LEAD EXCHANGE INTO

ZEOLITE AND CLAY MINERALS

BY

JIAN-JIE LIANG

A Thesis
Submitted to the Faculty of Graduate Studies
in Partial Fulfilment of the Requirements
for the Degree of

MASTER OF SCIENCE

Department of Geological Sciences
University of Manitoba
Winnipeg, Manitoba

ISBN 0-315-77955-1

LEAD EXCHANGE INTO ZEOLITE AND CLAY MINERALS

BY

JIAN-JIE LIANG

A Thesis submitted to the Faculty of Graduate Studies of the University of Manitoba in partial fulfillment of the requirements for the degree of

MASTER OF SCIENCE

ACKNOWLEDGEMENT

I wish to thank my supervisor, Dr. Barbara L. Sherriff, for everything she did for me during the past years. I could have never gone this far without her guidance. I also owe my gratitude to Dave Teertstra and Dan MacDonald for their kindly help in familiarising the chemical analysis facilities, and the helpful discussions. I would also like to offer my thanks to my fellow student, Zhi Xu, who helped with running the NMR instrument, and for discussions on the NMR results. Bruker Ltd., Canada is thanked for the loan of the DOR probe.

I appreciate deeply the careful review of the thesis by Dr. Norman M. Halden at the Department of Geological Sciences, and Dr. Charlie C. Bigelow at the Department of Chemistry.

Special thanks goes to my family, for their supporting, their understanding, and their suffering.

I would like to extend my acknowledgement to the University of Manitoba for granting the graduate fellowship.

ABSTRACT

Zeolite and clay minerals can be used to remove lead, a toxic heavy element, from waste water. The clay minerals also play an important role in the lead distribution in the contaminated soils through the ion exchange processes.

Chabazite, vermiculite, montmorillonite, hectorite, and kaolinite were used to examine the mechanism of lead exchange into zeolite and clay minerals. The minerals were characterized by XRD, XRF, AAS, electron microprobe, and wet chemical analyses, and their lead content measured by a gravimetric method. The maximum lead contents, gained through the ion exchange from 0.01 M aqueous $Pb(NO_3)_2$ solution, were 27% for Na-chabazite, 16% for vermiculite, 9% for montmorillonite and hectorite, and 0.4% for kaolinite. The ion exchange reached equilibrium within 24 hours in chabazite and vermiculite, but in less than 5 minutes in montmorillonite and hectorite. Na-chabazite took up more lead than natural Ca(Na)-chabazite, which had about 7% maximum lead content, whereas no such difference was observed in the clay minerals with respect to different cation forms of the minerals. Calcite impurities associated with clay minerals can very effectively remove lead from the aqueous solution by the precipitation of cerussite ($PbCO_3$).

^{29}Si, ^{27}Al, ^{23}Na, ^{7}Li, and ^{207}Pb magic angle spinning (MAS) NMR and ^{23}Na double angle rotation (DOR) NMR, as well as variable temperature MAS NMR were used to study the ion exchange mechanism. The fast chemical exchange of Na^+ cations at room temperature in Na-chabazite was slowed below -50 °C. The exchangeable cations in chabazite and vermiculite were found to be close to the SiO_4 and AlO_4 tetrahedra, while those in the other clay minerals were more distant. Two sites for exchangeable cations were observed in hectorite. The behaviour of the exchangeable cations in the interlayer is similar in all clay minerals studied.

TABLE OF CONTENT

	Pages
ACKNOWLEDGMENTS	I
ABSTRACT	II
LIST OF FIGURES	VI
LIST OF TABLES	IX
LIST OF ABBREVIATIONS	X
Chapter 1. LEAD OCCURRENCES, USES, AND TOXICITY	1
1.1. Introduction	1
1.2. Natural occurrences of lead on the Earth's surface	2
1.3. The use of lead	3
1.3.1. Historic times	3
1.3.2. Present day uses	4
1.4. Lead contamination of the environment	5
1.5. The toxicity of lead	7
Chapter 2. LITERATURE REVIEW	9
2.1. Ion exchange theory of the mineral exchanger	9
2.2. Chemistry of lead	10
2.3. Lead exchange into zeolite and clay minerals	13
2.3.1. Chabazite	13
2.3.2. Montmorillonite and kaolinite	15
2.4. Crystal chemistry of the zeolite and clay minerals	17

2.4.1. Chabazite 17

2.4.2. Vermiculite 17

2.4.3. Montmorillonite 22

2.4.4. Hectorite 24

2.4.5. Kaolinite 24

2.5. Solid state NMR study of the zeolite and clay minerals 26

2.5.1. Principles of nuclear magnetic resonance 26

2.5.2. Solid state NMR 28

2.5.3. Solid state NMR of the zeolite and clay minerals 32

Chapter 3. EXPERIMENTAL PROCEDURES 42

3.1. The ion exchange experiment 42

3.2. Materials 43

3.3. Wet Chemical analysis of the lead uptake 46

3.4. Electron microprobe analysis 49

3.5. Other chemical analyses 51

3.6. Water content measurement 52

3.7. Powder X-ray diffraction analysis 52

3.8. Nuclear magnetic resonance spectroscopy 54

Chapter 4. RESULTS AND DISCUSSION 56

4.1. Characterization of the ion exchangers 56

4.2. Lead exchange into zeolite and clay minerals 56

4.3. Reaction of calcite with lead nitrate solution 63

4.4. Solid state NMR study 65

4.4.1. ^{29}Si 65

4.4.2. ^{27}Al 70

4.4.3. ^{23}Na 72

4.4.4. ^{7}Li 85

4.4.5. ^{207}Pb 85

Chapter 5. THE ION EXCHANGE MECHANISM IN THE ZEOLITE AND CLAY MINERALS 89

5.1. Chabazite 89

5.2. The clay minerals 100

5.3. Conclusion 103

REFERENCES 106

LIST OF FIGURES

	Pages
Fig. 2.1. Types of isotherms showing differences in the cation selectivity of an ion exchanger	11
Fig. 2.2. Hydrolysis of Pb(II) of different concentrations and under varying conditions of pHs	14
Fig. 2.3. $2Na^+ \rightarrow Pb^{2+}$ exchange isotherm at 25°C	16
Fig. 2.4. Crystal structure model of natural chabazite	18
Fig. 2.5. Coordination of the three different sites of the exchangeable cations in chabazite	19
Fig. 2.6. Crystal structure model of the 2:1 clay minerals	20
Fig. 2.7. Schematic representation of the stacking disorder in vermiculite	23
Fig. 2.8. Crystal structure model of 1:1 clay minerals	25
Fig. 2.9. Schematic representation of magic angle sample spinning in the MAS NMR experiment	30
Fig. 2.10. Energy level for a spin I=3/2 nucleus	33
Fig. 2.11. Ranges of ^{29}Si chemical shift of Q^n units in solid silicates	34
Fig. 2.12. Ranges of ^{29}Si chemical shift of $Q^4(mAl)$ units in aluminosilicates	36
Fig. 2.13. Isotropic chemical shift ranges of selected aluminum compounds	37
Fig. 2.14. Chart of ^{207}Pb chemical shift ranges	41

Fig. 3.1. Filter disc adsorption of lead in different $Pb(NO_3)_2$ concentrations 50

Fig. 4.1. Lead uptake rate of chabazite and vermiculite in 0.01 M $Pb(NO_3)_2$ solution 58

Fig. 4.2. Lead uptake rate of hectorite and montmorillonite in 0.01 M $Pb(NO_3)_2$ solution 60

Fig. 4.3. Solid/solution equilibrium surface in the lead carbonate system at 25°C 64

Fig. 4.4. ^{29}Si MAS NMR of the zeolite and clay minerals before lead exchange 67

Fig. 4.5. ^{29}Si MAS NMR of Na-chabazite before and after lead exchange 68

Fig. 4.6. ^{29}Si MAS NMR of vermiculite before and after lead exchange 69

Fig. 4.7. ^{27}Al MAS NMR of Na-chabazite before and after lead exchange 71

Fig. 4.8. ^{27}Al MAS NMR of vermiculite before and after lead exchange 73

Fig. 4.9. ^{27}Al MAS NMR of montmorillonite before and after lead exchange 74

Fig. 4.10. ^{27}Al MAS NMR of hectorite before and after lead exchange 75

Fig. 4.11. ^{27}Al MAS NMR of kaolinite before and after lead exchange 76

Fig. 4.12. ^{23}Na MAS NMR of Na-chabazite before and after lead exchange 77

Fig. 4.13. ^{23}Na MAS NMR of Na-vermiculite before and after lead exchange 78

Fig. 4.14. ^{23}Na MAS NMR of hectorite before and after lead exchange 80

Fig. 4.15. Computer simulation (right) of ^{23}Na MAS NMR line shape of the centre band of the central transition from a powder with C_Q = 4.47 MHz, η_Q = 0.706 83

Fig. 4.16. ^{23}Na MAS NMR of montmorillonite before and after lead exchange 84

Fig. 4.17. ^{23}Na MAS NMR of kaolinite before and after lead exchange 86

Fig. 4.18. ^{7}Li MAS NMR of hectorite before and after lead exchange 87

Fig. 4.19. ^{207}Pb MAS NMR of cerussite in 8.4 T magnet 88

Fig. 5.1. Computer simulation of ^{27}Al MAS NMR peak width and shape using the computer program of Power and co-workers (1990) 92

Fig. 5.2. DOR NMR of Na-chabazite (8.4 T magnetic field) 95

Fig. 5.3. NMR peak shapes and widths of two exchanging chemical environment with different exchanging rate 97

Fig. 5.4. ^{23}Na variable temperature MAS NMR of Na-chabazite 98

Fig. 5.5. ^{23}Na MAS NMR spectra of the clay minerals before lead exchange 101

Fig. 5.6. ^{23}Na MAS NMR spectra of the clay minerals after lead exchange compared to that before lead exchange 102

LIST OF TABLES

	Pages
Table 2.1. Principle lead(II) compounds	12
Table 2.2. Effective ionic radii of lead	13
Table 2.3. Unit cell dimension of different cation forms of chabazite	21
Table 2.4. NMR parameters of the selected nuclei	28
Table 2.5. ^{29}Si chemical shift of the selected zeolite and clay minerals	35
Table 2.6. ^{27}Al MAS NMR peak position at 11.74 T of the selected zeolite and clay minerals	38
Table 2.7 ^{207}Pb chemical shifts of the selected solid Pb(II) inorganic compounds	40
Table 3.1. The zeolite and clay minerals selected in the lead exchange experiment	44
Table 3.2. Lead nitrate adsorption of the filter disc during filtration of lead nitrate solution	47
Table 3.3. Calibration of the gravimetric method using duplicate samples	48
Table 4.1. Chemical analysis from XRAL of the ion exchangers	57
Table 4.2. Electron microprobe analyses of the ion exchangers	59
Table 4.3. Electron microprobe analyses of the zeolite and clay minerals after lead exchange	61
Table 4.4. Lead uptake rate of the zeolite and clay minerals in 0.01 M $Pb(NO_3)_2$ solution	62
Table 4.5. ^{29}Si MAS NMR data of the zeolite and clay minerals	66

Table 4.6. ^{27}Al MAS NMR data of the zeolite and clay minerals 70

Table 4.7. ^{23}Na MAS NMR data of the exchangeable cation Na^+ in the zeolite and clay minerals 79

Table 5.1. ^{29}Si and ^{27}Al MAS NMR peak positions and peak widths of chabazite 90

Table 5.2. Chemical bonding of the cation sites of the exchangeable cations in chabazite 91

Table 5.3. ^{23}Na variable temperature MAS NMR data of Na-chabazite 99

LIST OF ABBREVIATIONS

AAS: Atomic Absorption Spectrascopy

CEC: Cation Exchange Capacity

CMS: Clay Mineral Society

DOR: (sample) Double Rotation

EFG: Electronic Field Gradient

FWHM: Full Width at Half Maximum

MAS: (sample) Magic Angle Spinning

meq: milli-equivalent

NMR: Nuclear Magnetic Resonance

XRD: X-ray Diffraction

XRF: X-ray Fluorescence

XRAL: X-ray Assay Laboratory

CHAPTER 1. LEAD OCCURRENCES, USES, AND TOXICITY

1.1. Introduction

Lead is a metal with a long history of use despite its toxicity which was recognized very early in history. In spite of the potential hazardous effects which it may cause, lead still finds an extensive application in the modern society, including gasoline additives and batteries for automobile industry, as well as paints and insecticides (Winship, 1989). Therefore, it is necessary to control the amount of lead released into the environment.

The objective of this study is to use natural zeolite and clay minerals to remove lead from the aqueous solution, and to examine the mechanism of the ion exchange process. Natural clays and zeolites are cheap and readily available minerals which should be considered in the lead removal processes. The behaviour of lead during the ion exchange processes in the zeolite and clay minerals is not well understood. This imposes difficulties in improving the efficiency of lead removal by these ion exchangers, and ultimately their use in environmental control. In addition, clay minerals are major components of soil and sediments. The elemental distribution of Pb in these materials is governed by ion exchange processes (Maes & Cremers, 1985). Therefore, understanding the ion exchange mechanism is critical in the cleanup of the lead contaminated soil and

modern sediments.

1.2 Natural Occurrence of Lead in the Earth's Surface

Lead, Pb, is the most metallic member of group IV elements in the Periodic Table, with the atomic number of 82. It has four naturally occurring isotopes: ^{208}Pb (51.55%), ^{206}Pb (26.26%), ^{207}Pb (20.8%), and ^{204}Pb (1.37%), and 10 unstable isotopes. Lead is a trace element in the Earth's crust, but ranks 27th among the elements in concentration in sea water, with 3 metric tons per cubic kilometre (Considine and Considine, 1984).

The average content of lead in the earth's crust is 16 ppm (de Treville, 1964). Felsic rocks have higher lead content than the mafic rocks, with a content ratio of approximately 20:8 by weight. Galena (PbS), the most abundant lead mineral, is used to produce lead. Other common lead minerals are cerussite ($PbCO_3$) and anglesite ($PbSO_4$). The element can also occur in bournonite ($PbCuSbS_3$), crocoite ($PbCrO_4$), wulfenite ($PbMoO_4$), pyromorphite ($Pb_5Cl(PO)_3$), and vanadinite ($Pb_5Cl(VO_3)_3$).

The average lead content in uncontaminated soil is 16 ppm (Stubbs, 1972), and the atmospheric concentration is 0.0005-0.0006 $\mu g/m^3$ (Patterson, 1965). An estimate for the lead concentration in drinking water is approximately 0.0005 ppm (Patterson, 1965).The sources of lead for uncontaminated soil can be the weathering of crustal rocks and atmospheric precipitation. Atmospheric lead comes from silicate dust from soils, volcanic ashes and smoke, as well as forest fires.

1.3 The Use of Lead

1.3.1. Historic Uses

Lead has been used through out civilization (Waldron and Stöfen, 1974). The Egyptians made human and animal figures, amulets, sinkers (for fishing nets), rings, dishes, trays and other ornaments from metallic lead (Waldron and Stöfen, 1974) which was also used as a core for bronze statuettes and bronze weights. Lead compounds were used extensively for eye paints (Partington, 1935).

In the Mediterranean cultures (Waldron and Stöfen, 1974), lead was frequently used in construction as binding and fastening materials. It was widely used in ship building, as sheets to protect the bottom of ships against worms, and as components for anchors. The Mediterranean cultures also used lead as sinkers for fishing nets. In writing, lead was used both as a stylus and as a slate on which letters could be easily scratched. In social life, lead was used to make tickets, visiting cards, trade marks, and coins.

In the Roman Empire, lead use reached its first apex. The maximum consumption of lead was 4 kg/citizen/year (Patterson, 1965), a figure approaching the rate of consumption in the USA, in the 1970s, of 6kg/citizen/year (Waldron and Stöfen, 1974). Most of the lead was used for water pipes which were made of lead sheet banded around a core and soldered (Waldron and Stöfen, 1974). Lead was used extensively in cooking, as an inner lining of bronze pots which otherwise gave a bitter taste to food. Lead compounds were added to food and wine because of the sweetening quality of some lead

compounds, such as lead acetates ($Pb(C_2H_3O_2)_2 \cdot H_2O$). These practices caused severe contamination of food and drinks, and it has been suggested that the fall of the Roman Empire is largely due to the widespread lead poisoning (Gilfillan, 1965).

Following the fall of the Roman Empire, the use of lead declined, but the practice of sweetening wine with lead and its salts became more widespread (Waldron and Stöfen, 1974). Lead contamination of wine continued till the recent times.

1.3.2. Present day Uses

The battery industry now consumes about half of the total lead produced, of about 1.3×10^5 T (Irwin, 1985). A lead storage battery consists of a negative plate of porous lead, a positive plate of lead peroxide, and an electrolyte of sulphuric acid solution. The chemical reactions may be represented as (Parker, 1983):

$$PbO_2 + 2H_2SO_4 + Pb \underset{\text{charge}}{\overset{\text{discharge}}{\rightleftharpoons}} 2PbSO_4 + 2H_2O$$

Another major portion of lead goes to the production of gasoline additives, the antiknock agents of tetraethyllead and tetramethyllead. When these compounds are added into gasoline, the compression ratio can be increased and the engine runs more efficiently. Introduced in the late 1920's, these additives were used everywhere around the world, and are still in use in most of the countries in Europe, Asia and Australia. The production of tetraethyllead is through the reaction of ethyl chloride with an alloy of sodium and lead (Parker, 1983):

$$4PbNa + 4C_2H_2Cl \rightarrow (C_2H_5)_4Pb + 4NaCl + 3Pb$$

Lead is also used in paints and coatings. In fact, basic lead carbonate,

$Pb_3(CO_3)_2(OH)_2$, was the only white pigment used in paint for over 2,000 years, until the late 1940's, when titanium oxide was introduced (Partington, 1973). Lead paints were widely used on interior and exterior walls, on furniture, and on toys. Today red lead (lead oxide) and lead chromate are still used in the paint industry, for corrosion protection of bridges and other exterior steel structures (Cloghesy, 1985) and in traffic markings. Lead phosphate is a wetting or dispersing agent to help make a smooth and uniform product in the water-based paints.

Lead is also passed to human through solders. Foods, beer and carbonate beverages used to be canned with lead-soldered side seams. Metal containers, which are not for food or drinks are still soldered with lead (Grant, 1985). Lead solders made connections in plumbing and automobile radiators, and lead-tin alloy is important for connections in electrical circuitry.

Lead is used in the plastics industry as a stablizer, and in glass industry to make optical and flint glasses, or photographic and other special lenses. Lead can be found in colour TV tubes, in gamma radiation shielding glasses and in mirror manufacture. There is lead in bronze and brass, in Pb-As-Mo-Sn cable and Pb-Sb cable coatings, in type metal (Pb-Sb-Sn), in shots and weights, in ceramics (lead silicates), in lubricating oils (organolead), in clutch and brake linings (lead oxides), in insecticides, and even in medicine and cosmetics (Winship, 1989).

1.4 Lead Contamination of the Environment

Contamination is inevitable due to the extensive use of lead. Industrial activities account for the present day elevated level of lead in the atmosphere. The sources include gasoline and oil contamination, waste incineration, coal combustion, lead production, industrial application of lead, metal production, wood combustion, and cement manufacture (Nriagü, 1986). Among these, gasoline production and combustion, lead and other metal production, and coal combustion are the most prominent sources.

Lead in the air can be absorbed by the vegetables grown alongside highways, which may contain two to three times the lead content of the vegetables grown well away from traffic (Wijin et al., 1983).

Soil is a major sink for atmospheric lead. Contamination from lead industry, coal ash, paint, sewage sludge, mining and smelting, as well as fallout from airborne gasoline lead have led to general soil pollution (Elwood, 1986). In urban areas in the industrialized countries, soil lead content is high (Elwood, 1986), especially in those around lead smelters or mining sites, which can have up to 3% lead (Nriagü, 1986).

Widespread and frequent use of lead-containing paint is one of the cause of elevated house hold lead levels which ranges from 600 to 922 ppm in the U.S.A. (Lin-Fu, 1982). High lead levels occur most frequently in old properties and in less privileged areas such as "down-town" urban areas, where water supply is not free of lead plumbing (Pocock et al., 1983). The first few litres of tap water are usually high in lead, which can reach 0.11 ppm (Karalekas et al., 1983).

Apart from air and water, it is determined that the major human exposure to lead is in the diet (Sherlock, et al., 1983). Vegetables adsorb lead from water during cooking,

and the amount adsorbed from soft water is greater than from hard water (Little et al., 1981). Alcoholic drinks can contain lead (Grandjean et al., 1981). Young children ingest lead from licking their hands after playing in dirt (Gallacher et al., 1984).

1.5 The Toxicity of Lead

Most lead compounds are toxic. The fatal dose of absorbed lead is estimated at 500 mg (Winship, 1989). Low dose lead exposure, through inhalation, ingestion, or skin absorption, will cause chronic poisoning (Waldron and Stöfen, 1974; Hotz, 1986; Winship, 1989).

Perhaps the issue which draws the most public attention are the effects of lead on mental development of young children. In the 1960's, there were frequent findings of raised blood lead concentration in children with mental handicaps or severe behavioural disorders (Bicknell et al., 1968). Most of these showed no clinical signs of exposure of lead poisoning. Later studies revealed a significant relationship between blood lead level and IQ in children aged between 6-9 years (Fulton et al., 1987). The blood lead level of infants can be high if the mother has elevated blood lead level (Singh et al., 1978). These infants can have delayed cognitive skills such as imitation tasks (Jenkins and Mellins, 1957).

Lead poisoning affects human reproduction. Both organic and inorganic lead compounds can cause abortions (Oliver, 1911), low sperm counts (Barlow and Sullivan, 1982), and endocrine and reproductive dysfunction (Cullen et al, 1984). Deformities of

fetus have been caused by lead poisoning in some animal species (Gilani, 1973). One similar human deformity occurred when the pregnant mother consumed Pb contaminated whisky (Palmisano et al., 1969).

There is evidence that smelter and battery workers may have higher expectations of developing lung and digestive tract cancer (Cooper, 1976). Smelter workers have developed carcinoma similar in appearance to lead induced tumours in animals (Cooper, 1976).

The central nervous system is also affected by lead poisoning. Low dose chronic poisoning can cause visual disturbance and auditory defects, while more rapid and intense lead adsorption will result in clumsiness, confusion, or even loss of memory (Crutcher, 1963). Young children, especially those between 12 and 48 months of age are most severely affected (Byers, 1959). 25% of the survivors of acute poisoning have permanent neurological damges, with brain damage usually occurring on reexposure (Byers and Lord, 1943). The peripheral nerve conduction velocity my be slowed when blood lead level is raised to over 3 ppm in adults (Schwartz et al., 1988). This was observed with workers in lead industries where lead level was considered safe and when there was no obvious tissue damage or other noticeable clinic effects (Boey and Jeyaratnam, 1988).

Renal failure was frequently observed among industrially exposed workers and long term drinkers of lead contaminated whisky (Lillis et al., 1968). Intense short term poisoning will produce renal tubular damage, especially among young children (Goyer et al., 1972). The gastrointestinal effects of lead poisoning are epigastric pains, indigestion, nausea, and constipation (Klaussen, 1980).

CHAPTER 2. LITERATURE REVIEW

2.1. Ion Exchange Theory of a Mineral Exchanger

In a system containing two exchanging cations A and B, the ion exchange process can be expressed as (Breck, 1974):

$$Z_A B_{(m)}^{Z_B+} + Z_B A_{(S)}^{Z_A+} \rightleftarrows Z_A B_{(S)}^{Z_B+} + Z_B A_{(m)}^{Z_A+}$$

where Z_A and Z_B are the charges of the exchangeable cations A and B, and the subscripts $_m$ and $_s$ denote the mineral ion exchanger and the solution respectively.

The equivalent fractions, taking the sum of those of A and B as 1, of the exchanging cations A in the solution and in the mineral can be given as:

$$A_S = \frac{Z_A (M_A)_S}{Z_A (M_A)_S + Z_B (M_B)_S}$$

where M is the mole concentration (mole/l), and

$$A_m = \frac{Z_A (M_A)_m}{Z_A (M_A)_m + Z_B (M_B)_m}$$

By varying the initial concentration A_{SI} in a system, while maintaining the total initial concentration $A_{SI} + B_{SI}$ as well as the solution temperature constant, a series of points (A_S, A_m) can be obtained. A plot of A_S as a function of A_m gives an ion

exchange isotherm. The shape of the isotherm gives information on the relative ease of a cation entering the mineral (Fig. 2.1). When the isotherm lies below the diagonal (curve 3), the mineral shows a preference for the entering cation A, whereas, when the isotherm lies above the diagonal (curve 2), cation A is less preferred than cation B. When the isotherm has a sigmoidal shape (curve 1), the selectivity of the mineral changes during the ion exchange process. Curve 1 shows that when the equivalent fraction of cation A in the mineral approaches 0.4, the preference of the mineral shifts from A to B. That is to say that greater ion exchange potential, e.g. greater concentration of A, has to be built up before further exchange of cation B by cation A.

The cation exchange capacity (CEC) is expressed in milli-equivalent of the exchangeable cations per hundred grams of the mineral (meq/100g). A large CEC indicates a strong ion exchange capacity.

2.2 Chemistry of Lead

As the electronic configuration of a lead atom is

$$1s^2 2s^2 2p^6 3s^2 3p^6 3d^{10} 4s^2 4p^6 4d^{10} 4f^{14} 5s^2 5P^6 5d^{10} 6s^2 6p^2,$$

two valence states, lead (II) and lead (IV), are expected (Considine and Considine, 1984):

$$Pb \rightarrow Pb^{2+} + 2e^- \qquad 0.126 \text{ eV}$$

$$Pb^{2+} + 2H_2O \rightarrow PbO_2 + 4H^+ + 2e^- \qquad -1.456 \text{ eV}$$

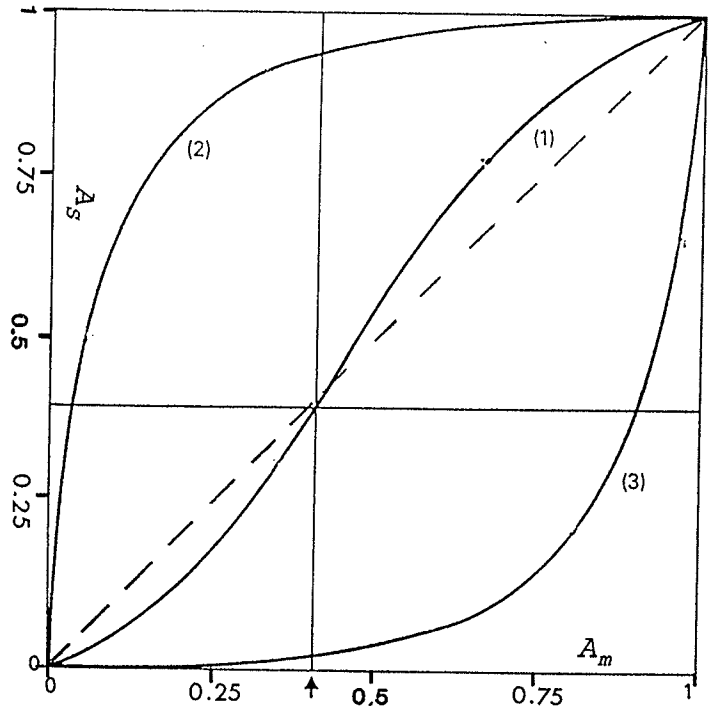

Fig. 2.1 Types of isotherms showing differences in the cation selectivity of an ion exchanger (modified from Townsend, 1984)

Pb(II) is relatively stable, formed by the loss of the $6p^2$ electrons. Pb(IV) is of much more covalent character, exhibiting sp^3 hybridization. Lead(II) forms compounds with most of the common anions (Table 2.1).

Table 2.1. Principle lead(II) compounds

compounds	formula	solubility (g / 100 ml)
Acetate	$Pb(C_2H_3O_2)_2 \cdot H_2O$	44.30
Arsenate	$Pb_3(AsO_4)_2$	very slightly soluble
Azide	PbN_6	0.023
Borate	$Pb(BO_2)_2$	insoluble
Carbonate	$PbCO_3$	0.00011
Chromates	$PbCrO_4$	0.0000058
Nitrates	$Pb(NO_3)_2$	37.65
Oxide	PbO	0.0023
Oxalate	PbC_2O_4	0.00016
Phosphate	$Pb_3(PO_4)_2$	0.000014
Sulphates	$Pb(SO_4)_2$	0.00425
Sulphide	PbS	0.000086

More than five hundred organometallic compounds of lead have been reported, in most of which lead is tetravalent and is covalently bonded (Considine and Considine, 1984). Eight and four coordination states exist for lead(II) and lead(IV) respectively (Shannon, 1976), and these are listed with the corresponding ionic radii in Table 2.2.

Table 2.2. Effective ionic radii of lead (Å) (from Shannon, 1976)

Coord. #	IV	V	VI	VII	VIII	IX	X	XI	XII
Pb^{+2}	0.98		1.19	1.23	1.29	1.35	1.40	1.45	1.49
pb^{+4}	0.65	0.73	0.775		0.94				

The hydrolysis of inorganic lead compounds dominates the migration of lead in aqueous solution. There are eight species of hydrated lead, including the uncomplexed Pb^{2+}, which exist under widely varying conditions of pH and Pb^{2+} concentration (Baes and Mesmer, 1976). The hydrolysis products can be represented as: $[Pb_p(OH)_q]^{(2p-q)+}$, where the (p,q) terms take the value of (1,0), (1,1), (1,2), (1,3), (2,1), (3,4), (4,4), (6,8). The dominant hydrolysed product in a solution, at constant temperature, is determined by the total Pb(II) concentration and the solution pH (Fig. 2.2). When the Pb(II) concentration is high (Fig. 2.2.a), the dominant species at pH 5 - 7 are Pb^{2+} and $Pb_4(OH)_4^{4+}$; when the Pb(II) concentration is low (Fig. 2.2.b), only Pb^{2+} is dominant at the same pH range, with small amount of $Pb(OH)^+$. Regardless of the Pb(II) concentration, when the solution is acidic, there is only one dominant species, Pb^{2+} (Sylva et al., 1980; Saether, et al., 1988). As the solution becomes more basic, species with greater q:p ratio, eg. $Pb_6(OH)_8^{4+}$, $Pb_3(OH)_4^{2+}$, and $Pb(OH)_3^-$, become dominant.

2.3. Lead exchange into zeolite and clay minerals

2.3.1. Chabazite

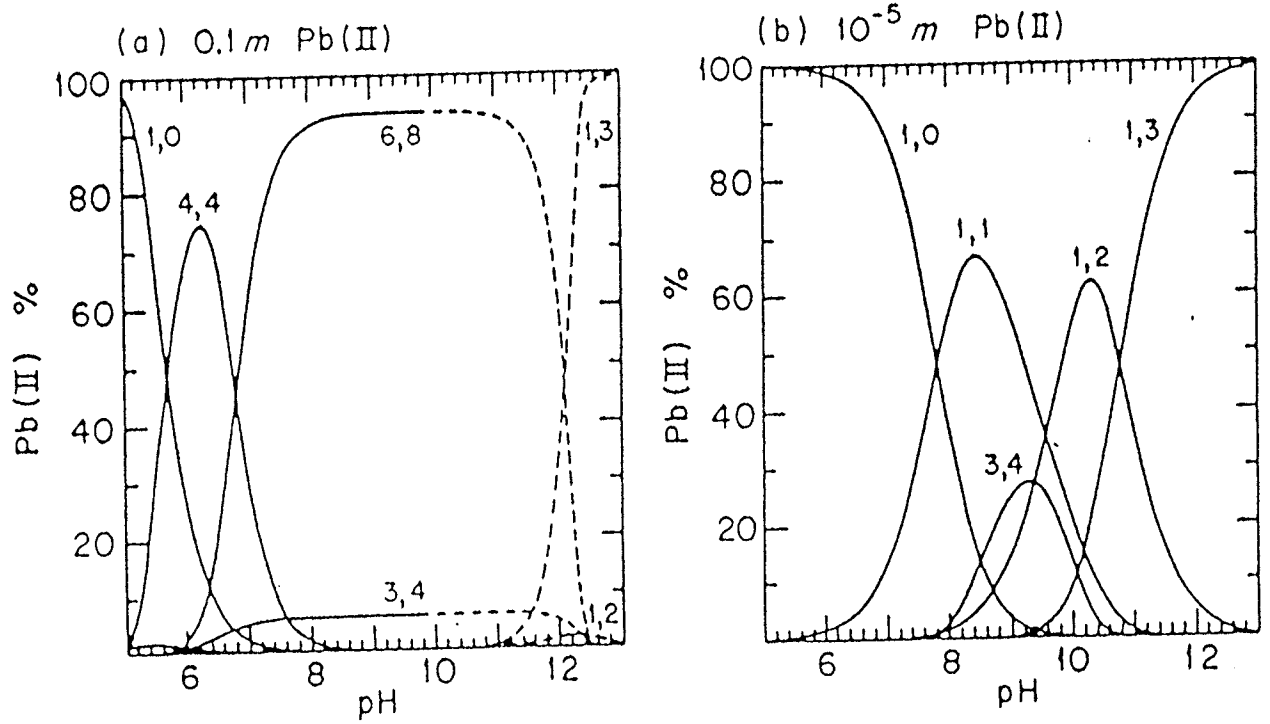

Fig. 2.2 Hydrolysis of Pb(II) of different concentration and under varying pH. (From Baes & Mesmer, 1974)

The first attempt of using natural chabazite to remove lead from the aqueous solution was reported in 1955 (Barrer and Sammon, 1955). Chabazite was heated in a lead nitrate solution at 95 °C. A considerable exchange of $Ca^{2+} \rightarrow Pb^{2+}$ occurred in the chabazite. Further experiments with Na saturated chabazite (Barrer et al, 1969) determined the $2Na^{+} \rightarrow Pb^{2+}$ exchange isotherm (Fig. 2.3), which shows the strong preference of Pb over Na in chabazite. An abrupt selectivity change happens at about $Pb_Z = 0.8 \sim 0.9$ (Pb_Z is the equivalent fraction of Pb in chabazite). It is difficult to exchange the last 0.2 equivalent fraction of Na^{+} for Pb^{2+} in chabazite. The $2Na^{+} \rightarrow Pb^{2+}$ exchange reaches equilibrium after 7 days of exchange. Pb was believed to be exchanged as the divalent ion Pb^{2+}, not as $PbOH^{+}$ (Barrer et al., 1969). Zamzow and the co-workers (1990) discovered that lead uptake is influenced by the initial cation form of the chabazite sample in the order Na^{+}, $NH_4^{+} > K^{+} > Ca^{2+} > Mg^{2+}$, and that the chabazite sample did not decompose with a pH lower than 2.

2.3.2. Montmorillonite & Kaolinite

The maximum uptake of lead from aqueous solutions containing 2×10^{-4} and 1×10^{-3} M Pb^{2+} are about 32 meq/100g for montmorillonite, and about 6 meq/100g for kaolinite (Srivastava et al., 1989). The amount of lead taken up by the minerals decreases with the initial concentration of lead of the solution. In acidic solution (pH 2-4) pH influences the lead uptake of the two minerals differently, with montmorillonite taking up more lead at higher pH, and kaolinite at lower pH. Increasing the solution temperature decreases the Pb uptake in both minerals.

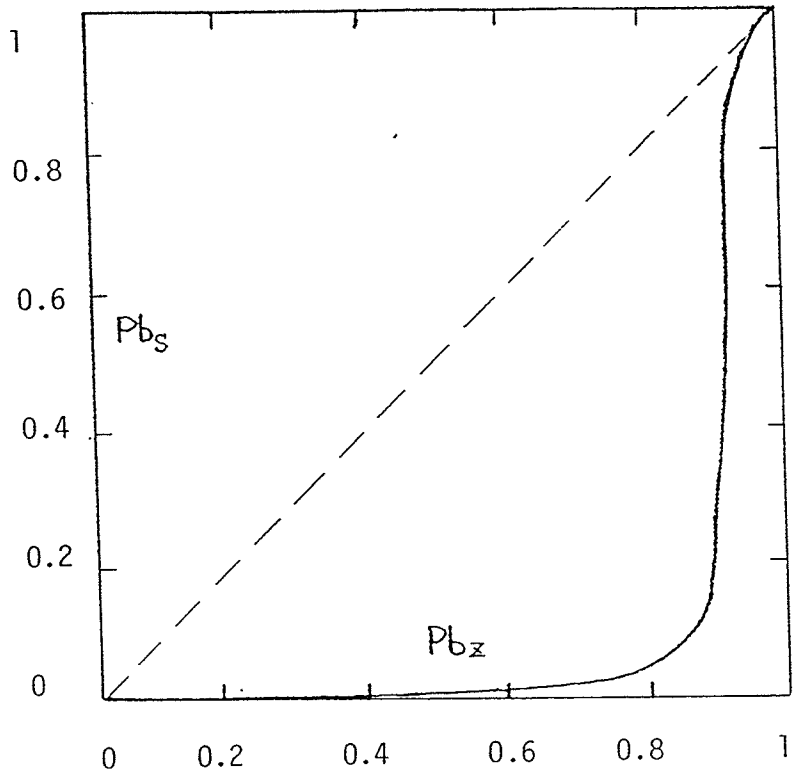

Fig. 2.3 $2Na^+ \rightarrow Pb^{2+}$ exchange isotherm at 25°C (From Barrer et al., 1969)

2.4. Crystal Chemistry of the Zeolite and Clay Minerals

2.4.1. Chabazite

Chabazite is a hydrated tectosilicate consisting of double six membered ring of the $Si(Al)O_4$ tetrahedra which are packed in an ABCABC sequence and linked by four membered rings (Fig. 2.4). Rhombohedral symmetry with space group $R\bar{3}M$ is widely accepted although there is evidence of lower triclinic symmetry (Smith et al., 1964, Mazzi & Galli, 1983) due to the local ordering of Al and Si in the tetrahedral sites.

Three exchangeable cation sites were resolved (Calligaris et al., 1982) along the [111] diagonal at x = y = z = 0.204 [CS1], x = y = z = 0.407 [CS2], x = y = z = 0 [CS3] (Fig. 2.4). They are all six coordinated but with different anions (Fig. 2.5). CS1 coordinates to 3 framework oxygen (CS1−O(4) = 2.685 Å) and three water molecules (CS1-O(7) = 2.82 Å). CS2 coordinates to water molecules only (CS2 - O(5) = 2.88 Å, CS2 - O(7) = 2.28 Å), while CS3 to the framework oxygens only (CS3-O(4) = 3.069 Å), but at considerably greater distance than that for CS1. Unit cell dimensions have little variation with differing exchangeable cations, with a = 9.35 ~ 9.50 Å, and α = 94.05° ~ 95.32° (Table 2.3).

2.4.2 Vermiculite

Vermiculite is a 2:1 hydrated phyllosilicate with each layer of the crystal structure having two tetrahedral sheets, and one octahedral sheet (Fig. 2.6). The

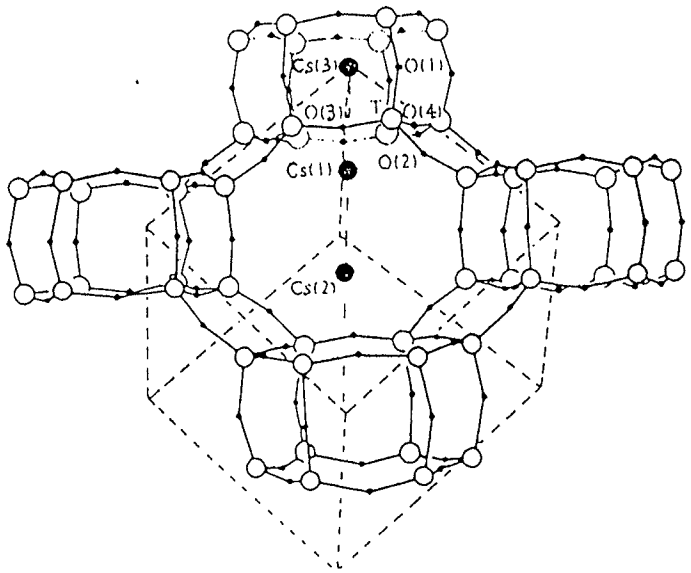

Fig. 2.4 Crystal structure model of natural chabazite (From Calligaris et al, 1982)
small dots: O
open circle: Si(Al)
large dots: exchangeable cation sites (CS)

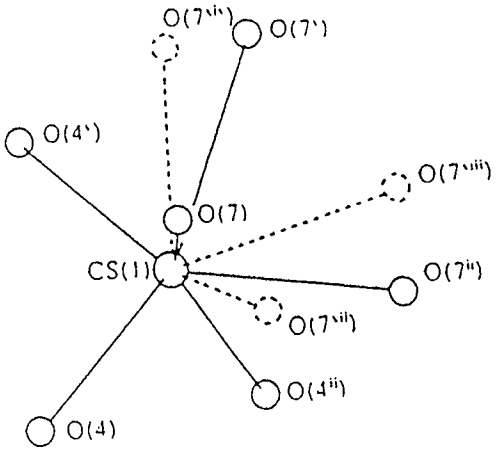

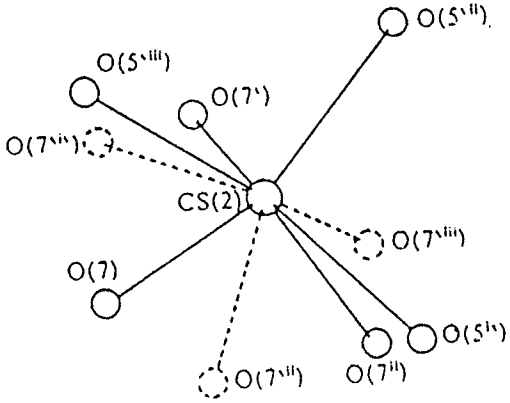

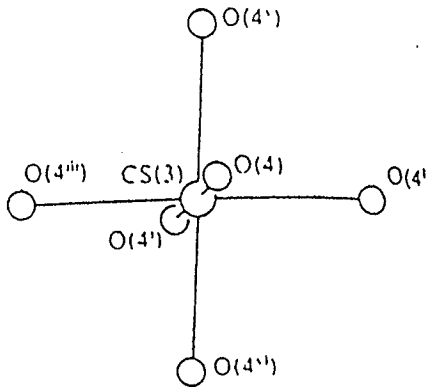

Fig. 2.5. Coordination of the three different sites of the exchangeable cations in chabazite (From Calligris et al., 1982)
O(7), O(5): Oxygen in the water molecules
O(4): Framework oxygens

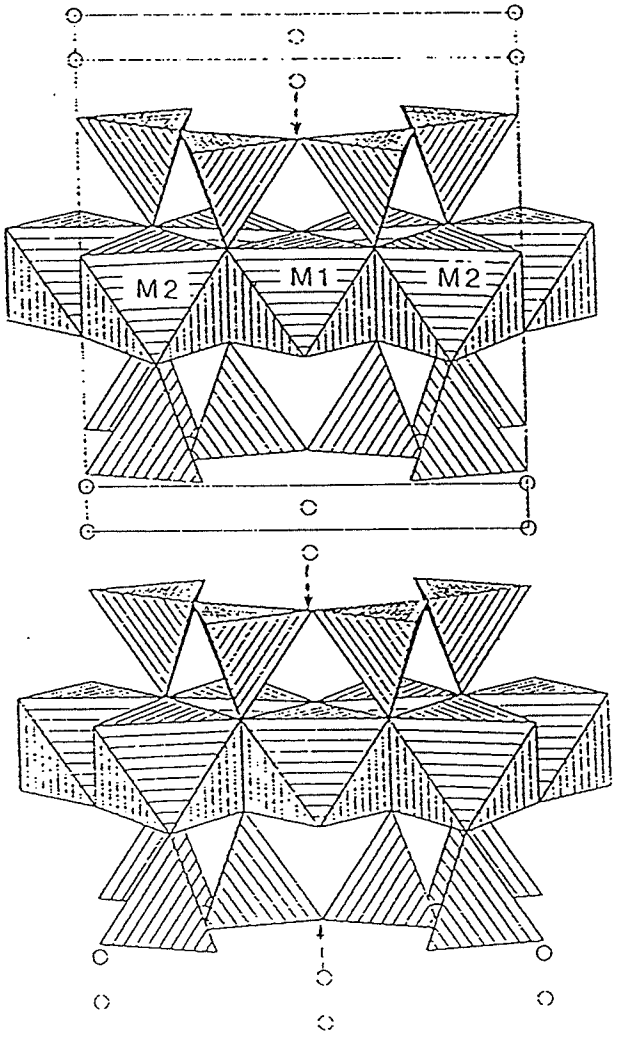

Fig. 2.6 Crystal structure model of the 2:1 clay minerals (From Smyth & Bish, 1988)

O Exchangeable Cation

Table 2.3 Unit Cell Dimension of Different Cation Forms of Chabazite

Chabazite Forms	a(Å)	α(degree)	Reference
hydrated Ca	9.45	94.47	Smith, 1962
hydrated Ca	9.43	94.45	Barrer & Sammon, 1955
hydrated Ca,Na	9.35	94.62	Nowacki, et al., 1958
hydrated Na	9.40	94.1	Smith, 1962
hydrated Na	9.50	94.05	Barrer & Sammon, 1955
hydrated Ag	9.45	94.30	Smith et al., 1963
hydrated Ba	9.47	94.05	Smith et al., 1963
hydrated Ca,Sr,Na,K	9.421	94.20	Calligaris et al., 1982
hydrated Cu	9.411	95.32	Pluth et al., 1977

octahedral cations are mostly Mg^{2+} with a small amount (0.16 out of 3 mole fraction) of Al^{3+}. They are coordinated to hydroxyl anions, OH^-, of the octahedral sheet, and the apical oxygens of the tetrahedral sheet. Cations in the tetrahedra are Si and Al. Each $Si(Al)O_4$ tetrahedron shares three apical oxygens with neighbouring tetrahedra to form a 6-membered ring. Al^{3+} instead of Si^{4+} results in an excessive negative charge. As each unit cell has 1.18 tetrahedral Al, there is a negative charge of 1.18 in the tetrahedral sheet, which is compensated by the positive charge generated by Al^{3+} in the octahedral sheet and by the interlayer cations which compensate for the remaining 1.02 excessive charge.

The space group derived is C2/c, with a = 5.349, b = 9.255, c = 28.89 Å, and β = 97°07' (Shirozu & Bailey, 1966). Partial tetrahedral cation (Si and Al) ordering

is indicated by the difference in the average T-O bond lengths (T_1-O = 1.673 Å, T_2-O = 1.641 Å), and by the difference in the temperature factors for these cations (B = 1.03 for T_1 and 0.83 for T_2) when similar scattering factors are assumed for both. T_1 site is occupied by Al and T_2 by Si. The exchangeable cations are between equivalent T_1 sites in the tetrahedral sheets above and below. There are stacking disorder in between the individual layers along both x and y axes (Fig.2.7).

2.4.3. Montmorillonite

Montmorillonite is also a 2:1 hydrated phyllosilicate. It is di-octahedral, with only two out of three octahedra in the unit cell filled with the octahedral cations Al^{3+} and Mg^{2+}. No structural refinement is available because of the structural disorder and distortion, as well as fine grain size (Güven, 1988). The space group of C2/m (Zvyagin & Pinsker, 1949) or C2 (Méring and Oberlin, 1971) is suggested from the powder diffraction data and theoretical calculation.

The excessive negative charge originates from the di-valent cation, Mg^{2+}, in the octahedral sheet occupying the site for the tri-valent cations Al^{3+}. It is in this aspect, together with a lower net negative charge, that montmorillonite differs from vermiculite which has its excess negative charge developed in the tetrahedral sheet. Two general sites for the exchangeable cations are possible (Nrigü, 1988). One of them is between the 6-membered rings of the tetrahedral sheets in the adjacent layers, with bonds to the oxygens in the two corresponding layers. The other site is inside the 6-membered ring where the exchangeable cation bonds to only one

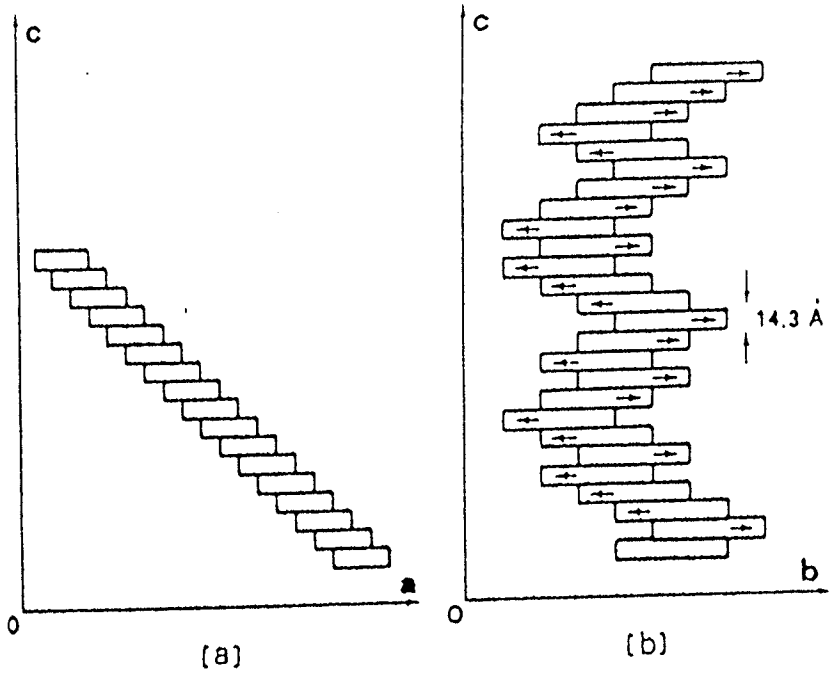

Fig. 2.7 Schematic representation of the stacking disorder in vermiculite (From de la Calle & Suquet, 1988).
a) (010) view
b) (100) view

montmorillonite layer (Fig. 2.6).

2.4.4 Hectorite

Hectorite is the tri-octahedral analogue of montmorillonite. All three octahedra in the unit cell are filled by Mg^{2+} or Li^{+}. The charge imbalance is again in the octahedral sheet due to monovalent Li^{+} in the place of the divalent Mg^{2+}. The exchangeable cations are assumed to be distributed into sites similar to those in montmorillonite (Nrigü, 1988).

Hectorite is an even less understood species with respect to the crystal structure. No structural refinement is available.

2.4.5 Kaolinite

The symmetry of kaolinite is triclinic, with space group C1. A recent Rietveld structural refinement (Bish and Von Dreele, 1988) determined the unit cell parameters as:

$a = 5.15560(10)$ Å; $b = 8.94460(17)$ Å; $c = 7.40485(17)$ Å,

$\alpha = 91.697(2)°$; $\beta = 104.862(2)°$; $\gamma = 89.823(2)°$.

Kaolinite is a di-octahedral 1:1 hydrated phyllosilicate (Fig. 2.8). Al is coordinated by six oxygens and hydroxyls to form the octahedral layer, while Si is coordinated by four oxygens to form the tetrahedral sheet. There is a small amount of exchangeable cations in between the layers, due to trace amounts of lower valent cations either in the octahedral or the tetrahedral sheet, eg. Al^{3+} or Fe^{3+} in the place

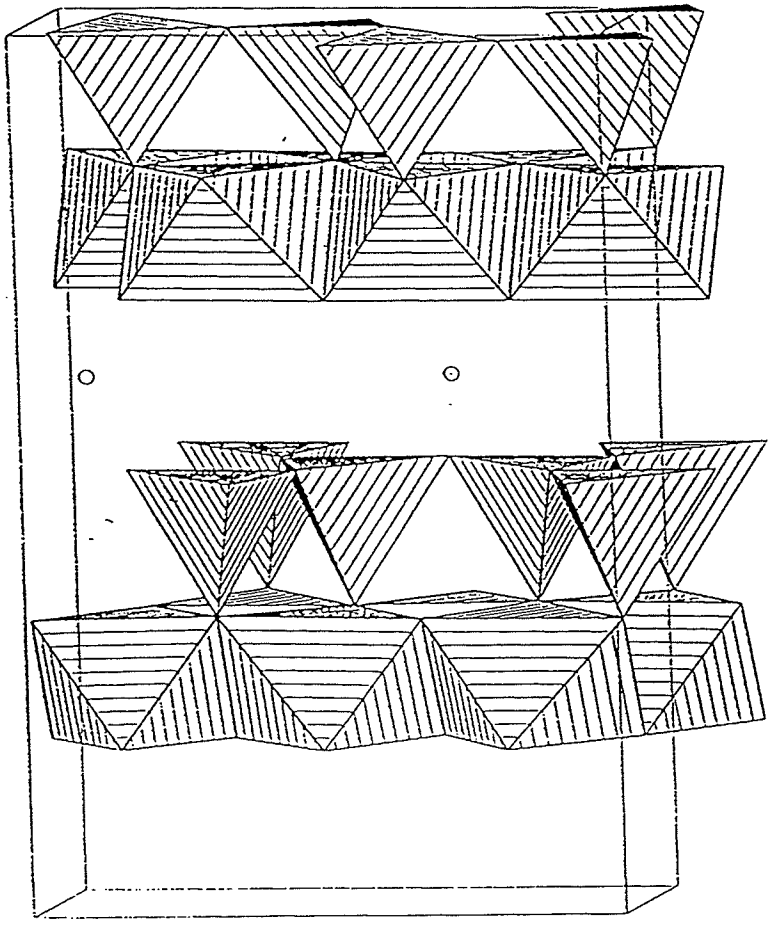

Fig. 2.8 Crystal structure model of 1:1 clay minerals.

o Exchangeable cations

of tetrahedral Si^{4+}; Mg^{2+} or Fe^{2+} in the place of the octahedral Al^{3+}.

2.5 Solid State NMR Study of Zeolite and Clay Minerals

2.5.1 Principles of Nuclear Magnetic Resonance

Each element in the Periodic Table has at least one isotope whose nucleus possesses a nuclear spin, i.e. with a nuclear spin number $I > 0$. Such a nucleus, when placed in a magnetic field, will undergo a precession about the field direction. The frequency of the precession in Hz (Larmor precession frequency) is given by:

$$\nu_0 = \gamma B_0/2\pi$$

in which B_0 is the applied magnetic field and γ the magnetogyric ratio which is a different constant for each isotope. When electromagnetic energy in the form of radio waves, with the same frequency as the precessing nucleus, is applied to the system, this energy will be absorbed, and the nucleus resonates. Such resonance can be detected and the precessing frequency of the nucleus measured.

For a certain nucleus, such as ^{29}Si, the exact precession frequency in a given magnetic field will differ slightly in response to the difference in the chemical environment of the nucleus, i.e. bonding, coordination, etc. The nucleus is surrounded by a cloud of electrons which are also charged particles. When placed in a magnetic field B_0, currents are induced in the electron clouds, which give rise to a small, local magnetic field which is always proportional to B_0, but opposite in direction. The nucleus is thus said to be shielded from B_0. The actual magnetic field B_{eff} acting on the nucleus is:

$$B_{eft} = B_0(1 - \sigma)$$

in which σ, the chemical shielding tensor, is dependent on the chemical environment of the nucleus. Information about the chemical environment of a nucleus can therefore be gained from the resonant frequency, which can be expressed as

$$\nu_s = \gamma B_{eft}/2\pi$$

$$= \gamma B_0(1 - \sigma_s)/2\pi$$

For a given nucleus, the resonant frequencies ν_s of different chemical environments differ by the order of Hz to 10^3 Hz. Such differences are small compared to the resonant frequency, which is in the order of 10^6 Hz. It is therefore convenient to deal with the relative differences in between different chemical environments which are expressed with respect to a reference (Becker, 1980):

$$\delta = (\nu_s - \nu_r)/\nu_r \cdot 10^6$$

in which δ is the chemical shift, and ν_s, ν_r are the resonant frequencies of the sample and of the reference respectively. Chemical shift is given in parts per million (ppm) of the magnetic field.

The relaxation time is the time for the nucleus to release the absorbed energy and to return to its ground state. Nuclei like ^{27}Al, ^{23}Na, and ^{7}Li which have nuclear spin > 1/2 possess an efficient quadrupolar relaxation mechanism, and hence have a relatively short relaxation time. Spin 1/2 nuclei like ^{29}Si and ^{207}Pb have longer relaxation times. The NMR technique has to repeat the process of excitation → data acquisition → relaxation hundreds to thousands of times in order to obtain an acceptable signal to noise ratio.

The relative ease of NMR observation varies with the relative isotopic abundance and the magnetic sensitivity of the nucleus. In this study, ^{27}Al and ^{23}Na, which have 100% natural abundance, and ^{7}Li at 92% abundance (Table 2.4) are the most easily observed nuclei. ^{29}Si and ^{207}Pb have low natural abundance and are difficult to observe.

Table 2.4 NMR parameters of the selected nuclei

Isotope	NMR frequency* (MHz)	Natural abundance(%)	Relative sensitivity#	Spin I
^{29}Si	99.320	4.7	$7.85 \cdot 10^{-3}$	1/2
^{27}Al	130.244	100	0.207	5/2
^{23}Na	132.216	100	$9.27 \cdot 10^{-2}$	3/2
^{7}Li	194.262	92.57	0.294	3/2
^{207}Pb†	74.752	21.11	$9.13 \cdot 10^{-3}$	1/2

*: in 11.74 T magnetic field
†: in 8.4 T magnetic field
#: relative to the sensitivity of ^{1}H at constant magnetic field (From Bovey, 1988)

2.5.2 Solid State NMR

The chemical shielding tensor σ is orientation dependent. In the powder sample of a crystalline solid, all orientations of the crystallites with respect to the applied magnetic field are possible. Each orientation will produce a resonance line with a slightly different frequency. The resulting spectrum is a broad envelope of these peaks which renders interpretation difficult. Chemical shift anisotropies, dipole-dipole interactions, and quadrupolar interactions are main causes of line broadening.

1). Chemical shift anisotropy Chemical shift anisotropy originates from the three dimensional property of the shielding tensor σ. To average this to an isotropic quantity, the sample is mechanically rotated at speeds between 3 and 20 KHz. The observed electronic shielding σ_{obs} of the rotating sample is (Pines et al., 1973):

$$\sigma_{obs}=\frac{3}{2}\sigma_{iso}Sin^2\theta+\frac{1}{2}(3\cos^2\theta-1)\cdot\sum_p\sigma_p\cos^2\chi_p$$

where θ is the angle between the sample rotation axis and the magnetic field direction $\mathbf{B}_0$ (Fig. 2.9), χ_p the angles related to the orientation of the crystallite in the sample, and σ_p the effective shielding components of the shielding tensor σ of the crystallites. If θ = 54.7°, then $\cos^2\theta$ = 1/3, $\sin^2\theta$ = 2/3, and the above equation reduces to:

$$\sigma_{obs} = \sigma_{iso}$$

Therefore, by spinning the sample at the angle θ = 54.7° (the 'magic angle'), chemical shift anisotropy can be averaged to an isotropic value. The relationship between the isotropic shielding, σ_{iso}, and the isotropic chemical shift, δ_{iso}, is:

$$\sigma_{iso} = -\delta_{iso}$$

It can be informative to extract the parameters of the electronic shielding anisotropy. The isotropic shielding tensor is related to the principle values σ_{11}, σ_{22}, σ_{33} by (Becker, 1980):

$$\sigma_{iso} = (\sigma_{11} + \sigma_{22} + \sigma_{33})/3$$

and the shielding anisotropy is defined as (Becker, 1980):

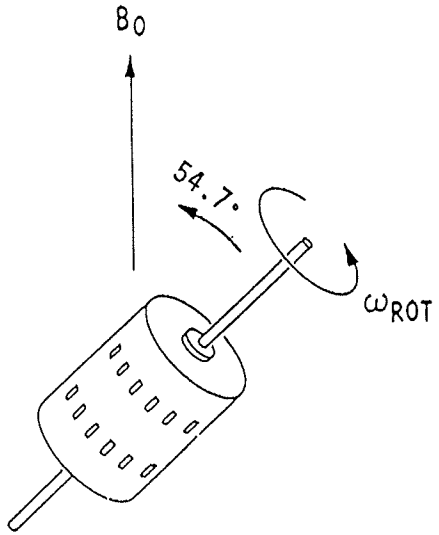

Fig. 2.9 Schematic representation of magic angle sample spinning in the MAS NMR experiment (From Bovey, 1988).

$$\eta = \frac{\sigma_{22} - \sigma_{11}}{\sigma_{33} - \sigma_{iso}}$$

2). Dipolar Interaction The spinning nuclei can be considered as small magnetic dipoles. When the internuclear distance is sufficiently small (the distance of two covalent bonded atoms), there will be interaction between the dipoles. The interaction can be visualized in a way that one spinning nucleus adds a small local magnetic field to the static applied magnetic field $\mathbf{B_0}$ which is experienced by its neighbour. Such interaction is of the form (Fukushima and Roeder, 1981):

$$(A/R_{ij}^3)(3\cos^2\Theta - 1)$$

in which A is a constant, R_{ij} the distance between nuclei i and j, Θ the angle between the internuclear vector $\mathbf{R_{ij}}$ and the magnetic field $\mathbf{B_0}$. When a powder sample is rotated rapidly, the averaged internuclear vector $\mathbf{R_{ij}}$ between any given pair of nuclei i and j will coincide with the rotation axis (Fukushima and Roeder, 1981). By placing the rotation axis at the magic angle $\Theta = 54.7°$, the term $3\cos^2\Theta - 1$ in the equation above vanishes, and so does the dipolar interaction. Therefore the MAS technique can also eliminate the dipolar interaction in solids.

3). Quadrupolar Interaction Nuclei with spin number $I > 1/2$, the quadrupolar nuclei such as ^{27}Al (I=5/2) and ^{23}Na (I=3/2), have spheroidal nuclear charge distributions and hence electric quadruple moments. Such nuclei interact with an electric field gradient (EFG) which exists in a site with non-spherical symmetry in a solid. Since both the nuclear charge distribution and the EFG are three dimensional, the quadrupolar interaction is orientation dependent.

There are 2I+1 energy levels for a spin I, eg. for I = 3/2, there are 4 energy levels (Fig. 2.10). In the absence of quadrupolar effects, i.e. when the EFG distribution is spherical, the four energy levels are equally spaced (Fig. 2.10A), and there is only one transition frequency ν_0, the Larmor frequency. When a small quadrupolar interaction is present, the energy levels will be shifted and three different transition frequencies are possible (fig. 2.10B). In many cases, the differences between the three transition frequencies are so great that NMR instrument can register only the central transition which is the least affected one by the quadrupolar interaction.

The quadrupolar interaction causes broadening of the central peak and shifts it from the isotropic chemical shift. Both the broadening and the shift are reduced when a stronger applied magnetic field is used. Rotating the sample at the magic angle also helps reduce the broadening but does not remove it.

2.5.3 Solid State NMR of the Zeolite and Clay Minerals

^{29}Si ^{29}Si NMR Chemical shift in silicates and aluminosilicates is affected by the number of SiOT bridges between the tetrahedra, and the number of Al atoms in the second coordination sphere of the Si. ^{29}Si chemical shift value becomes increasingly negative (Fig. 2.11) in the sequence of sorosilicates (Q^0) →chain silicates (Q^1) → nesosilicates (Q^2) → phyllosilicates (Q^3) → tectosilicates (Q^4), corresponding to increasing electronic shielding of ^{29}Si.

An empirical relationship was discovered between ^{29}Si chemical shift and the environments of Si atoms (Sherriff et al., 1991) which can be used to allocate peaks to

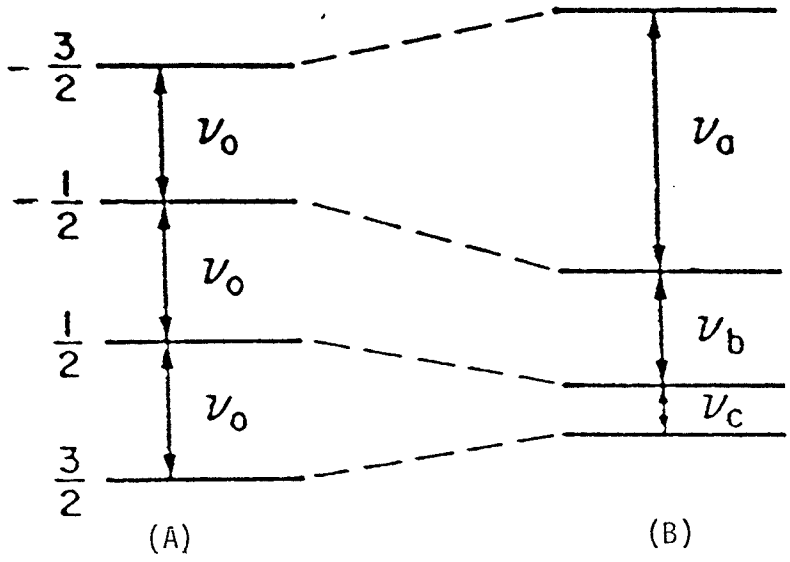

Fig. 2. 10. Energy level for a spin I=3/2 nucleus
(A) no electrical quadrupole interaction;
(B) small quadrupole interaction present.
From Fyfe, 1983

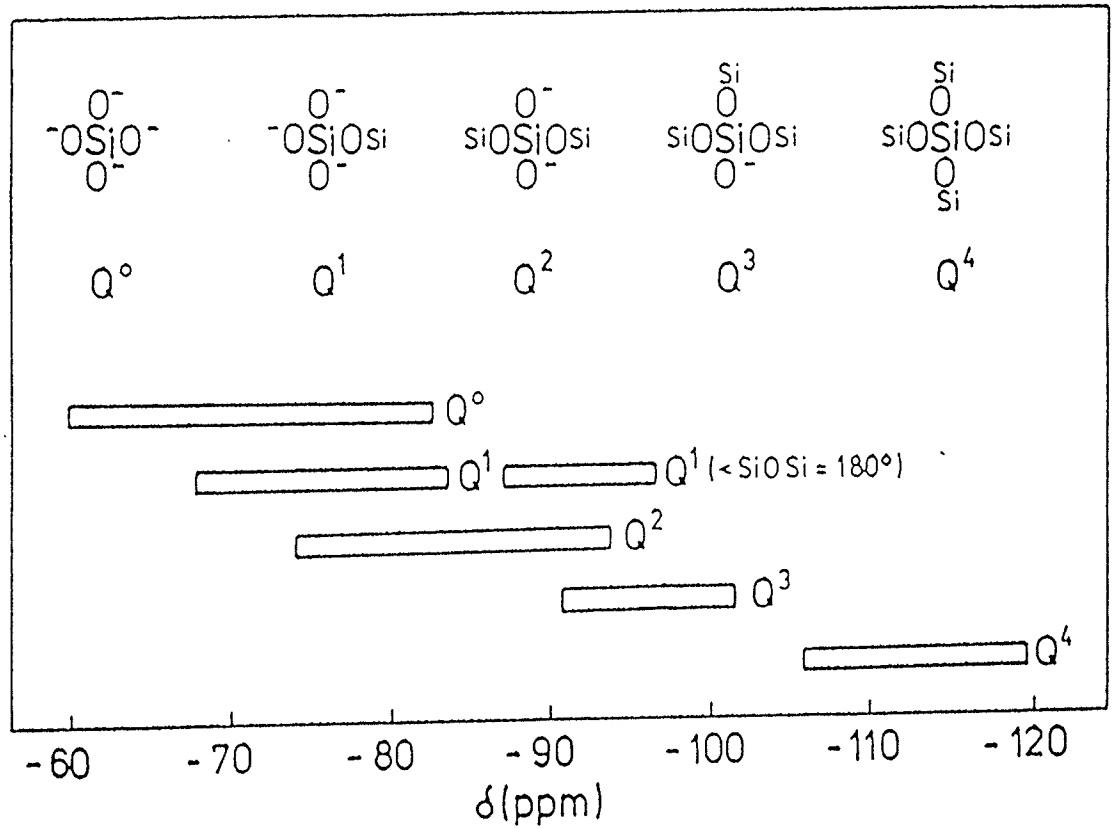

Fig. 2.11 Ranges of ^{29}Si chemical shift of Q^n units in solid silicates (from Mägi et al., 1984)

Si sites when there are multiple sites in a structure.

It is difficult to use X-ray diffraction to distinguish between Si and Al because of their similar scattering factors. NMR however is sensitive to whether the second nearest neighbour is Si or Al. Si surrounded by Si atoms is most highly shielded. With each substitution of Si by Al, there will be about 5 ppm shift in the direction of decreased shielding (Fig. 2.12).

^{29}Si chemical shift data of selected zeolite and clay minerals are listed in Table 2.5.

Table 2.5 ^{29}Si chemical shift of the selected zeolite and clay minerals

Mineral	Chemical shift (ppm)				Reference
	Si(3Al)	Si(2Al)	Si(1Al)	Si(0Al)	
Chabazite	94.0	99.4	104.8	110.0	Lippmaa, 1981
Vermiculite		84.6	88.7	92.9	Thompson, 1984
Montmoril-lonite				93.7	Komarneni et al., 1986
Kaolinite				91.5	Mägi et al., 1984

^{27}Al ^{27}Al MAS NMR can be used to determine the coordination number of Al (Fig. 2.13). ^{27}Al isotropic chemical shifts are between +50 and +80 ppm when tetrahedrally coordinated, between +30 and +40 ppm when 5-coordinated , and between -10 and +20 ppm when octahedrally coordinated.

Most of the ^{27}Al chemical shift data was reported uncorrected for the quadrupolar distortion. A list of such ^{27}Al MAS NMR apparent chemical shift (peak position) data is

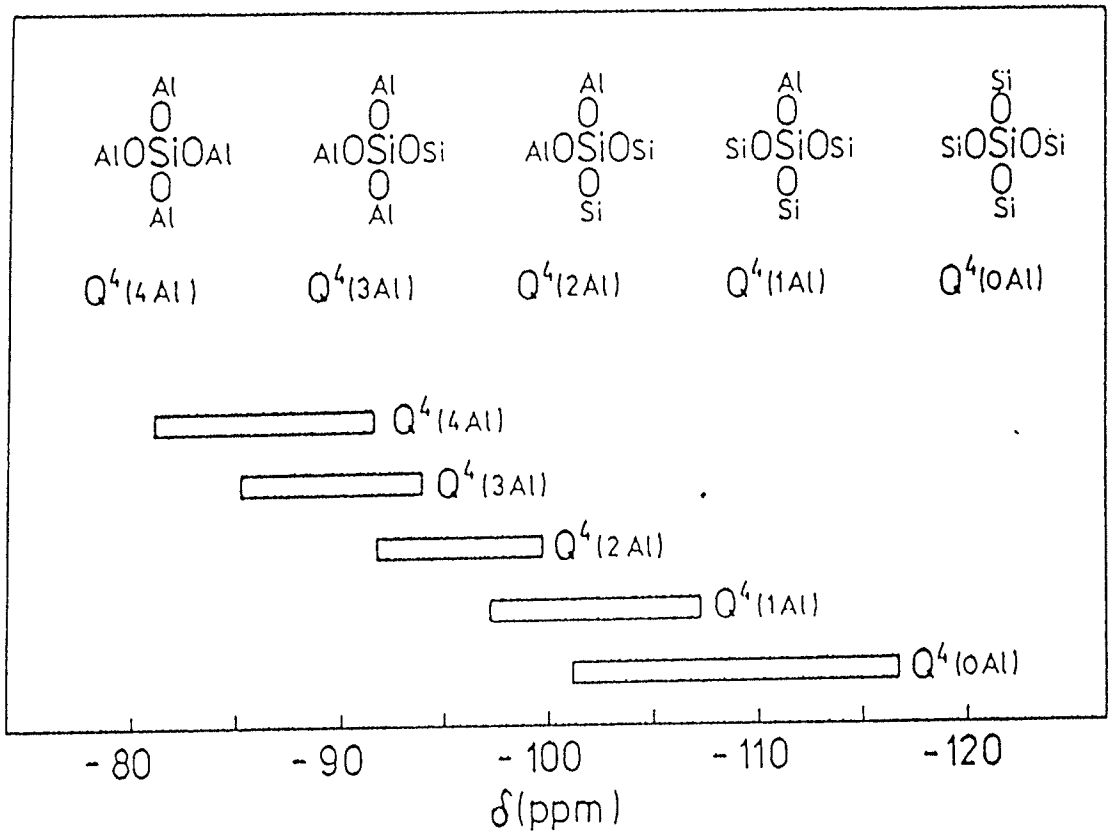

Fig. 2.12 Ranges of ^{29}Si chemical shift of $Q^4(mAl)$ units in aluminosilicates (from Engelhardt and Michel, 1987)

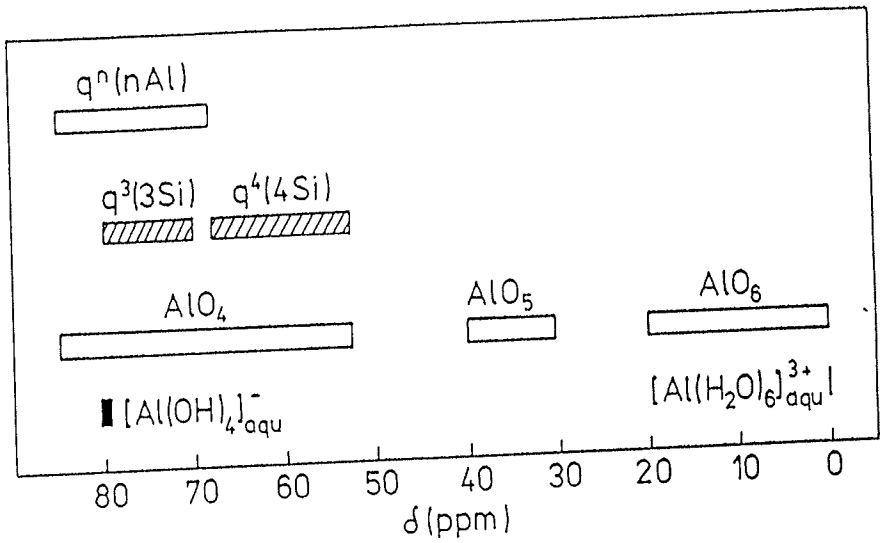

Fig. 2.13 Isotropic chemical shift ranges of selected aluminum compounds (from Engelhardt & Michel, 1987)
$q^n(nAl)$: aluminates
$q^3(3Al)$,$q^4(4Al)$: aluminosilicates
AlO_n: AlO_n polyhedra

shown in Table 2.6.

Table 2.6 ^{27}Al MAS NMR peak position at 11.74 T of the selected zeolite and clay minerals

Mineral	Peak position (ppm)		Reference
	Tetrahedral Al	Octahedral Al	
Chabazite	58.4	---	Lippmaa et al., 1986
Vermiculite	66.6	8.3	Woessner, 1989
Montmoril-lonite1	68.8	3.2	"
Montmoril-lonite2	----	3.2	"
Montmoril-lonite3	----	2.7	"

^{23}Na Na^+ is the exchangeable cation in the zeolite and clay minerals. The study of ^{23}Na MAS NMR can help understand the exchangeable cation distribution and observe directly the ion exchange process.

Under ambient condition of temperature and humidity, Laperche et al. (1990) observed a small quadrupolar coupling constant (C_Q) of about 0.46 MHz for the ^{23}Na in vermiculite. A C_Q of 0.46 MHz will cause only 0.3 ppm shift of the peak position from the isotropic chemical shift, within the experimental error (Lapperche et al., 1990). Therefore ^{23}Na MAS NMR peak position of vermiculite can be taken directly as the isotropic chemical shift. Another parameter, the quadrupolar asymmetry constant, was determined to be approaching 1. The corresponding line has a symmetrical shape.

^{207}Pb NMR Most of ^{207}Pb NMR studies have been on the organolead

compounds. ^{207}Pb chemical shift values cover a range of about 16,000 ppm (Fig. 2.14). Coordination number (c.n.) of lead is a major factor affecting the chemical shift of ^{207}Pb, as the electronic shielding of the lead nucleus increases with coordination. ^{207}Pb chemical shift is also influenced by the nature of the solvent (Harrison et al., 1983; Wrackmeyer, 1981; Lucchini and Wells, 1980), the type of the coordinating anions and the interbond angles (Nizam et al., 1989).

Some static ^{207}Pb NMR data of the powdered solid lead compounds (Piette and Weaver, 1958; Weinberg, 1962) used a variety of references. The isotropic chemical shifts, along with the corresponding principle values of the shielding tensor of ^{207}Pb, were reported by Nolle (1977) on lead nitrate, carbonate, chromate, molybdenate, and tungstate(Table 2.7). Recent work (Sherriff et al., in prep.) includes measured chemical shifts and relaxation times of an assortment of lead minerals. Most minerals have relaxation times between 4 and 16 s, with the exception of galena of 0.5 s. There are some discrepancies between the chemical shifts obtained by different workers for certain compounds (Table 2.7). This could be due to the enormous chemical shift anisotropy which makes the determination of isotropic chemical shift difficult, and the normally low signal to noise ratio characteristic of many static solid state NMR experiments.

Table 2.7 ^{207}Pb chemical shifts of the selected solid Pb(II) inorganic compounds

Compounds	δ ^{207}Pb(ppm)	Reference
$PbCl_2$	-1174	Piette & Weaver, 1958
$TlPbI_3$	+371	Sharma et al, 1987
$Pb(NO_3)_2$	-3480	Piette & Weaver,1958
$Pb(SO_4)$	-2500±880 -3575	Sherriff et al., (in prep.) Piette & Weaver, 1958
$PbCO_2$	-2719	Nolle, 1977
$PbCrO_4$	-2360	Nolle, 1977
$PbMoO_4$	-2449±40 -2078	Sherriff et al., (in prep.) Nolle, 1977
$PbWO_4$	-2071	Nolle, 1977
PbO(yellow)	+2750±40 +3770	Sherriff et al., (in prep.) Nolle, 1977
PbO(red)	+38	Nolle, 1977
PbS	+1680±40 +1076	Sherriff et al., (in prep.) Weinberg, 1962
$Pb_2Sb_2O_6(OH)$	+400±40	Sherriff et al., (in prep.)
$Pb_3Cl_2O_2$	+100±40(site 1) +100±40(site 2) +300±40(site 3)	Sherriff et al., (in prep.)
$Pb_2CO_3Cl_2$	-3550±60	Sherriff et al., (in prep.)
$Pb_5(PO_4)_3Cl$	-2800±780(site 1) -2000±760(site 2)	Sherriff et al., (in prep.)
$Pb_5(AsO_4)_3Cl$	-2330±1500(site 1) -1500±2100(site 2)	Sherriff et al., (in prep.)
Pb_3O_4	1000±5000(site 1) -500±3000(site 2)	Sherriff et al., (in prep.)

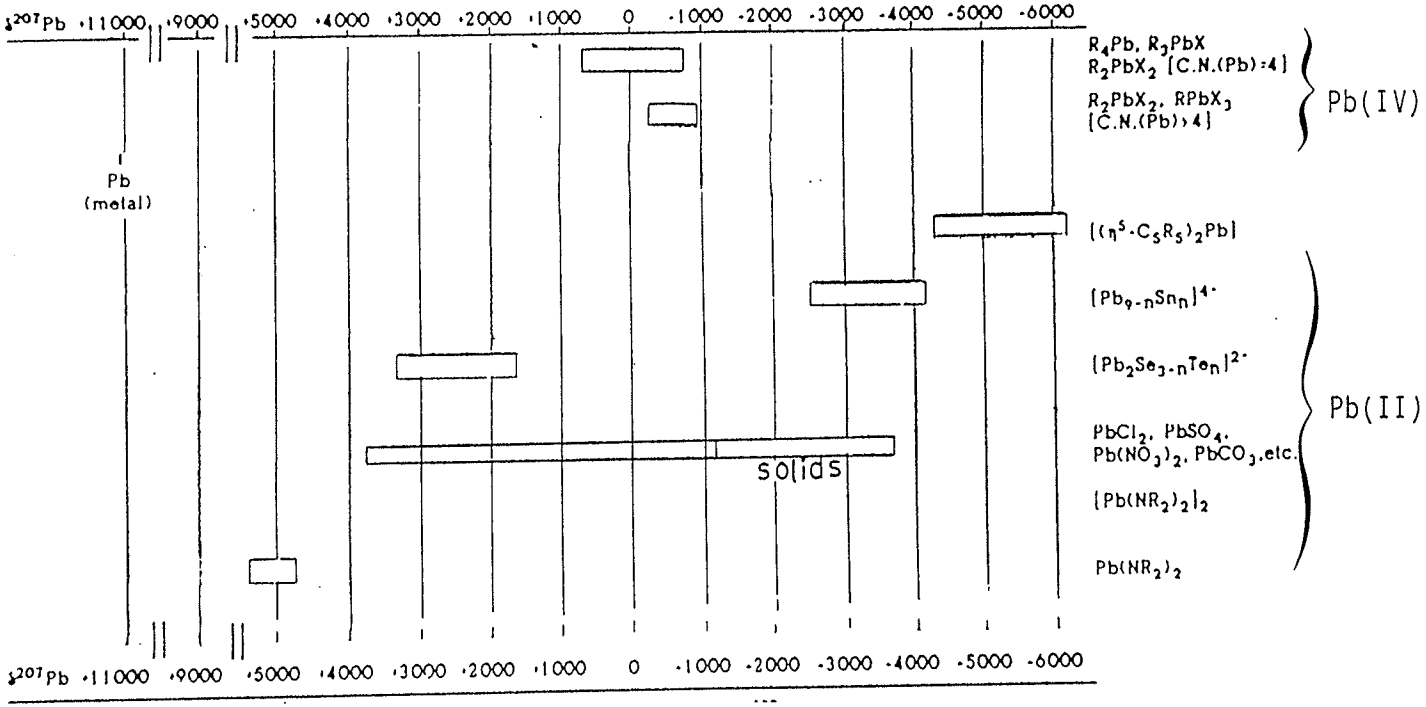

Fig. 2.14 Chart of ^{207}Pb chemical shift (from Wrackmeyer & Horchler, 1989)

CHAPTER 3. EXPERIMENTAL PROCEDURES

3.1. The Ion Exchange Experiment

In the ion exchange experiment, in addition of being involved in the ion exchange reactions, lead could also be adsorbed along with NO_3^- anions (Townsand, 1984). As such adsorption is small, it is included in the discussion of the ion exchange study.

The ion exchange experiments were done in a 0.01 M $Pb(NO_3)_2$ solution at room temperature. The pH of the $Pb(NO_3)_2$ solution, which was about 5, was not adjusted, to prevent the addition of competing cations (Breck, 1974), such as Na^+ and H^+, by the acid or base. The mineral:solution ratio was generally 0.25 g : 100 ml. After the mineral was added into the solution, the mixture was stirred until the mineral had thoroughly dis-aggregated. There was no further stirring until the solid phase was separated from the solution. The solid phase was then washed with distilled waster, and air dried. X-ray diffraction showed that there was no solid $Pb(NO_3)_2$ left in the lead exchanged minerals.

In the ion exchange experiment, adsorption by the glass surface (White and Yee, 1986) was minimized by saturating the walls of the glass containers (flasks, funnels, etc.) before use, by washing them with 0.01 M $Pb(NO_3)_2$ solution. The glassware was then rinsed with distilled water to remove the residual $Pb(NO_3)_2$ solution.

3.2 Materials

One zeolite, chabazite, and four clay minerals, vermiculite, hectorite, montmorillonite, and kaolinite, were used as an ion exchanger (Table 3.1). Chabazite was crushed, hand picked, and ground to less than 60 μm. Powder X-ray diffraction indicates a single chabazite phase, with a similar powder pattern to that of the chabazite sample, from Wasson's Bluff, Nova Scotia, on the Powder Diffraction Data card 34-137. The exchangeable cation of the unmodified sample is mostly Ca^{2+}.

As different cation forms of chabazite vary in lead uptake capacity, chabazite was also transformed into Na-form by the ion exchange of $2Na^{+} \rightarrow Ca^{2+}$. The chabazite powder was put in the 0.1 M NaCl solution at room temperature. More than 90% of Ca^{2+} could be replaced by Na^{+} by changing the NaCl solution once a day for about 30 days, with a solid:solution ratio of 10 g : 1000 ml. The same result was obtained by placing the ion exchange system into an autoclave operating at about 23 psi and 106°C for two days and with only 6 changes of the solution. Neither X-ray diffraction nor NMR spectroscopy show differences between the samples developed by these two methods. The CEC of chabazite is 349 meq/100 g (Barrer et al., 1969), ie. if chabazite is saturated with Pb(II), there will be $207.19(349 \times 10^{-3}/2) = 36.2$ g lead in 100 g such chabazite.

The four clay species were ordered from the Clay Mineral Society (CMS), USA. Vermiculite (CMS-VTx-1) is well crystallized and was hand picked. Because of the platy nature of the mineral, it can only be ground to less than 0.1 mm, using a pestle and mortar. X-ray powder diffraction revealed that the hand-picked sample to be pure

Table 3.1. The zeolite and clay minerals selected in the lead exchange experiment.

Minerals	Structural Formulae	Sample #	Localities
Chabazite	$(Ca,Na)_x(Si,Al)_6O_{12}nH_2O$		Nova Scotia
Vermiculite	$(Mg,Ca)_x[(Mg,Al)_3(Si,Al)_4O_{10}(OH)_2]nH_2O$	CMS-VTx-1	Texas
Montmorillonite	$(Ca,Na)_x[(Al,Mg)_2Si_4O_{10}(OH)_2]nH_2O$	CMS-STx-1	"
Hectorite	$(Na,K)_x[(Mg,Li)_3Si_4O_{10}(OH,F)_2]nH_2O$	CMS-SHCa-1	California
Kaolinite	$Al_2O_3SiO_2$	CMS-KGa-1	Georgia

vermiculite. The CEC of vermiculite is 230 meq/100g (Laperche et al., 1990), corresponding to a maximum lead content of 23.8%.

The hectorite sample is a composite powder, CMS-SHCa-1, which contains about 27% calcite and traces of quartz (van Olphen & Fripiat, 1979). A combined mechanical and chemical treatment was used to obtain pure hectorite. The powdered sample was firstly mixed with distilled water to form a thick slurry, and left to precipitate the larger, granular grains consisting mainly of calcite and quartz. Because the thickness of the slurry, the smaller and platy grains of hectorite, which are less than 10 μm, stay suspended regardless of how long the slurry was left. The suspended portion was then poured into another beaker carefully in order to separate the precipitate from the suspension which contained no quartz, but minor calcite.

A chemical treatment recommended by Moore and Reynolds (1989) was used to remove the remaining calcite. 82 g sodium acetate, and 27 ml glacial acetic acid, were added to 900 ml of the clay suspension. The system was stirred, and the slurry pH adjusted to 5 by the addition of sodium acetate or acetic acid. The volume of the slurry was then increased to 1000 ml by adding more distilled water, and placed in a hot water bath at approximately 90°C. It was stirred occasionally over a period of 24 hours to ensure that the calcite was dissolved. The solid phase of pure hectorite was then separated from the solution containing CH_3COO^-, Cl^-, Na^+, and Ca^{2+} by centrifuging, and was washed by distilled water. X-ray diffraction showed the resultant solid to be pure hectorite, with a powder pattern similar to that given by Brindley (1980). The CEC of hectorite is 56 meq/100g (Weiss et al., 1990), corresponding to a maximum lead

content of 5.8%.

Kaolinite sample, CMS-KGa-1, contains pure kaolinite. The powder sample gave an X-ray powder pattern identical to that of Brindley (1980) for the Georgia kaolinite. The CEC of kaolinite is 1.9 meq/100g (van Olphen and Fripiat, 1979), corresponding to a maximum lead content of 0.20%.

There is small amount of silica associated with montmorillonite sample, CMS-STx-1. The silica phase is present even in the $< 2.5\ \mu m$ separates of the powder sample. Single grain electron microprobe analysis revealed high SiO_2 content (see Chapter 4), suggesting that the silica phase may be physically incorporated into the montmorillonite grains, probably as surface coating or along the grain boundaries. This silica phase was identified as low cristobalite which gives a characteristic reflection at d=4.05 Å on the powder pattern. The CEC of montmorillonite is 80 meq/100g, corresponding to a maximum lead content of 8.3%.

3.3. Wet Chemical Analysis of the Lead Uptake

Gravimetric methods were used to determine the amount of lead taken up by the minerals during the ion exchange experiment, as quick and dynamic monitoring of the extent of lead uptake was required. In addition, gravimetric methods are economic and efficient, and can be easily done in a chemistry laboratory.

In the ion exchange experiment, the solution originally contains only one type of cation, Pb^{2+}, and one type of anion, NO_3^-. After certain period of time, the solution loses

some of its Pb^{2+}, and gains equivalent amount of Na^{+}, Ca^{2+}, or Mg^{2+} from the mineral. When sodium sulphate is added into the solution, Pb^{2+} will react with the SO_4^{2-} anions to precipitate $PbSO_4$. The Pb concentration of the solution can be calculated from the weight of the $PbSO_4$ precipitate.

Table 3.2. Lead nitrate adsorption of the filter disc during filtration of lead nitrate solution.

solution concentration (M)	filter disc weight (g)		$Pb(NO_3)_2$ adsorbed (g)
	before filtration	after filtration	
0.14	0.3547	0.3700	0.0153
0.12	0.3486	0.3622	0.0136
0.10	0.3580	0.3700	0.0120
0.08	0.3563	0.3654	0.0091
0.06	0.3595	0.3681	0.0086
0.04	0.3585	0.3665	0.0080
0.02	0.3632	0.3677	0.0045
0.01	0.3680	0.3683	0.0003
0.008	0.3541	0.3534	-0.0007
0.006	0.3545	0.3543	-0.0002
0.004	0.3720	0.3721	0.0001
0.002	0.3666	0.3674	0.0008

The amount of lead taken up by the ion exchanger is determined indirectly, with the assumption that lead removed from the solution is completely taken up by the mineral ion exchanger. However, lead can also be adsorbed by the filter paper during the separation of the lead exchanged minerals and the $Pb(NO_3)_2$ solution. To monitor such

adsorption, 100 ml of $Pb(NO_3)_2$ solution with concentrations from 0.14 M to 0.002 M (Table 3.2.) were passed through a weighed filter disc which were then dried in an oven at 90 - 100°. The weight increase was taken as the amount of the adsorbed $Pb(NO_3)_2$. When the $Pb(NO_3)_2$ concentration is not greater than 0.01 M (Table 3.2), the amount of the adsorbed $Pb(NO_3)_2$ by the filter disc is within the error range of the weighing procedure. The negative figures in the amount of $Pb(NO_3)_2$ adsorbed from the 0.008 and 0.006 M solution indicate that the precision of the weighing procedure is 0.001 g.

Table 3.3. Calibration of the gravimetric method using duplicate experiments

Set	Pb^{2+} Concentration (M)		
	Standard	Measured	Difference
set 1			
	0.01000	0.00992	-0.00008
	0.00796	0.00788	-0.00008
	0.00584	0.00574	-0.00010
	0.00385	0.00379	-0.00006
	0.00212	0.00211	-0.00001
	0.000878	0.00082	-0.00006
set 2			
	0.01000	0.00989	-0.00011
	0.00794	0.00788	-0.00006
	0.00585	0.00577	-0.00008
	0.00386	0.00376	-0.00010
	0.00213	0.00204	-0.00009
	0.000884	0.00082	-0.00006

The filter disc adsorption from solutions with greater than 0.01 M $Pb(NO_3)_2$ is, however, significant and increases with concentration. A linear relationship ($R^2 = 0.96$) was derived between the original solution lead concentration $Pb_{solution}$(M) and the filter disc adsorption of lead nitrate (Fig. 3.1). Expressing the adsorption as the concentration decrease Pb_{loss} (M) of the solution, there is a relationship of:

$$Pb_{loss} = 2.533 \times 10^{-2}\ Pb_{solution}(M) + 0.0001.$$

The gravimetric method was calibrated with duplicate sets of samples of varying concentration from 0.01 M to 0.00878 M (Table 3.3). Duplicate measurements were reproducible. A systematic error occurred, causing all measurements to be an average of 0.00007 M lower than the true concentration. The overall random error spans a range of 0.00010 M, with a standard deviation of 0.00003 M.

3.4. Electron Microprobe Analysis

The analyses were done on a CAMECA CAMEBAX SX-50 electron microprobe. The standards used in the quantitative analysis were albite (SiKα, NaKα), anorthite (CaKα, AlKα), PbTe (PbKα), olivine (MgKα), orthoclase (KKα), fayalite (FeKα), spessartine (MnKα), and strontianite (SrKα). Data reduction was done using the 'PAP' Φ (ρz) routine of Pouchou & Pichoir (1985).

Because the zeolite and clay minerals are very soft, care was needed to obtain well polished surfaces of the grain mount. The grain mounts were prepared by drilling 10 shallow holes in plastic glass discs of 2.5 cm in diameter, filling the holes with epoxy

Fig.3.1 Filter Disc Adsoption of Lead

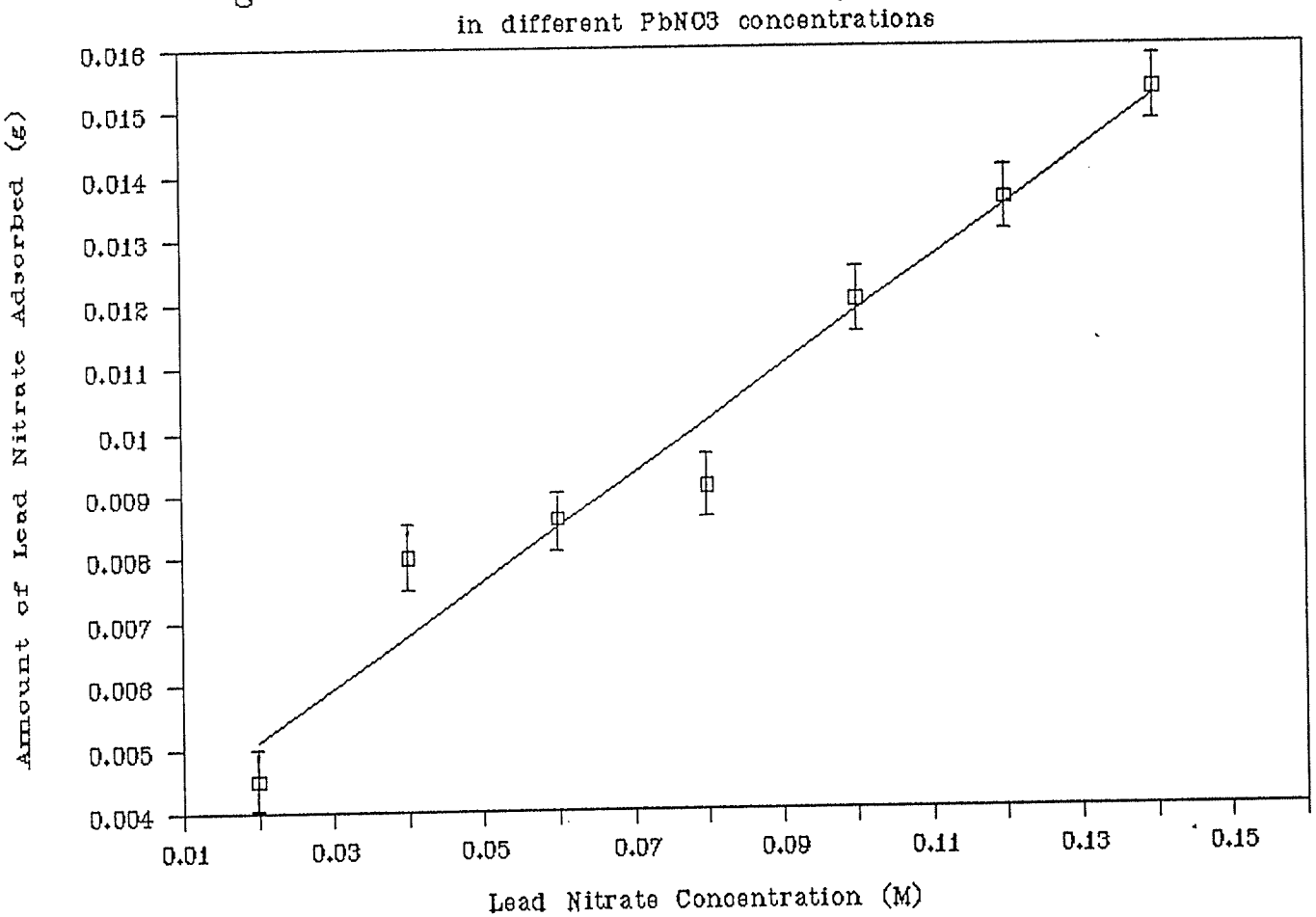

resin mixed with the powder sample, and immediate curing without allowing the grains to settle. Many grains on the polished surface, especially in the montmorillonite and hectorite samples, were either too small (less than 5 μm) or with rough surfaces. To obtain a sufficient number of suitable grains, usually not less than 2, the same mounts were often repolished and reanalysed.

A qualitative energy dispersion scan was made to estimate the elements existing in significant amount in the mineral. As short element list as possible for a given sample was determined before the quantitative continual wave dispersion analysis. This is necessary not only to save the instrumental time, but also to reduce the evaporation and dispersion of the volatile and mobile ions, such as OH^-, F^-, and Na^+, by prolonged exposure to the high energy beam and extreme vacuum. Back scattered electron images were also acquired to estimate the degree of uniform distribution of the elements in the sample.

3.5. Other chemical analyses

The zeolite and clay minerals before lead exchange were sent for analysis at the X-Ray Assay Laboratories (XRAL), a Division of SGS Supervision Services INC., Don Mills, Ontario. The normal abundance elements (Si, Al, Ca, Na, K, Fe, Mn, Mg, P) analyses were done with X-ray fluorescence (XRF), Li by atomic absorption, and F by wet chemical analysis. The detection limit for these analyses were 0.01%, 1 ppm, and 0.01% respectively.

3.6. Water Content Measurement

The water content of the zeolite and clay minerals were measured with the Mitsubishi moisturemeter Model CA-06. The water is driven out of the sample by heating in a furnace and reacts with iodine:

$$I_2 + SO_2 + H_2O \rightarrow 2HI + SO_3$$

One mole of iodine reacts with one mole of water. The iodine required in the titration is generated electrolytically. By measuring the electricity consumed in the electrolysis, the amount of iodine generated, and therefore the water released by the sample can be calculated.

The precision of the moisturemeter is dependent on the amount of water given off by the sample. For samples which can generate no less than 1 mg water, the moisturemeter has a precision of $\pm 0.3\%$. Each sample measured here yielded 3 $\sim$ 6 mg water from about 30 mg of sample. Therefore, the precision of the water measurement is better than $\pm 0.3\%$. The furnace temperature was set at 900°C so that water, including hydroxyls, could be driven out in less than 25 minutes of heating.

3.7. Powder X-ray Diffraction Analysis

Powder X-ray diffraction was used for the sample identification. A Phillips Automated Powder Diffractometer System PW1710 using CuKα radiation (λ = 1.54178 Å) with generator settings of 40 KV and 40 mA, and fast scan within the 2Θ range of

3 to 63°, was used.

Smear mounts were used in the preparation of the zeolite samples. For the clay minerals, a basal plane oriented smear sample was prepared by pipetting the suspended fraction of the clay minerals in water onto a glass slide. The sample was dried at room temperature and humidity. Portions of different grain sizes in the suspension can be obtained by changing the settling times. If no settling time was allowed, all sizes were present, whereas for the < 2.5 μm portion, 3 to 4 hours was required to allow the larger grains to settle. When randomly oriented sample were needed, the powder sample was loaded into an aluminum sample holder with a glass insert to support the powder. The sample surface was chopped gently with a blade to randomize the crystallite orientation.

Chabazite and the non-clay impurities were identified using a computer automated powder diffraction pattern search-match package. However, most clay minerals can not be identified by this automated approach. Clay minerals differ from each other by characteristic basal spacings. For a given clay species, the basal spacing varies according to different cation forms and adsorbed molecules; e.g. the basal spacing of Mg,Ca-vermiculite is 14.5 Å, while that of the Na-vermiculite is 12.5 Å; and for the Na-vermiculite, when the adsorbed molecules is water, the spacing is 12.5 Å, but when the molecule is ethylene glycol, it becomes 14.5 Å (Brown and Brindley, 1980). The matter gets more complicated when the sample prepared has different degrees of preferred orientation. Therefore, for most clay mineral identifications the diffractograms were compared visually with the published powder patterns of clay minerals, following the schemes proposed by Moore and Reynolds (1990).

3.8. Nuclear Magnetic Resonance Spectroscopy

The spectra were collected using a Bruker AMX-500 console with two magnets of 11.7 T and 8.4 T at the Prairie Regional Nuclear Magnetic Resonance Facility, Winnipeg, Manitoba. A Doty high speed MAS probe, equiped with a variable temperature unit, was used. The sample spinning speed can reach 14 KHz, but the routine operation speed is 8 to 10 KHz. A maximum sweep width of 125,000 Hz was used initially, but once the required frequency range was found, the sweep width was narrowed to improve the signal to noise ratio and to enhance resolution. The acquired data was processed with the online package UXNMR, Version 9.1, using digital filtering of exponential multiplication prior to Fourier Transform. ^{29}Si, ^{27}Al, ^{23}Na, and ^{7}Li were all run using the 11.7 T magnet and ^{207}Pb using the 8.4 T magnet. A single pulse program was used for data acquisition.

For ^{29}Si, 30° pulse, corresponding to a pulse length of 2.5 to 3 μs, was applied. The probe ring down time, i.e. the time required between the end of the excitation pulse, and the acquisition of signals from the probe, was 42.5 μs. Data acquisition lasts about 0.28 s. The delay between pulses varies from 1 to 5 s, depending on the effectiveness of the relaxation mechanism in the sample. The number of scans was 400. All ^{29}Si spectra were referenced to tetramethylsilane.

^{27}Al, ^{23}Na, and ^{7}Li are all quadrupolar nuclei. To ensure no intensity distortion occur (Samoson and Lippmaa, 1983), $\pi/12$ pulse of 0.4 μs, 0.4 μs, and 0.5 μs with probe ring down times of 8.8μs, 8.8 μs, and 8.25 μs, were used for ^{27}Al, ^{23}Na, and ^{7}Li

respectively. The delay between pulses was 0.1 s. 1000 to 6000 scans were recorded depending on the concentration of the nuclei in the sample. ^{27}Al and ^{23}Na were referenced to 1 M $AlCl_3$ and 1 M NaCl solutions respectively, while ^{7}Li spectra to LiBr.

For ^{207}Pb, 30° pulse, of the length of 1.5 μs, together with the probe ring down of 5 μs and a delay between pulses of 1 s, was used. The spectra were referenced to tetramethyllead.

The double angle rotation experiment was done using a Bruker DOR probe. The spinning speed of the inner rotor reaches 5 KHz, and the outer rotor 1 KHz. The applied magnetic field strength was 8.4 T. The pulse length was 1 μs, and the delay between pulses was 0.2 s.

CHAPTER 4 RESULTS AND DISCUSSION

4.1. Characterization of the ion exchangers

The chemical analyses of the zeolite and clay minerals, as well as the calculated unit formulae, are listed in Table 4.1, 4.2, and 4.3. Chabazite unit formulae were calculated to 12 oxygens, kaolinite to 7 oxygens, and the other clay minerals to 11 oxygens. The low total of 95.3% of hectorite was corrected by taking into account additional F and Li. F takes the place of the equal equivalents of oxygen. SiO_2 content of montmorillonite is high because the cristobalite phase is physically attached to the montmorillonite grains even down to the size of < 0.25 μm. Unit formulae for montmorillonite sample were therefore not calculated.

4.2. Lead Exchange into Zeolite and Clay Minerals

Pb content of Na-chabazite was up to 27% when equilibrated with the 0.01 M $Pb(NO_3)_2$ solution, whereas that of unmodified Ca(Na)-chabazite was only about 7% (Table 4.4). There is a rapid lead content increase in Na-chabazite during the first 15

Table 4.1 Chemical analyses from XRAL of the ion exchangers

	1	2	3	4	5	6
Weight percent						
SiO_2	52.6	53.0	35.3	61.6	55.3	44.6
Al_2O_3	16.8	17.1	14.3	13.7	0.53	39.4
CaO	7.74	0.78	0.19	1.43	0.45	<0.01
MgO	0.16	0.04	27.8	3.09	24.6	0.07
Na_2O	0.62	9.27	0.09	0.42	2.11	0.06
K_2O	0.86	<0.01	<0.01	0.03	0.14	<0.01
Fe_2O_3	0.04	<0.01	0.08	0.61	0.10	0.07
MnO	0.02	<0.03	0.03	0.03	0.02	0.02
TiO_2	<0.001	<0.001	0.248	0.183	<0.001	1.61
P_2O_5	<0.02	0.02	0.02	0.04	0.03	0.07
H_2O	20.5	19.7	21.8	19.1	12	14.5
Sum	100.1	100.3	100.0	100.3	95.3	100.5
Li					0.48	
F					4.53	
Total	100.1	100.3	100.0	100.3	97.9	100.5
Unit formulae						
Si	4.36	4.35	2.28		3.98	1.96
Al(IV)	1.64	1.65	1.18		0.02	
Al(VI)			0.16		0.02	2.04
Ca	0.69	0.07	0.02		0.03	
Mg(VI)			2.84		2.64	
Mg(ex)*	0.02		0.47			
Na	0.10	1.48	0.01		0.29	
K	0.09				0.01	
Fe						
Li					0.30	
F					1.02	
OH			2.00		0.98	2.00

*: Mg^{2+} as exchangeable cations
1: Ca(Na)-chabazite
2: Na-chabazite
3: Vermiculite
4: Montmorillonite
5: Hectorite
6: Kaolinite

hours of ion exchange (Fig. 4.1), with equilibrium reached in about 20 hours.

There is very little difference in lead uptake capacity between 16% of Mg-vermiculite, which is the natural form, and 17% of Na-vermiculite. There is an initial rapid lead uptake during the first 5 hours of ion exchange (Fig. 4.1), with a gradual

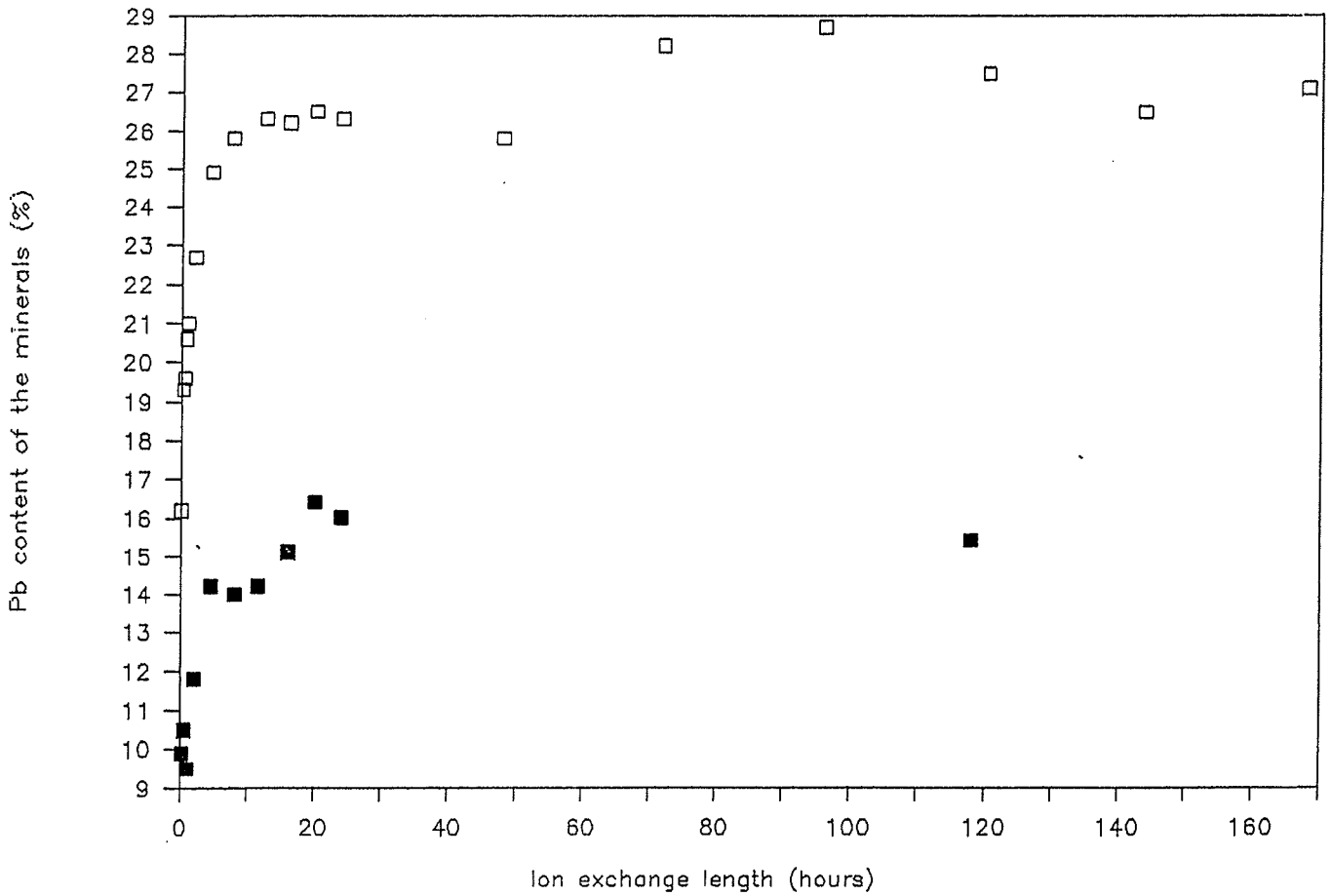

Fig. 4.1 Lead uptake rate of chabazite and vermiculite in 0.01 M $Pb(NO_3)_2$ solution
■ : Vermiculite
□: Na-chabazite

Table 4.2 Electron microprobe analyses of the ion exchangers (with H_2O measured by the Mitrubishi moisturmeter)

	1	2	3	4
Weight percent				
SiO_2	52.1	39.6	59.5	46.1
Al_2O_3	17.6	14.5	15.9	39.4
CaO	8.01	0.12	1.47	0.00
MgO	0.00	28.2	3.68	0.00
Na_2O	0.17	0.01	0.09	0.00
K_2O	1.50	0.05	0.12	0.04
Fe_2O_3	0.03	0.21	0.68	0.16
MnO	0.02	0.00	0.00	0.01
PbO	0.47	0.01	0.01	0.05
SrO	0.54	0.00	0.06	0.03
H_2O	21.0	20.8	15.4	14.0
Total	101.4	103.5	96.9	99.6
Unit formula				
Si	4.3	2.96		1.99
Al(IV)	1.71	1.04		2.00
Al(VI)		0.24		
Ca	0.71	0.01		
Mg(VI)		2.76		
Mg(ex)		0.38		
Na	0.03			
K	0.16			
Fe		0.01		
Pb	0.01	0.01		
Sr	0.03			
OH		2.00		

Mg(ex): Exchangeable Mg^{2+} cations
1: Ca(Na)-chabazite
2: Vermiculite
3: Montmorillonite
4: Kaolinite

increase in lead content until equilibrium being reached by about 20 hours.

The amount of lead taken up by hectorite and montmorillonite within a few minutes of ion exchange did not increase significantly over periods up to 120 hours (Fig. 4.2, Table 4.4).

The maximum lead content of kaolinite was only 0.4%.

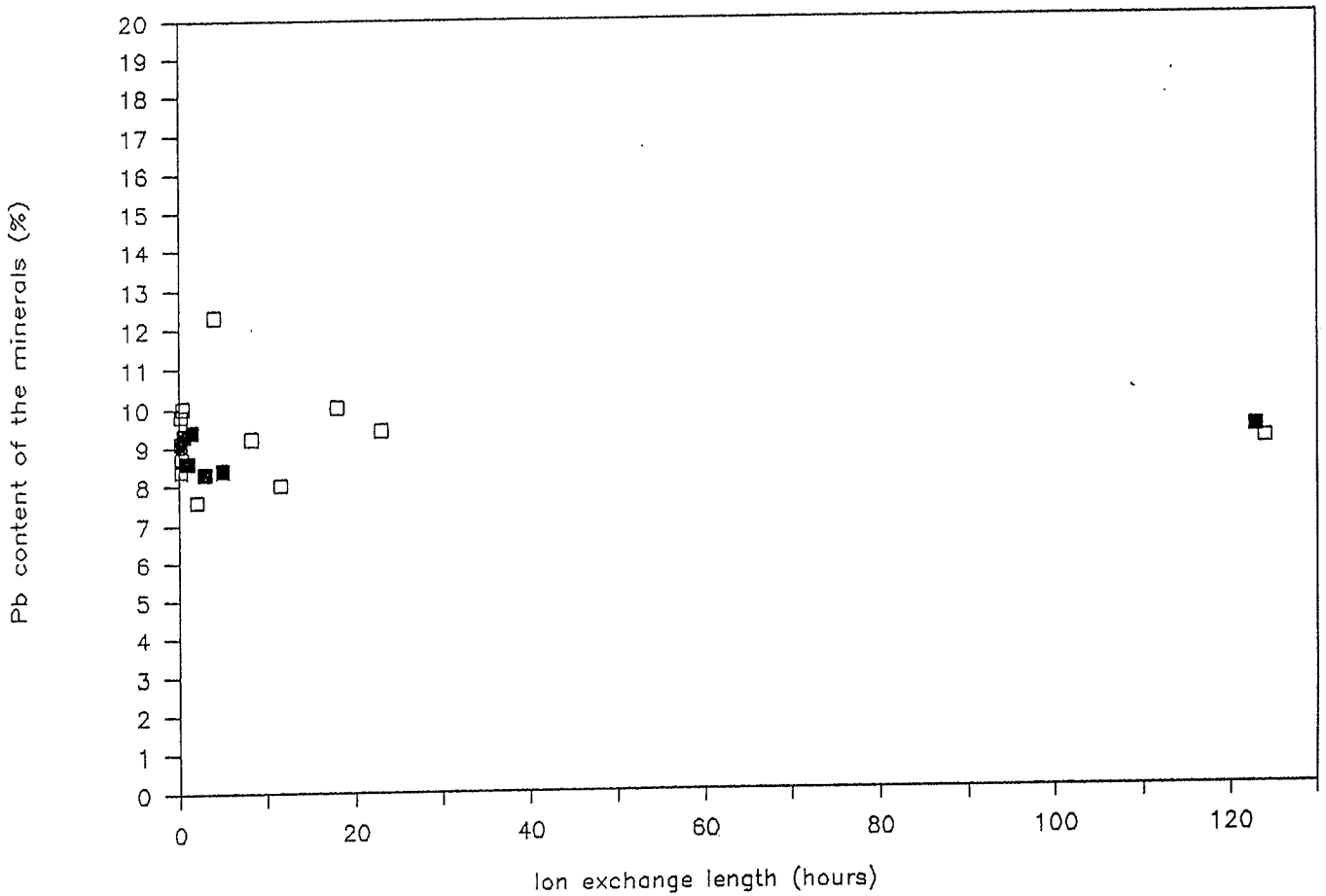

Fig.4.2. Lead uptake rate of hectorite and montmorillonite in 0.01 M $Pb(NO_3)_2$ solution
□: Hectorite
■ :Montmorillonite

Table 4.3 Electron microprobe analyses of the zeolite and clay minerals after lead exchange (with H_2O measured by the moisturemeter, Li by AAS, and F by wet chemical analysis)

	1	2	3	4	5	6
Weight percent						
SiO_2	52.0	39.5	32.4	63.1	49.5	46.2
Al_2O_3	17.8	14.9	13.3	10.7	0.16	39.7
CaO	6.96	0.02	<0.01	0.12	0.04	<0.01
MgO	0.11	<.01	23.1	2.03	22.2	<0.01
Na_2O	0.23	0.66	<0.01	0.01	0.002	0.02
K_2O	1.66	<.01	0.08	0.07	0.038	0.01
Fe_2O_3	<.01	<.01	0.20	0.24	0.069	0.08
MnO	<.01	<.01	0.04	0.01	0.014	<0.01
PbO	5.55	29.7	17.3	7.81	7.27	0.12
SrO	0.55	0.00	<0.01	0.01	0.008	<0.01
H_2O	19.2	15.7	14.3	12.2	11.7	14.2
Sum	103.5	100.7	100.7	96.3	91.0	100.5
Li					0.43	
F					4.06	
Total	103.5	100.7	100.7	96.3	94.3	100.5
Unit formulae						
Si	4.28	4.15	2.79		3.99	1.99
Al(IV)	1.72	1.84	1.21		0.01	
Al(VI)			0.14		0.005	2.00
Ca	0.61	0.02				
Mg(VI)			2.86		2.67	
Mg(ex)*	0.01		0.12			
Na	0.03	0.13				
K	0.17		0.01			
Fe			0.01			
Pb	0.12	0.84	0.40		0.16	
Sr	0.14					
Li					0.30	
F					1.15	
OH			2.00		0.85	2.00

*: Mg^{2+} as exchangeable cations
1: Ca(Na)-chabazite
2: Na-chabazite
3: Vermiculite
4: Montmorillonite
5: Hectorite
6: Kaolinite

Table 4.4. Lead uptake rate of the zeolite and clay minerals in 0.01 M $Pb(NO_3)_2$ solution

	Length of ion exchange (hours) / Pb content (Pb%) of the minerals
Na-chabazite	0.08/16.2, 0.25/19.3, 0.5/19.6, 0.75/20.6 1/21.0, 2/22.7, 4.5/24.9, 7.5/25.8, 12.5/26.3, 16/26.2, 20/26.5, 24/26.3, 48/25.8, 72/28.2, 96/28.7, 120/27.5, 144/26.5, 168/27.1
Ca(Na)-chabazite	28/3.7, 48/3.4, 69/4.2, 93/4.6, 118/6.9, 281/5.3
Mg-vermiculite	0.12/9.9, 0.2/9.9, 0.9/10.5, 1/9.5, 2/11.8, 4.5/14.2, 8/14.0, 11.5/14.2 16/15.1, 20/16.4, 24/16.0, 118/15.4
Na-vermiculite	5.5/17.1
Ca(Na)-montmorillonite	0.08/9.1, 0.25/8.7, 0.5/9.3, 1.5/9.4, 3/8.3, 123/9.3
Na-montmorillonite	5/8.4
Na-hectorite	0.08/9.8, 0.12/8.4, 0.35/10.0, 1/8.6, 2/7.6, 4/12.3, 8/9.2, 11.5/8.0, 18/9.9, 23/9.4, 124/9.2
Na(Ca)-hectorite	100/9.0
Ca-kaolinite	116/0.4
Na-kaolinite	5.5/0.3

4.3. Reaction of Calcite with Lead Nitrate Solution

The hectorite sample, CMS-SHCa-1, contained calcite, with grain size ranging from 0.1 mm to $< 10\ \mu m$. The calcite reacted with Pb^{2+} in the solution to form cerussite ($PbCO_3$). A further experiment with pure calcite of grain size between 60 and 10 μm, at the mole ratio of Pb^{2+}:$CaCO_3$ of 1:4, showed that all Pb^{2+} in 100 ml 0.01 M lead nitrate solution reacts with the calcite in less than 30 minutes at room temperature. There was no measurable grain size changes, and hence, no increase in the volume of the solid phase, after the formation of cerussite.

One of the most common methods for the removal of lead from waste water is based on precipitation of $Pb(OH)_2$ (Patterson, 1975; Maruyama et al., 1975; Nilsson, 1971). This generates large volume of sludge because of the very fine grain size and the hydrated nature of the precipitates. Another commonly used treatment is the precipitation of PbS which requires the removal of the excess S^{2-} from the treated solution (Mazzocco, 1977).

In aqueous carbonate solution, lead can also form hydrocerussite [$Pb_3(OH)_2(CO_3)_2$], plumbonacrite [$Pb_{10}O(OH)_6(CO_3)_6$], and litharge (PbO). Figure 4.3 shows the solid/solution equilibrium surface in the lead carbonate system at 25 °C (Taylor and Lopata, 1983). Total lead activity (the effective concentration), pPb_t, and total carbonate activity, pC_t, are plotted as the negative logarithms of the actual activities. In the carbonate activity range of $pC_t = 0$ to 3, corresponding to the actual total activity of 1 to 0.001 M, the most favourable solution pH range for precipitating lead as cerussite

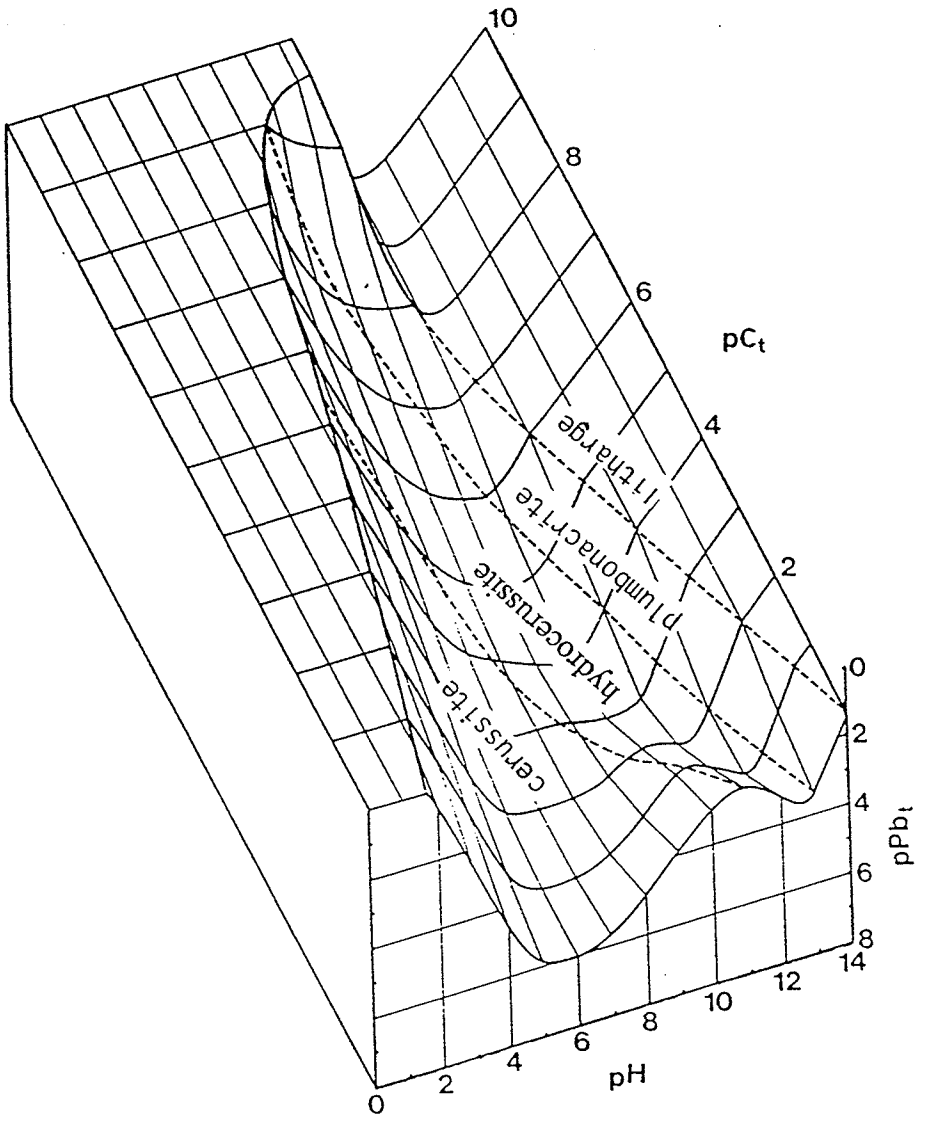

Fig. 4.3 Solid/solution equilibrium surface in the lead carbonate system at 25°C (From Taylor and Lopata, 1983).

is from 5 to 7. The cerussite phase predominates in the acidic solution even at a total carbonate activity down to $pC_t = 6$, or 0.000001 M. The total lead activity will be as low as $pPb_t = 6$, or 0.000001 M, if the total carbonate activity is 1 M and the solution acidity is about pH6.

4.4. Solid State NMR Study

4.4.1. ^{29}Si

The four peaks at -92, -98, -103, and -109 ppm in the ^{29}Si MAS NMR spectrum of natural chabazite (Table 4.5, Fig. 4.4) correspond to Si(3Al), Si(2Al), Si(1Al), and Si(0Al) of Si in the tetrahedral site. The full width at half maximum (FWHM) of the peaks range from 230 to 320 Hz (Table 4.5). There are the same number of the peaks for Na-chabazite and the peak positions do not differ significantly from those for the natural chabazite. However the FWHM of all peaks are smaller for Na-chabazite, especially at Si(0Al). After lead exchange, all four peak positions for both Ca(Na)-chabazite and Na-chabazite shifted 1 to 2 ppm to more negative values (Table 4.5, Fig. 4.5).

There are three overlapping peaks in the spectrum of vermiculite at -84.4, -88.8, and -92.4 ppm (Fig. 4.4, Table 4.5), corresponding to Si(2Al), Si(1Al), and Si(0Al). After lead exchange, all three peaks shifted 1 ppm to more negative values (Table 4.5, Fig. 4.6).

Montmorillonite, hectorite, and kaolinite give only one peak each at -93.5, -95.3,

Table 4.5. ^{29}Si MAS NMR data of the zeolite and clay minerals (11.74 T magnetic field)

	δ ^{29}Si (ppm) / FWHM (Hz)			
	Si(3Al)	Si(2AL)	Si(1AL)	Si(0Al)
Before Pb exchange				
Ca(Na)-chabazite	-92.4/350	-98.2/320	-103.6/300	-109.0/230
Na-chabazite	-93.0/210	-98.8/300	-104.3/240	-109.6/160
Vermiculite		-84.4	-88.8	-92.4
Montmorillonite				-93.5/400
Hectorite				-95.3/340
Kaolinite				-91.3/250
After Pb exchange				
Ca(Na)-chabazite	-95.0/220	-100.3/260	-105.8/280	-111.0/260
Na-chabazite	-94.4/250	-100.0/240	-105.4/240	-111.0/160
Vermiculite		-85.2	-89.0	-93.2
Montmorillonite				-93.7/390
Hectorite				-95.4/310
Kaolinite				-91.3/250

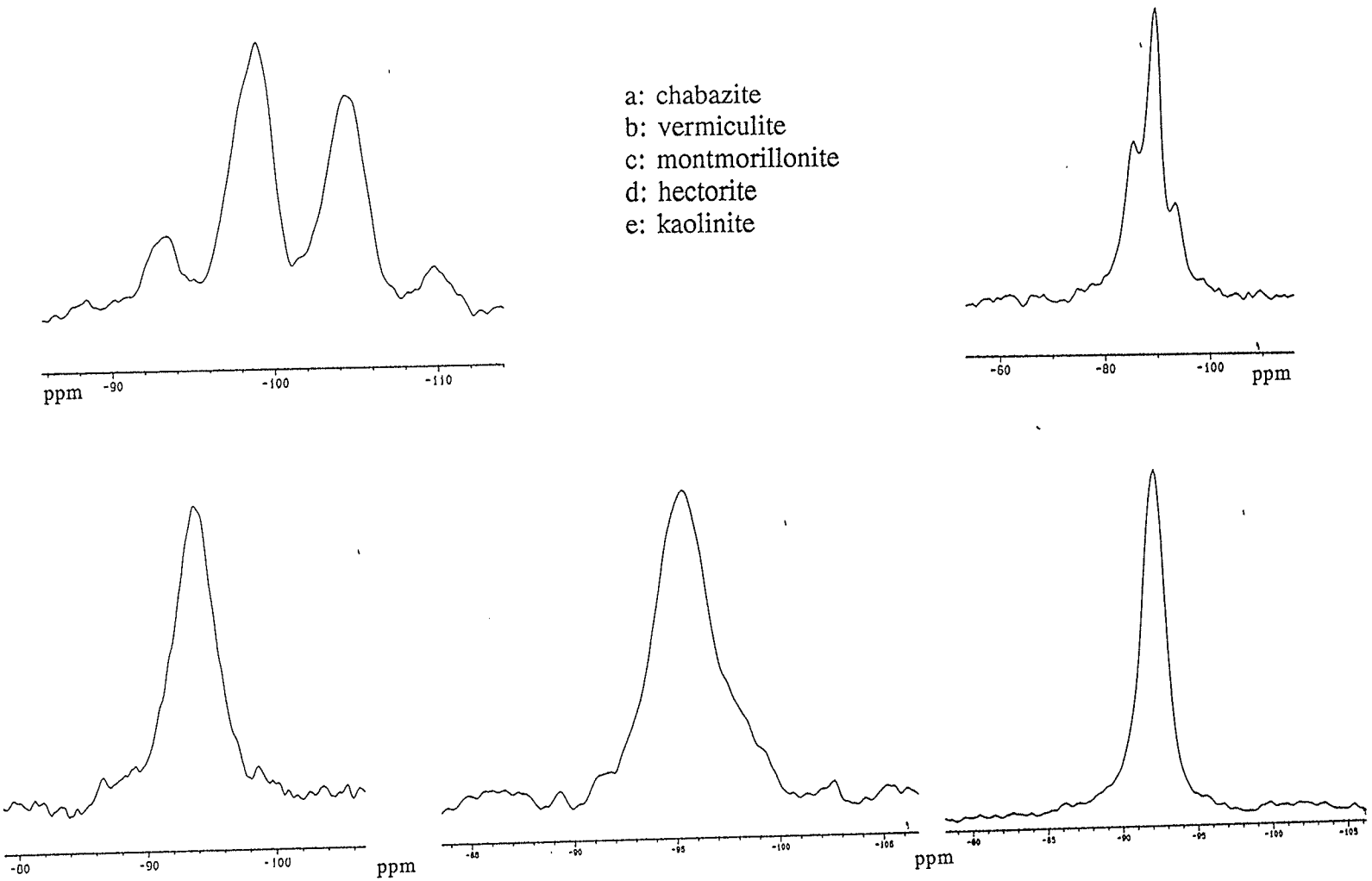

Fig. 4.4 ^{29}Si MAS NMR of the zeolite and clay minerals before lead exchange.

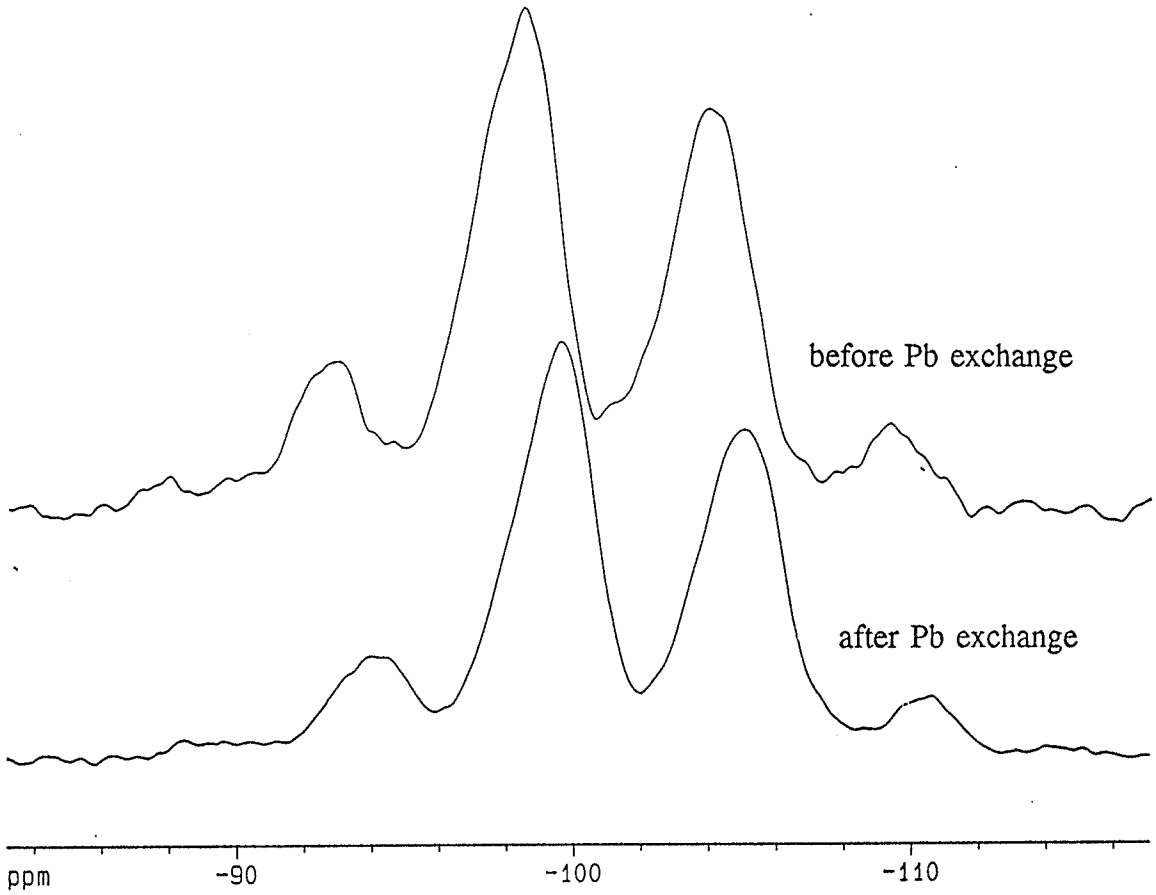

Fig. 4.5 ^{29}Si MAS NMR of Na-chabazite before and after lead exchange

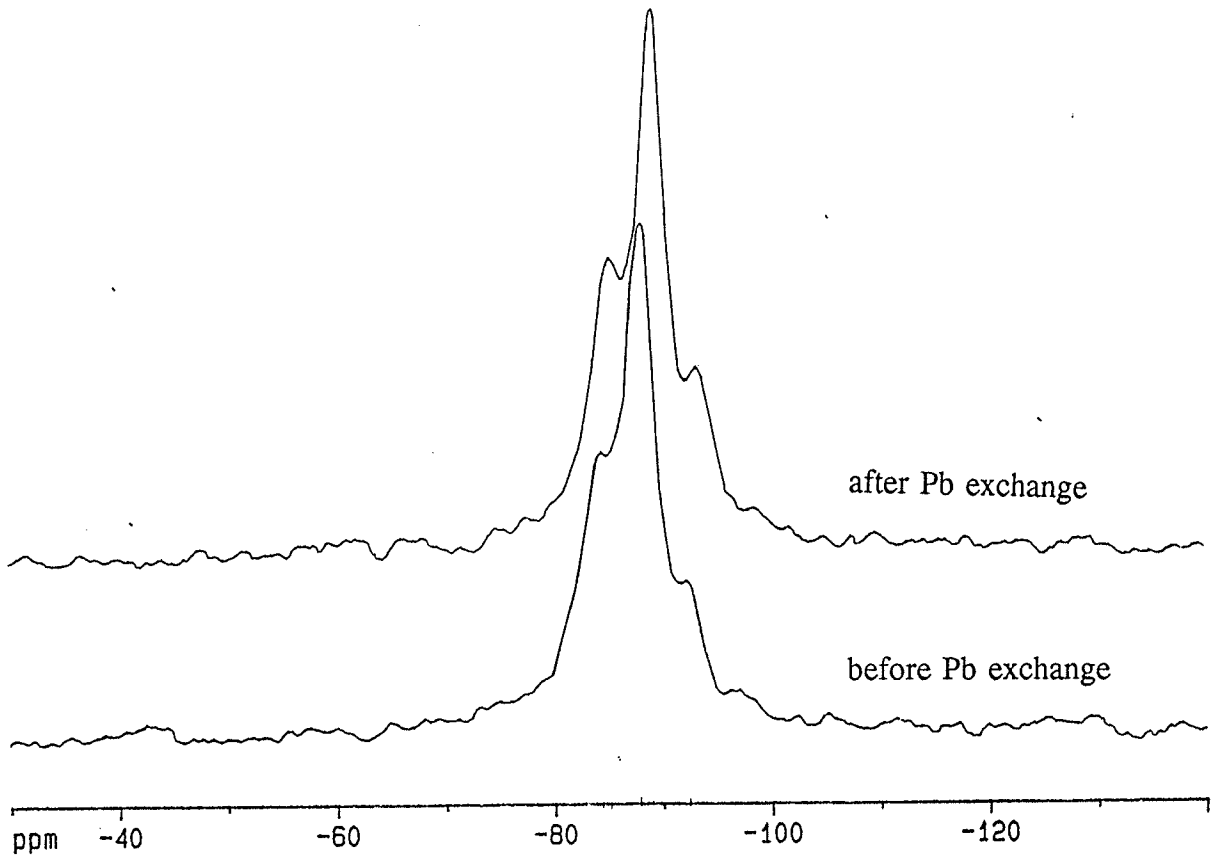

Fig. 4.6 ^{29}Si MAS NMR of vermiculite before and after lead exchange

and -91.3 ppm respectively (Fig. 4.4). There is no change either in peak positions or widths (Table 4.5) after lead exchange.

4.4.2 ^{27}Al

Al in chabazite gives a symmetrical peak at +59.9 ppm (Fig. 4.7). The peak position does not shift significantly after Ca(Na)-chabazite is converted into Na-chabazite,

Table 4.6 ^{27}Al MAS NMR data of the zeolite and clay minerals (11.7 T magnetic field)

	^{27}Al peak position (ppm) / FWHM (Hz)	
	Tetrahedral Al	Octahedral Al
Before Pb exchange		
Ca(Na)-chabazite	+59.9/650	
Na-chabazite	+59.0/570	
Vermiculite	+66.8/1560	+3/2600
Montmorillonite	+56/1300	+2.4/1560
Hectorite	+58.8/2080	
Kaolinite		+3.4/1040
After Pb exchange		
Ca(Na)-chabazite	+56.6/760	
Na-chabazite	+56.9/780	
Vermiculite	+66.0/1500	+3/2600
Montmorillonite	+56/1300	+2.3/1560
Hectorite	+59.0/2020	
Kaolinite		+3.2/1040

but the peak width decreased from 650 Hz to 570 Hz (Table 4.6). After lead exchange,

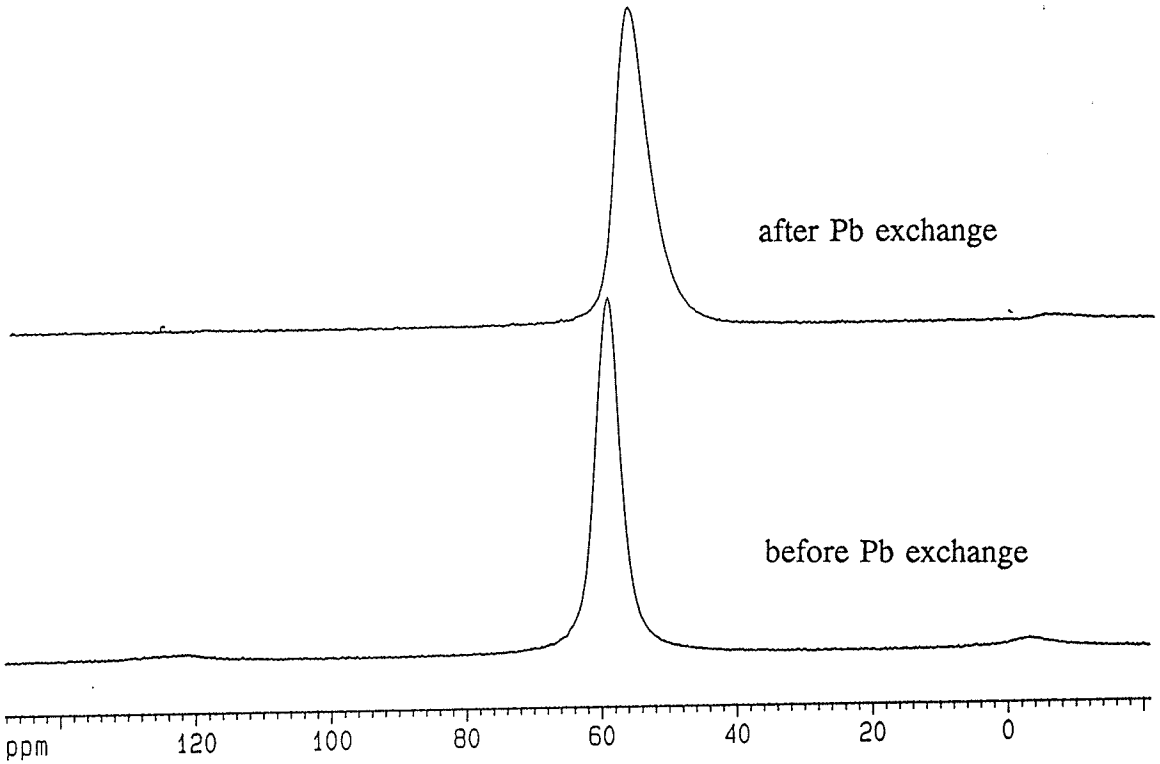

Fig. 4.7 ^{27}Al MAS NMR of Na-chabazite before and after lead exchange (11.74 T magnetic field)

of both Ca(Na)-chabazite and Na-chabazite, the ^{27}Al peak shifted 2 to 3 ppm to a more negative values, and the peak width increased by about 200 Hz (Table 4.6, Fig. 4.7).

Most of Al in vermiculite is in the tetrahedral site (Fig. 4.8). There is a slight shift of the peak in the Pb exchanged vermiculite from 66.8 ppm to 66.0 ppm (Fig. 4.8). The narrow peak overlapped with the octahedral peak is likely the spinning side band of the satellite transition.

Most of the Al in montmorillonite is in octahedral coordination (Fig. 4.9). The peak due to octahedral ^{27}Al at 2.3 ppm is asymmetrical. Neither the peak position nor width changed after lead exchange (Table 4.6, Fig 4.9).

Al in hectorite is mostly in tetrahedral site (Fig. 4.10). The peak positions and width of both the tetrahedral and octahedral peaks did not change after lead exchange (Fig. 4.10).

^{27}Al spectrum of kaolinite is a single symmetric octahedral peak at +3.2 ppm (Fig. 4.11). There is no change in peak position or width after lead exchange (Table 4.6 and Fig. 4.11).

4.4.3. ^{23}Na

there is only one ^{23}Na peak at about -6 ppm in the spectra of both Na- and Ca(Na)-chabazite (Table 4.7, Fig 4.12). ^{23}Na spectra of lead exchanged chabazite also show only one peak identical in position and shape to that before lead exchange.

Only one symmetrical peak at -8.6 ppm was observed in the ^{23}Na spectrum of vermiculite (Fig. 4.13). The intensity of this peak decreased after lead exchange. A

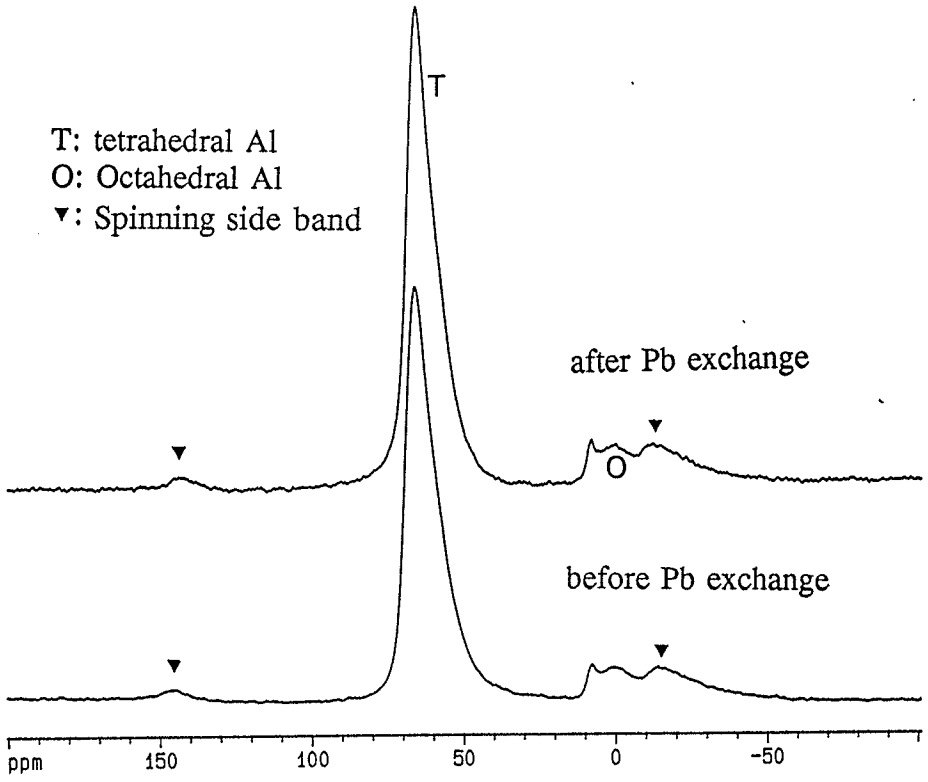

Fig. 4.8 ^{27}Al MAS NMR of vermiculite before and after lead exchange (11.74 T magnetic field)

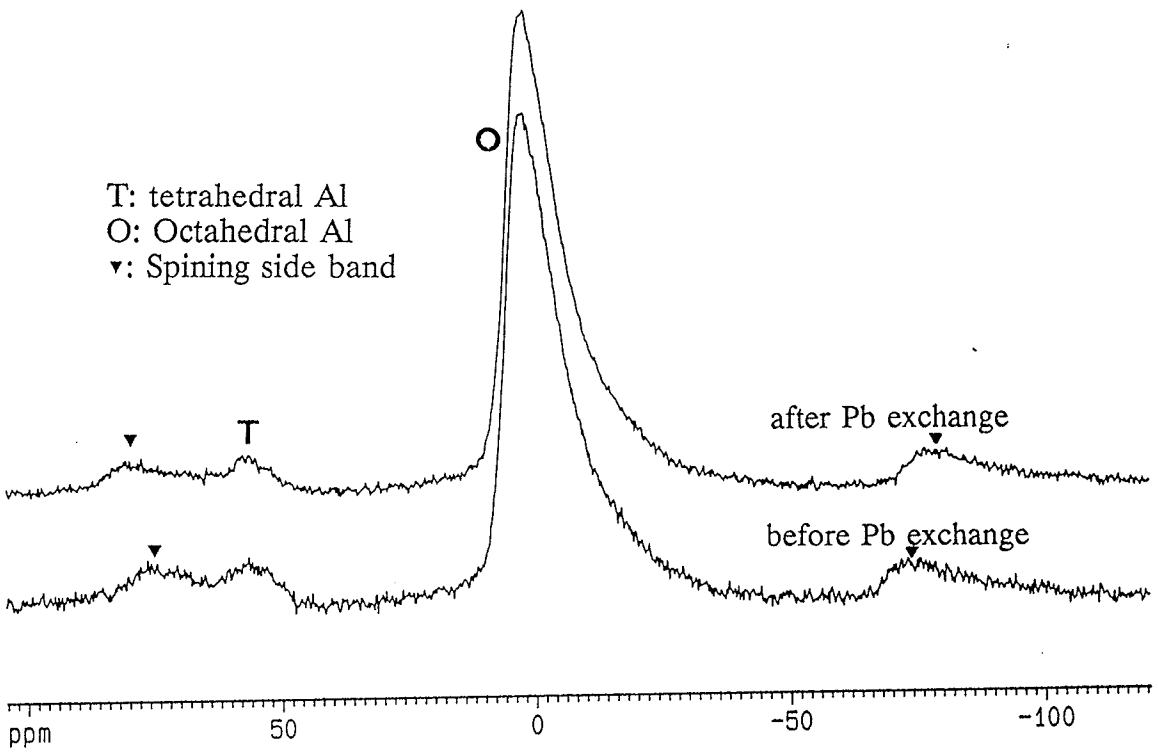

Fig. 4.9 ^{27}Al MAS NMR of montmorillonite before and after lead exchange (11.74 T magnetic field)

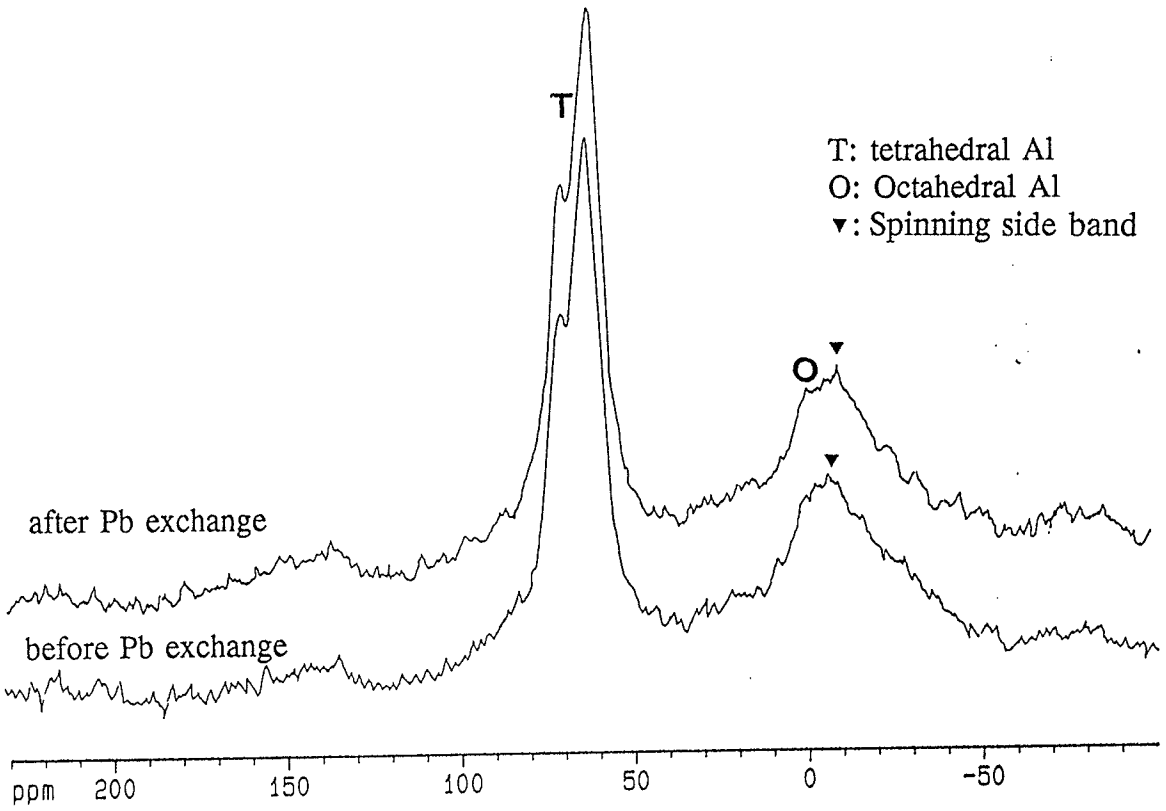

Fig. 4.10 ^{27}Al MAS NMR of hectorite before and after lead exchange (in 11.74 T magnetic field)

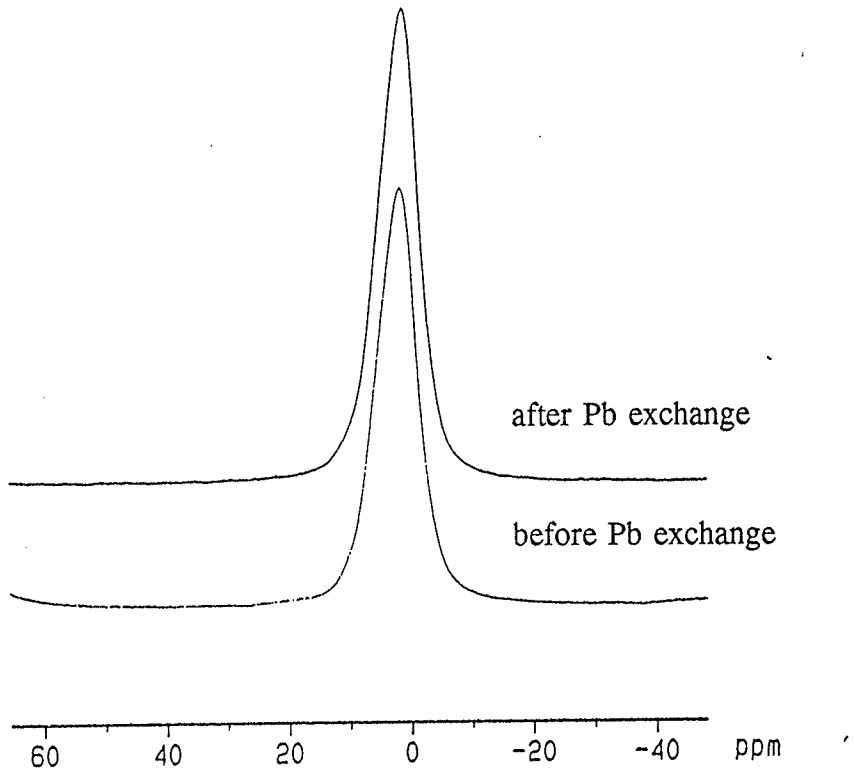

Fig. 4.11 ^{27}Al MAS NMR of kaolinite before and after lead exchange (11.74 T magnetic field)

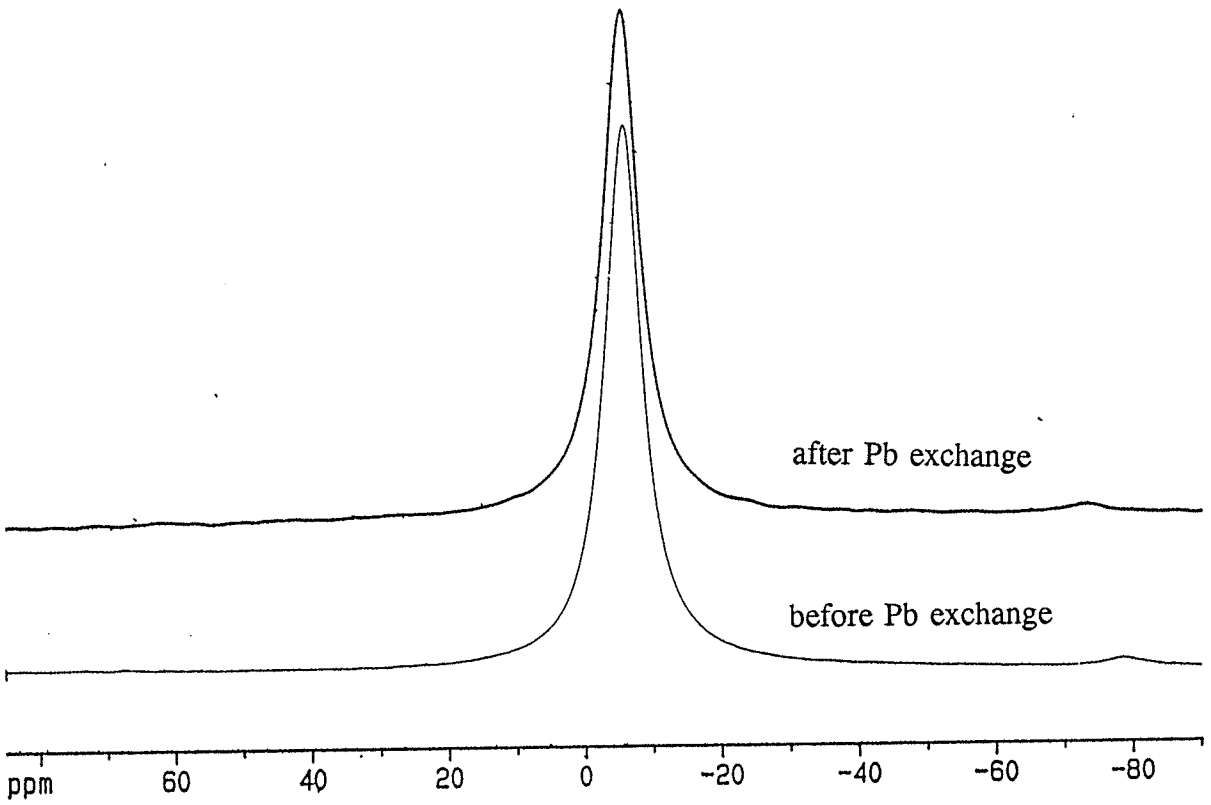

Fig. 4.12 ^{23}Na MAS NMR of Na-chabazite before and after lead exchange (in 11.74 T magnetic field)

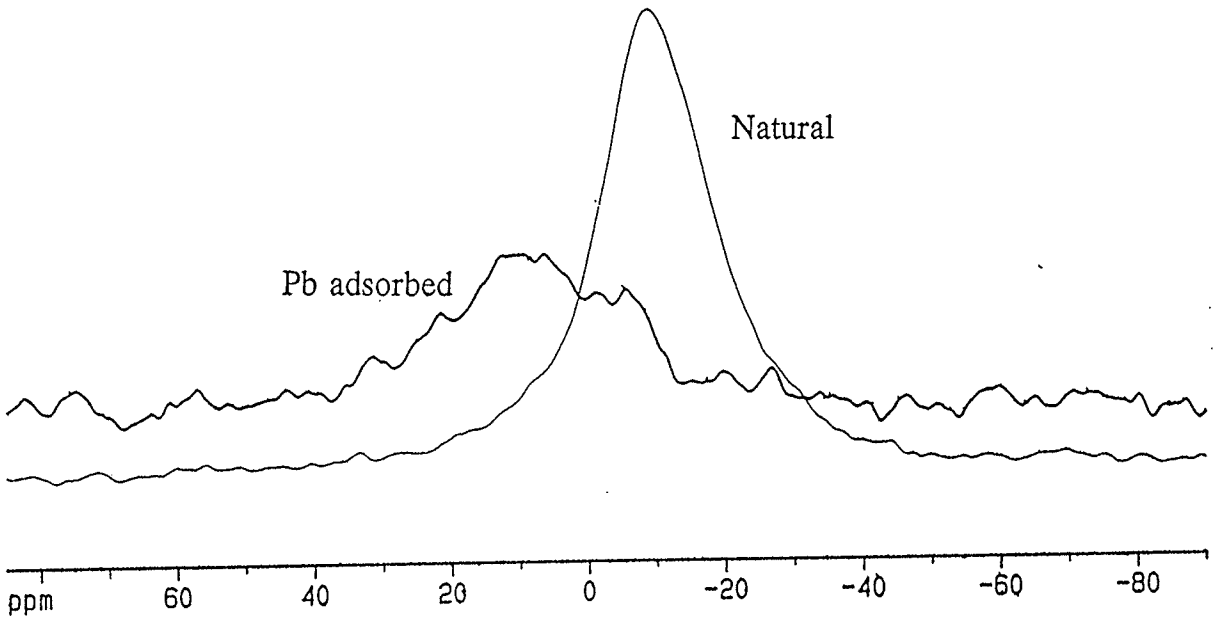

Fig. 4.13. ^{23}Na MAS NMR of Na-vermiculite before and after lead exchange (11.74 T magnetic field)

Table 4.7. ^{23}Na MAS NMR data of the exchangeable cation Na^+ in the zeolite and clay minerals (11.74 T magnetic field)

	^{23}Na peak position (ppm)	
	Before Pb exchange	After Pb exchange
Ca(Na)-chabazite	-6.3	-6.0
Na-chabazite	-6.3	-6.0
Vermiculite	-8.6	+8
Montmorillonite	-10.7	+8, -20
Hectorite	-8.4, -19.4	+8, -25
Kaolinite	-6.3	+6

broader and weaker peak shows on the spectrum of the lead exchanged sample at about +8 ppm. It was tentatively assigned to the non-crystallographic sites at the mineral grain boundaries.

There are two overlapping peaks in the ^{23}Na spectra of hectorite at -8.4 and -19.4 ppm (Table 4.7; Fig. 4.14). These peaks could represent two different chemical environments, or be the result of the quadrupolar splitting of a single peak. Under magic angle spinning condition, the theoretical line shape of the centre band of the central transition can include two singularities (Samoson et al., 1982). They will show as peak splitting when the EFG asymmetry factor η_Q is considerably less than 1 and when the line broadening factors, such as magnetic inhomogeneity and paramagnetic impurities, as well as dipolar and chemical shift interactions, are minimized. A single peak will occur when η_Q approaches 1.

When splitting occurs, the positions of the singularities do not move from the

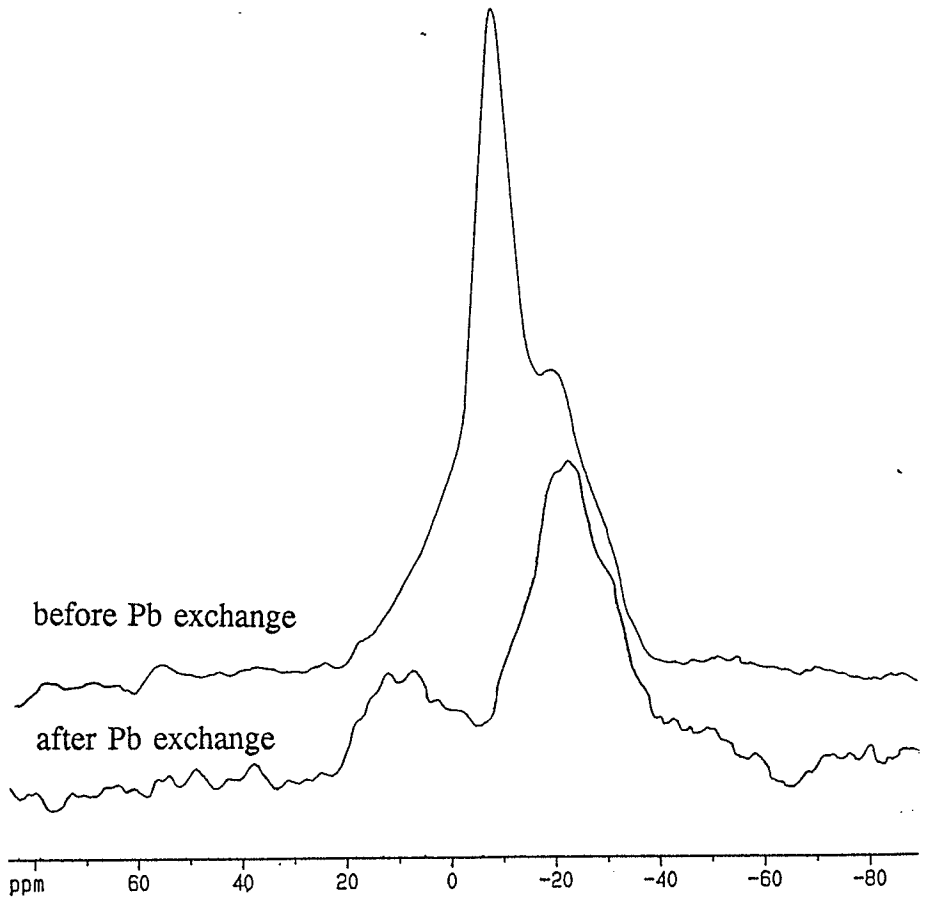

Fig. 4.14 ^{23}Na MAS NMR of hectorite before and after lead exchange (in 11.74 T magnet)

calculated positions even if the peaks are broadened (Samoson et al., 1982). The frequencies of the two singularities, ω_{P1} and ω_{P2}, taking the position of the isotropic chemical shift as the zero point, can be expressed in Hz as:

$$\omega_{P1} = -\left(\frac{5}{8} - \frac{1}{4}\eta_Q + \frac{7}{24}\eta_Q^2\right) a, \qquad when \quad 0 \le \eta_Q \le \frac{3}{7},$$
$$or \quad -\frac{4}{7}a, \qquad when \quad \frac{3}{7} \le \eta_Q \le 1,$$

and

$$\omega_{P2} = -\frac{1}{7}(1+\eta_Q)^2 a$$

$$a = \frac{3}{32}\frac{C_Q^2}{[I(2I-1)\hbar]^2 \nu_L}[2I(I+1) - 14m(m-1) - 5]$$

Under MAS conditions, the relative quadrupolar shift of the centre of gravity of the centre band, $\sigma_{QS}(m)$, of a single quantum (m,m-1) transition, in ppm, is (Lippmaa, 1986):

$$\sigma_{QS}(m) = -\frac{3}{40}\left(\frac{C_Q}{I(I-1)\nu_L}\right)^2 [I(I+1) - 9m(m-1) - 3]\left(1 + \frac{\eta_Q^2}{3}\right)$$

For the ^{23}Na central transition, with both ν_L and C_Q in MHz, the quadrupolar shift, relative to the isotropic chemical shift σ_{iso} in Hz, can be written as:

$$\sigma_{QS}\left(\frac{1}{2}\right) = \sigma_{CG} - \sigma_{iso} = -25000\frac{C_Q^2}{\nu_L}\left(1 + \frac{\eta_Q^2}{3}\right)$$

where σ_{CG} is the centre of gravity of the central transition line.

If the two peaks of hectorite are due to the splitting caused by the quadrupolar interaction, then

$$\omega_{P1} = (-8.4 - \sigma_{iso}) \cdot 132.3,$$

$$\omega_{P2} = (-19.4 - \sigma_{iso}) \cdot 132.3,$$

$$\sigma_{QS} = (-11.2 - \sigma_{iso}) \cdot 132.3.$$

Substituting these parameters into the corresponding equations above, the quadrupolar parameters were calculated to be $\eta_Q = 0.706$, $C_Q = 4.45$ MHz.

An NMR line shape modelling computer program (Power et al. 1990) was used to simulate the quadrupolar line shape from these parameters. As the simulated spectrum was different from the observed (Fig. 4.15), it was concluded that the two observed peaks are not the result of the quadrupolar interaction, but are due to two different Na sites within hectorite.

The larger peak at -8.4 ppm is due to the less shielded environment and is tentatively assigned to the interlayer site of the exchangeable cations. The intensity of this peak diminished considerably after lead adsorption (Fig. 4.14), suggesting that lead has occupied the site. The other peak at -19.4 ppm has a relatively high proportion of residual intensity after lead adsorption. This suggests that lead cations have difficulty in entering this site. The site is tentatively assigned to the one within the 6-membered ring in the tetrahedral sheet. The broad and weak peak at +8 ppm was also observed for the lead exchanged hectorite.

The ^{23}Na MAS NMR spectrum of montmorillonite before lead exchange (Fig. 4.16) resembles that of hectorite in peak position, width and shape. The intensity of the peak at -10.7 ppm, representing the interlayer site, decreased after lead exchange, but in this case, the one representing the site in the 6-membered ring also decreased considerably (Fig. 4.16).

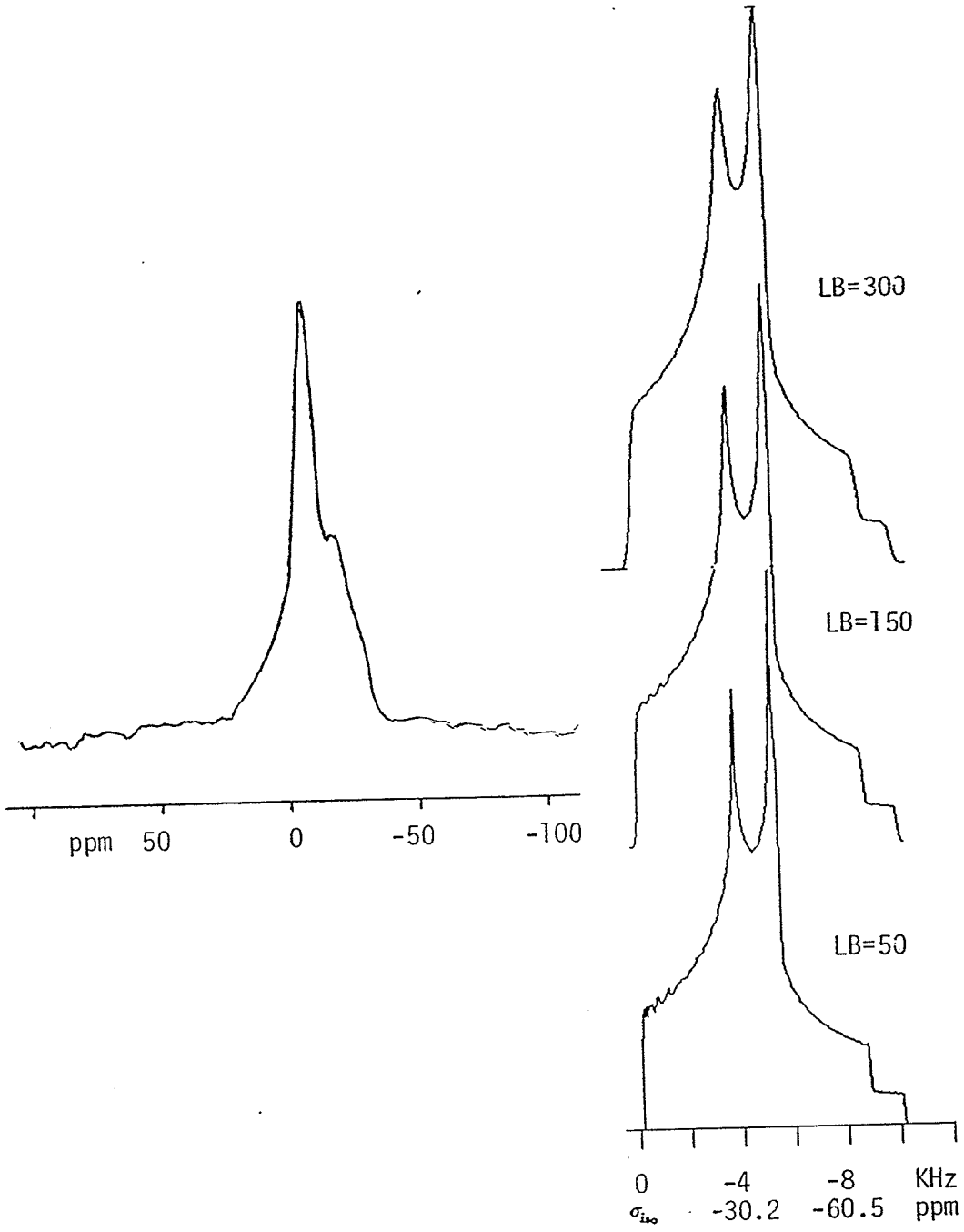

Fig. 4.15. Computer simulation (right) of ^{23}Na MAS NMR line shape of the centre band of the central transition from a powder with C_Q = 4.47 MHz, η_Q = 0.706 (11.74 T magnetic field). the spectrum on the left is the ^{23}Na MAS NMR spectrum of hectorite before lead exchange.

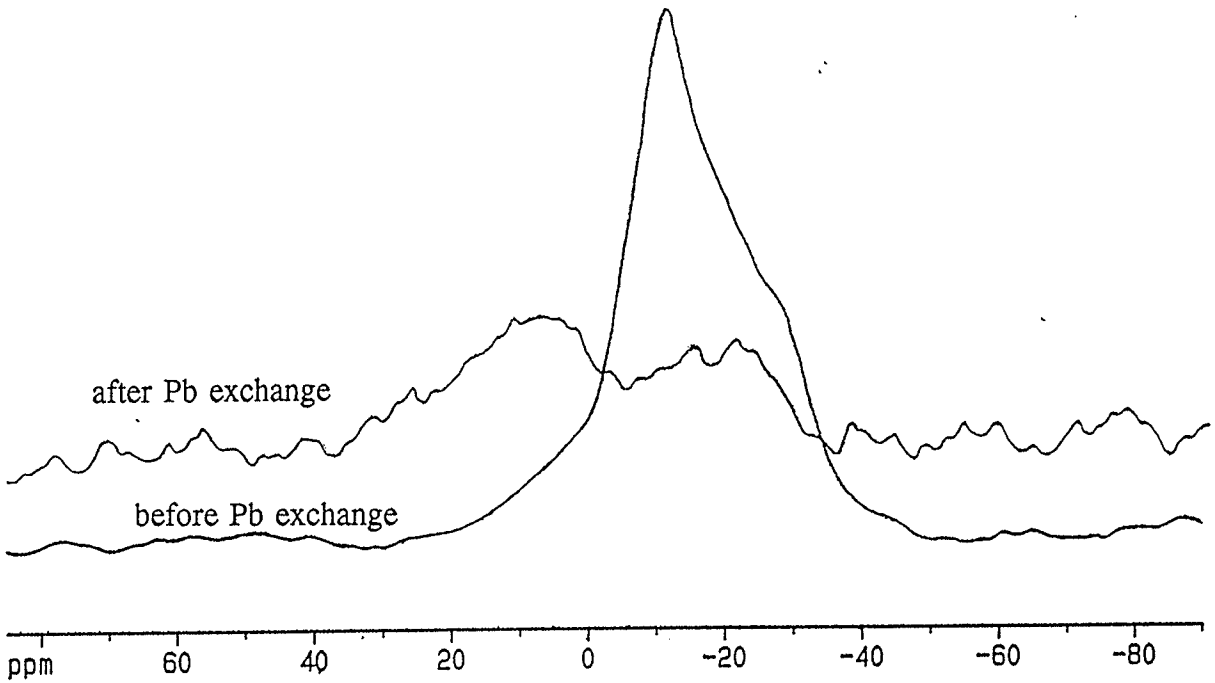

Fig. 4.16 ^{23}Na MAS NMR of montmorillonite before and after lead exchange (11.74 T magnetis field)

The ^{23}Na spectra of kaolinite has a relatively narrow peak at -6.3 ppm overlapped with a broad peak at about +8 ppm (Fig. 4.17). The peak at -6.3 ppm disappeared after lead exchange, while the broad peak remained unchanged.

4.4.4. ^{7}Li

^{7}Li MAS NMR spectra of hectorite samples showed one symmetrical peak at -2.2 ppm. There was no change in peak position, width, and peak shape after lead exchange (Fig. 4.18).

4.4.5. ^{207}Pb

A ^{207}Pb MAS NMR spectrum of cerussite (Fig. 4.19) gave an isotropic chemical shift of -2619 ppm. The principle values of the shielding tensor obtained by the graphical method of Herzfeld and Berger (1980), from the relative side band intensities, are σ_{11} = -2300, σ_{22} = -2500, σ_{33} = -3000 ppm.

No ^{207}Pb MAS NMR spectra were obtained for the lead exchanged zeolite and clay minerals. Several reasons may be possible for not receiving ^{207}Pb MAS NMR signals from these minerals. Firstly, the already huge chemical shift anisotropies of ^{207}Pb increases with magnetic field, and spread the spectrum out over the whole spectral width at high field. Secondly, T_2 relaxation may be too short so that the signals decayed before it can be collected. Finally, there was also a large ^{207}Pb background signal from the probe which would overwhelm any weak ^{207}Pb peak.

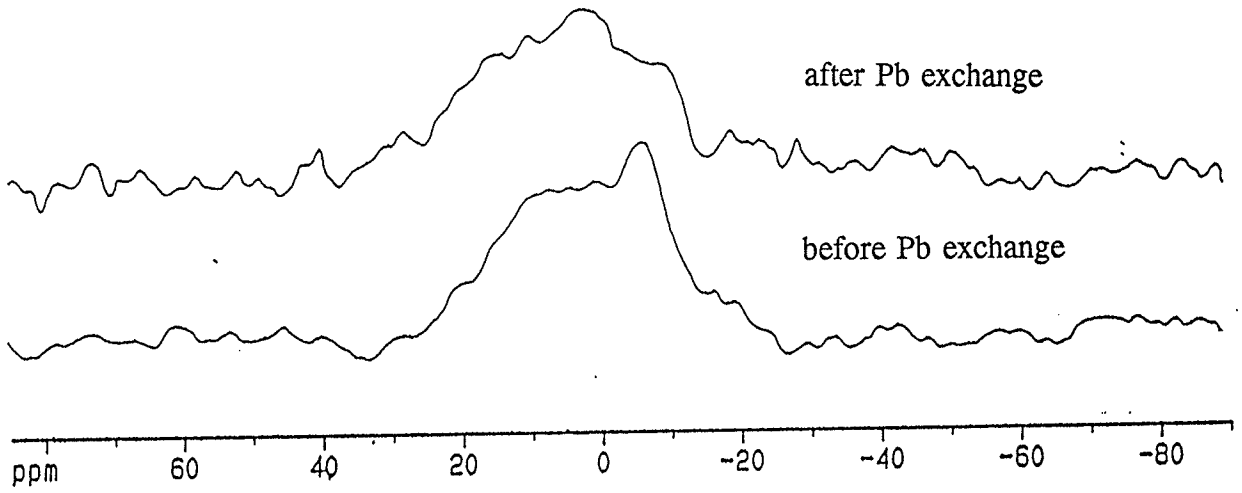

Fig. 4.17 ^{23}Na MAS NMR of kaolinite before and after lead exchange (11.74 T magnetic field)

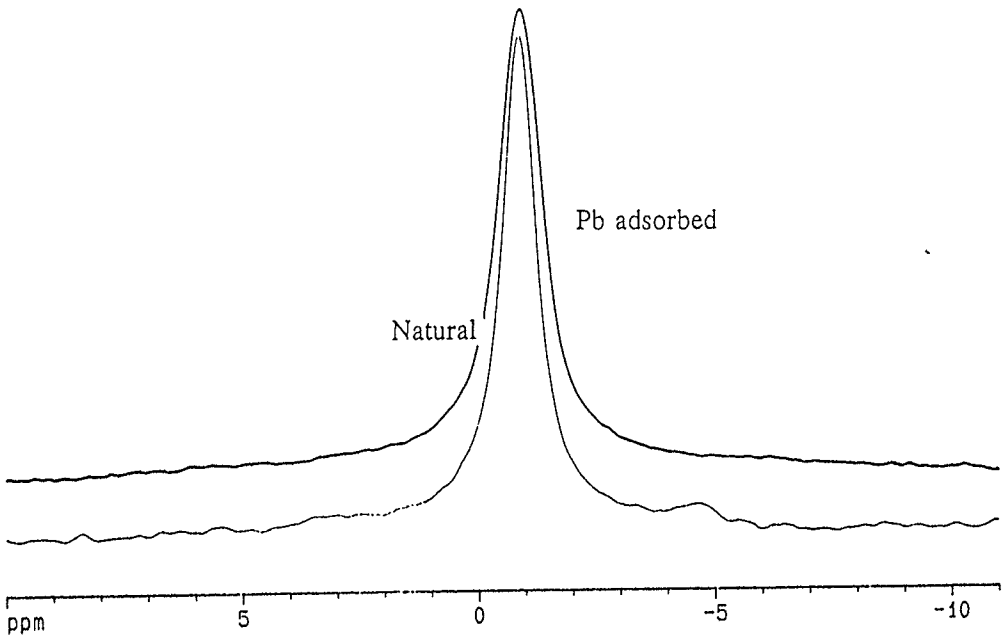

Fig. 4.18 ^{7}Li MAS NMR of hectorite before and after lead exchange (11.74 T magnetic field)

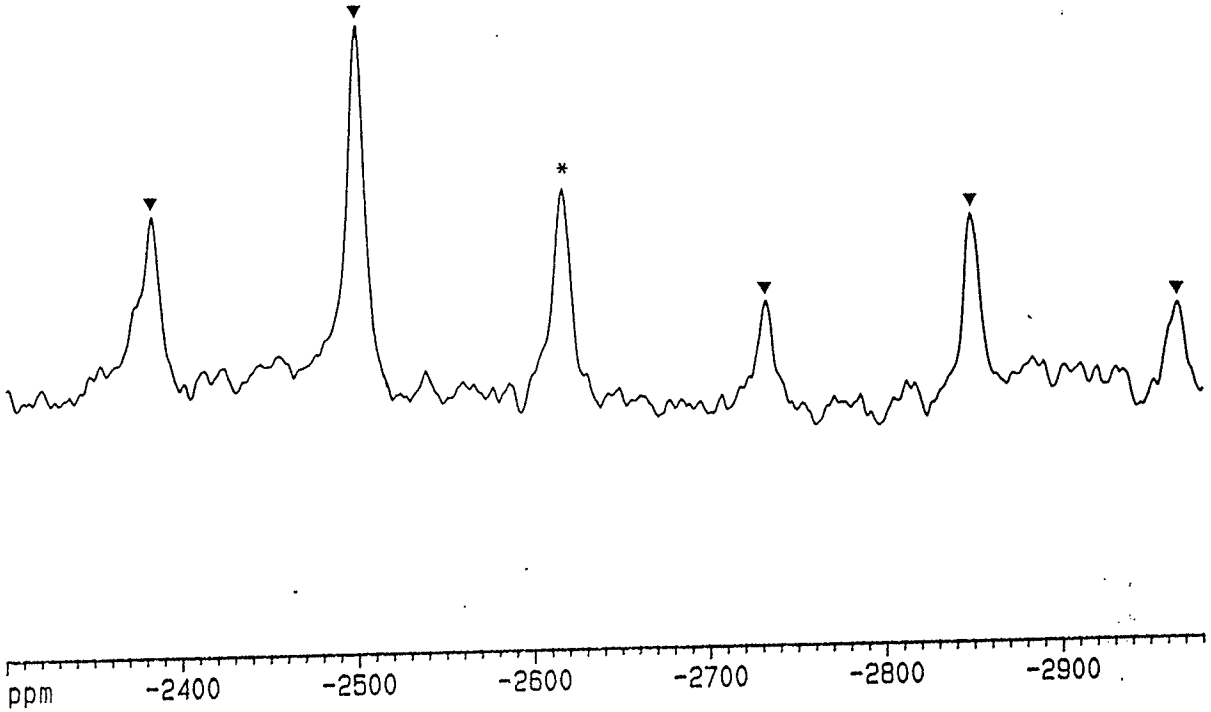

Fig. 4.19 ^{207}Pb MAS NMR of cerussite in 8.4 T magnet.
*: centre band
▾: spining side band

CHAPTER 5. THE ION EXCHANGE MECHANISM IN THE ZEOLITE AND CLAY MINERALS

5.1. Chabazite

In chabazite, both the ^{29}Si and ^{27}Al MAS NMR peak positions shift in the direction of increased electronic shielding when there is lead exchanged into the mineral (Table 5.1). As Si and Al are both tetrahedral cations in chabazite, this change in NMR peak position indicates a local chemical environment change at the tetrahedral site.

The ^{29}Si chemical shift of silicates and aluminosilicates can be calculated, from the crystal structure, using the relationship found by Sherriff, Grundy and Hartman (1991). This relationship was used to evaluate the relative importance of the three different exchangeable cation sites and of their occupancy by different cations, in influencing the ^{29}Si chemical shift. The chabazite structure model was based on that of Calligaris and co-workers (1982), and was built using the Chem-X crystal structure Modelling Package (developed and distributed by Chemical Design Ltd, Oxford, England).

It was discovered that among the three sites, only site 1 (Fig. 2.4), which has direct bonds to the framework oxygens, can make the ^{29}Si chemical shift more negative, when it is occupied by lead instead of Na or Ca. This corresponds to the peak position

Table 5.1. ^{29}Si and ^{27}Al MAS NMR peak positions and peak widths (11.7 T magnetic field)

	Before Lead Exchange		After Lead Exchange	
	Ca(Na)-chabazite	Na-chabazite	Ca(Na)-chabazite	Na-chabazite
^{29}Si peak position (ppm) / peak width (Hz)				
Si(3Al)	-92.4/350	-93.0/210	-95.0/220	-94.4/250
Si(2Al)	-98.2/320	-98.8/300	-100.3/260	-100.0/240
Si(1Al)	-103.6/300	-104.3/300	-105.8/280	-105.4/240
Si(0Al)	-109.0/230	-109.6/160	-110.0/260	-111.0/160
^{27}Al peak position (ppm) / peak width (Hz)				
	+59.9/660	+59.0/570	+56.6/760	+56.9/780

shift towards the increasing electronic shielding direction seen in the experimental results. The difference between the chemical environments of site 1 and site 2 and 3 (Fig. 2.4), is that site 1 has shortest bonds to the framework oxygens, and hence stronger influence on the chemical environment of the framework cation Si and Al. Site 2 is in the middle of the chabazite cavity, and is coordinated only by water molecules. Site 3 is coordinated to the framework oxygens, but has an exchangeable cation - oxygen bond distance of 3.07 Å, compared to that of the site 1 of 2.68 Å (Table 5.2). The increased electronic shielding of the tetrahedral site in the lead exchanged sample therefore indicates the occupancy of lead in site 1.

Table 5.2. Chemical bonding of the three cation sites of the exchangeable cations in chabazite (from Calligaris et al., 1982)

	Cation - O distance (Å)	Nature of the coordinating oxygens
Site 1	2.68	framework oxygens
	2.82	oxygens in water molecules
Site 2	2.88	oxygens in water molecules
	2.28	oxygens in water molecules
Site 3	3.07	framework oxygens

There are also differences in NMR peak width for the chabazite samples. The ^{29}Si peak width of Ca(Na)-chabazite decreased by about 70 Hz after being converted in to Na-chabazite, while that of ^{27}Al decreased by 80 Hz (Table 5.1). The NMR peak width reflects the chemical environment diversity at the nucleus observed, as the other line broadening mechanisms, such as chemical shift anisotropy and dipolar interactions, are effectively reduced under MAS condition. It has been experimentally observed (Mägi et

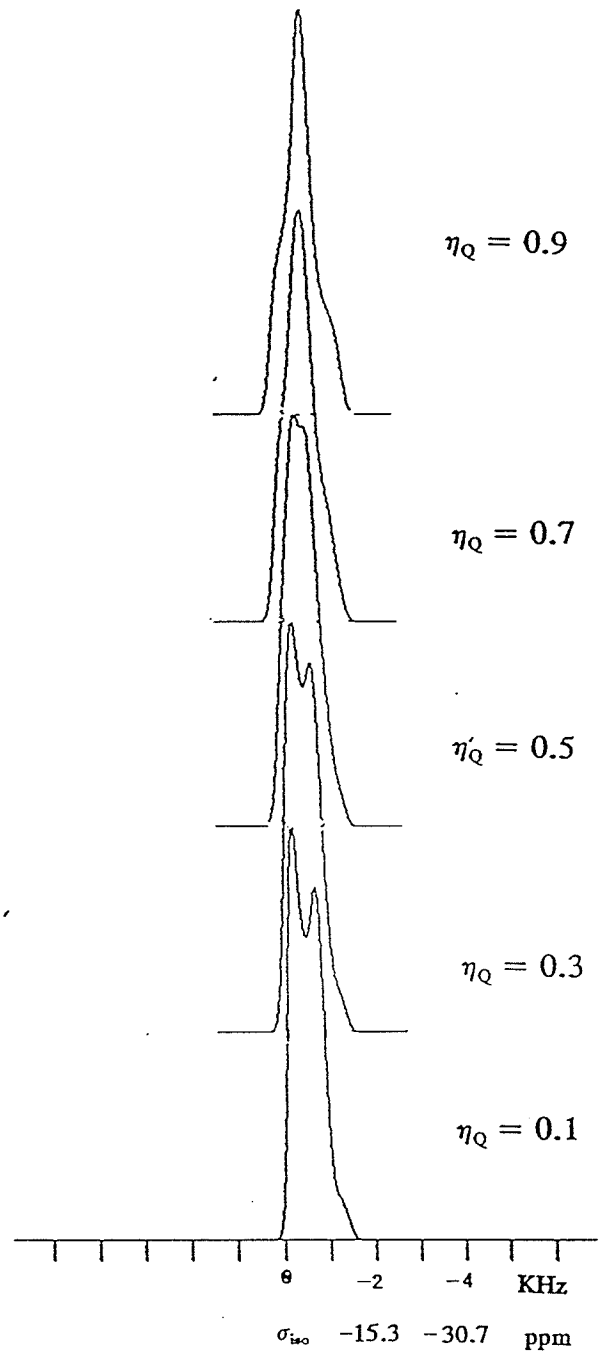

Fig. 5.1. Computer simulation of ^{27}Al MAS NMR peak width and shape using the computer program of Power and co-workers (1990). C_Q = 3.5 MHz, η_Q = 0.1 to 0.9 with 0.2 increment. LB = 250 Hz, B_0 = 11.74 T.

al., 1984) and calculated (Sherriff et al., 1987) that having either Na^+ or Ca^{2+} as adjacent cations will result in slightly different ^{29}Si chemical shift values which can cause overlapping peaks in disordered minerals such as scapolite (Sherriff et al., 1987). As there are both Ca^{2+} and Na^+ in Ca(Na)-chabazite, the ^{29}Si peak can be interpreted as an envelope containing peaks due to ^{29}Si adjacent to Ca^{2+} and to Na^+. In Na-chabazite, most ^{29}Si is close to Na^+ and therefore there are fewer overlapping peaks, and the ^{29}Si peaks are narrower.

After lead exchange, the peak width of ^{29}Si does not change, but that of ^{27}Al in the lead exchanged Na-chabazite increased by about 200 Hz. Such broadening is unlikely the indication of the chemical environment, of the tetrahedral cations Si and Al, becoming more diverse, because the corresponding ^{29}Si peak widths did not change. It can not be either the result of preferential concentration of the residual Na^+ cations near Al, causing overlapping Al(Na) and Al(Pb) peaks, because the ^{23}Na spectrum did not differ in peak position nor width from that before lead exchange (Table 4.7, Fig. 4.12). One possible explanation could be the increasing quadrupolar interaction at ^{27}Al caused by Pb^{2+} cations in the place of Na^+. The MAS peak width of the quadrupolar nucleus ^{27}Al is (from Samoson, 1982):

$$\Delta\nu(Hz) = -\frac{1}{7}(1-\eta)^2 a - [-\frac{1}{6}(6+\eta^2)a]$$
$$= \frac{3}{200}\frac{C_Q^2}{\nu_L}[\frac{1}{42}\eta^2 + \frac{2}{7}\eta + \frac{6}{7}]$$

in which only two factors, the asymmetry parameter η of the electric field gradient, and the quadrupolar coupling constant C_Q, vary. η has little influence on peak width, but can

significantly change the peak shape (Fig. 5.1). The ^{27}Al MAS NMR peak shape changes very little in the Na-chabazite after lead exchange (Fig. 4. 7), therefore changes in η would be very small. The peak width is proportional to the square of the quadrupolar coupling constant C_Q, which is a measure of the size of the electronic field gradient. Lead exchanged into chabazite possibly increases the electronic field gradient of Al in the framework.

In Na-chabazite, all three exchangeable cation sites are available to Na^+, but the ^{23}Na MAS NMR spectrum shows only one peak (Fig. 4.12). Quadrupolar broadening of the peaks may cause the three possible peaks to overlap. The double rotation (DOR) NMR technique, which rotate the sample simultaneously around two axis, reduces both quadrupolar broadening and chemical shift anisotropy + dipolar interactions (Wu et al., 1990), and often resolve peaks which overlap in MAS spectrum. The DOR NMR spectrum of Na-chabazite (Fig. 5.2), however, still shows only one broad peak, indicating that it is not just quadrupolar broadening which is causing these peaks to overlap.

Another possible explanation is the fast exchange of the Na^+ cations between the three sites. For two sites with $\Delta\nu$ (Hz) difference in the NMR frequency, if the nuclei in the two sites are exchanging at a rate greater than

$$K_{ex} = \pi (\Delta\nu) \cdot 2^{-1/2},$$

NMR spectroscopy will not be able to resolve the two peaks, and gives only one peak at an average frequency between the two (Sanders and Hunter, 1989). The maximum difference between the NMR frequencies of the two sites should be greater than or equal

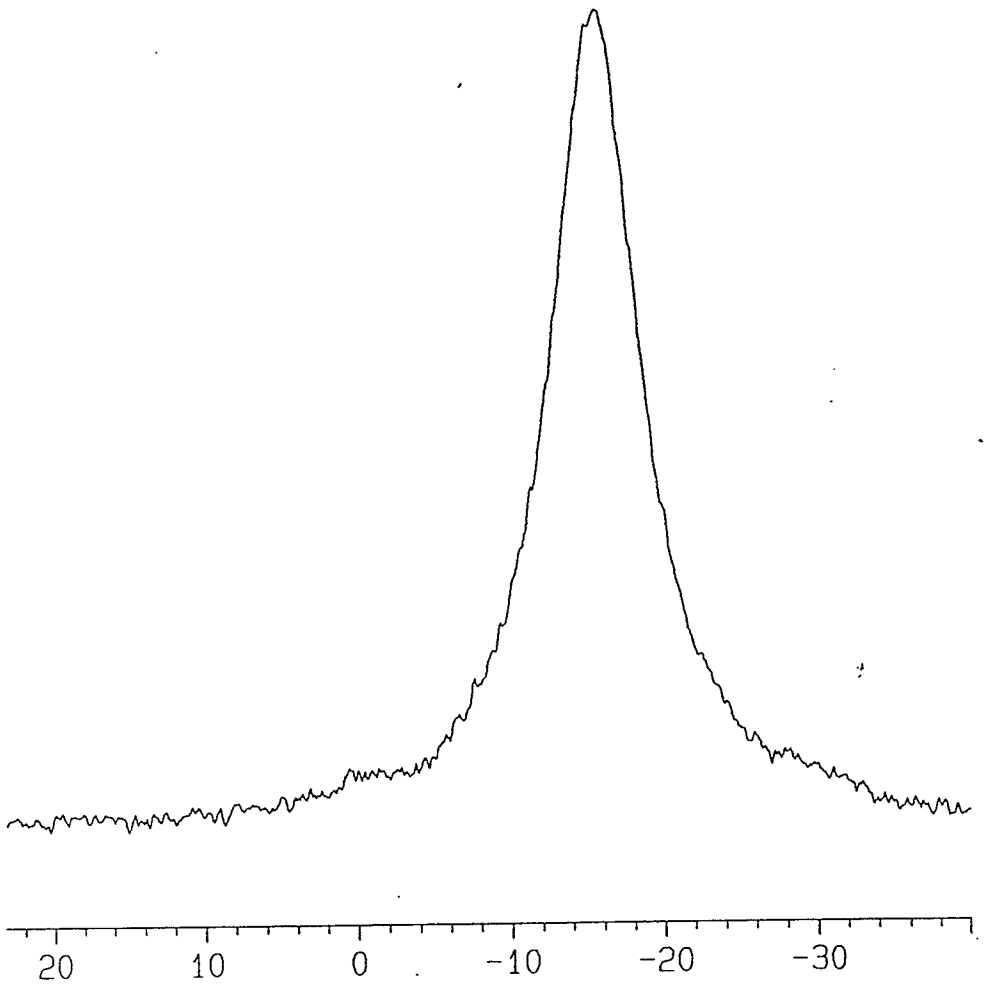

Fig. 5.2. ^{23}Na DOR NMR of Na-chabazite (8.4 T magnetic field)

to the full width of the average peak (Fig. 5.3), depending on the cation exchange rate (Sanders and Hunter, 1989). As the other line broadening factors, such as quadrupolar interaction, chemical shift anisotropy, and dipolar interaction, were reduced by the DOR technique, the peak width of the DOR NMR is probably due to the fast exchange of nuclei between the three sites. The full width of the ^{23}Na DOR NMR peak of chabazite is approximately 30 ppm, corresponding to an NMR frequency difference of 2.9×10^3 Hz. The maximum frequency difference between the three types of ^{23}Na nuclei in the three different sites is therefore greater than 30 ppm, or 2.9×10^3 Hz. Therefore, the cation exchange rate in these sites should be greater than

$$K_{ex} = \pi \times 2.9 \times 10^3 \times 2^{-1/2} = 6.4 \times 10^3 \ S^{-1}.$$

The average peak position is the same for Na-chabazite and Ca(Na)-chabazite, as well as for the lead exchanged samples, which suggests that Na^+ is exchanging rapidly between the same three sites regardless whether the dominant exchangeable cation is Na^+, Ca^{2+}, or Pb^{2+}. The other cations would have to exchange at a similar rate in order to maintain the electrical charge balance.

Variable temperature MAS NMR can provide information on thermal dynamics. Figure 5.4 and Table 5.3 show ^{23}Na MAS NMR data of Na-chabazite in the temperature range of +20 to -120 °C. From +20 °C to -20 °C, there is a systematic shift of peak position from about -6 to -9 ppm, and a decrease of peak width from 510 to 360 Hz. Further cooling causes a dramatic increase in peak width from 360 Hz at -20 °C, to 1230 at -50 °C, and to 2370 at -100 °C. There is a suggestion of 3 peaks in the -80 °C spectrum, but such trend did not continue with further cooling.

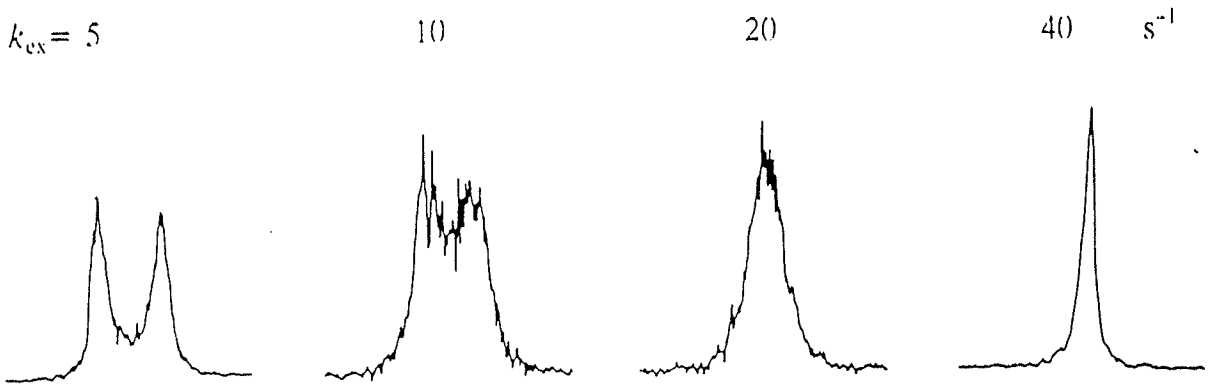

Fig. 5.3. NMR peak shapes and widths of two exchanging chemical environment with different exchanging rate (after Sanders and Hunter, 1989).

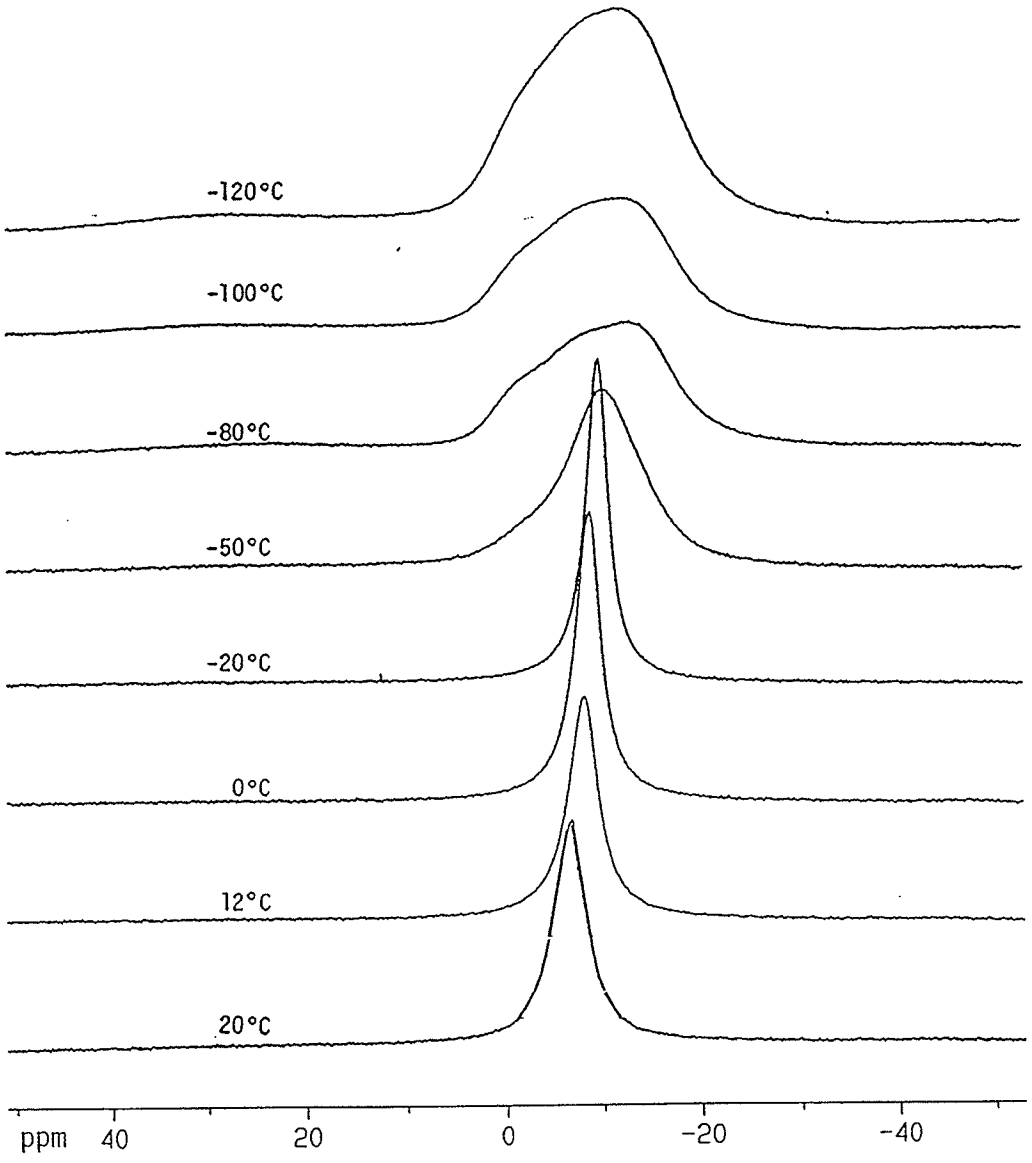

Fig. 5.4. ^{23}Na variable temperature MAS NMR of Na-chabazite (11.74 T magnetic field)

Table 5.3. ^{23}Na variable temperature MAS NMR data of Na-chabazite (11.74 T magnetic field)

Sample temperature (°C)	Peak position (ppm)	FWHM (Hz)
20	-6.3	510
12	-7.5	460
0	-7.9	410
-20	-8.8	360
-50	-9	1230
-80	-2, -8, -14	2260
-100	-9	2370
-120	-9	2340

The systematic change in peak position of the spectra from +20 to -20 °C could be the result of increasing quadrupolar interactions, or the preferential occupancy of Na^+ cations in the more highly shielded sites. The former is unlikely because an increase in quadrupolar interaction will also cause broadening of the peak, which is in contradiction with the experimental results. The dramatic increase of peak width at -50 °C indicates that the fast chemical exchange at room temperature of the Na^+ cations in Na-chabazite does not change above the temperature of -50 °C. The peak width continue to increase from 1230 Hz at -50 °C, to 2260 Hz at -80 °C, indicating that Na^+ cations are still exchanging positions in this temperature range, although at a slower rate than at room temperature. Further cooling had little effect on peak width, suggesting that chemical exchange was no longer a dominant factor in controlling peak width. Dipolar and quadrupolar interactions, and chemical shift anisotropy may be causing broad peaks at

temperatures below -80 °C.

5.2. The Clay Minerals

As in chabazite, the ^{29}Si and ^{27}Al peaks of vermiculite become increasingly shielded after lead exchange. Therefore the exchangeable cation site in vermiculite is close enough to the tetrahedral site to influence the electronic shielding of Si and Al, through the coordinating oxygens.

There are no peak position or width changes on the ^{29}Si and ^{27}Al spectra of montmorillonite, hectorite, and kaolinite after lead exchange. The exchangeable cation site which lead can occupy is, therefore, like site 2 in chabazite, not directly bonded to the coordinating oxygens of SiO_4 and AlO_4 tetrahedra. The occupancy of this site by lead will not affect the electronic shielding of the tetrahedral cation Si and Al, and hence their NMR frequencies.

Two peaks were observed in the ^{23}Na MAS NMR spectrum of hectorite before lead exchange, with the difference between the two peak positions being 11 ppm, or 1.4 $\times$ 10^3 Hz at a magnetic field of 11.7 T. Therefore the exchange rate of Na^+ between these two sites in hectorite will not be greater than

$$K_{ex} = \pi \times 1.4 \times 10^3 \times 2^{-1/2} = 3.2 \times 10^3\ S^{-1},$$

assuming that the quadrupolar broadening and shift is the same for both sites.

There are similarities among the ^{23}Na MAS NMR spectra of the clay minerals. Figure 5.5 shows the ^{23}Na spectra of the clay minerals before lead exchange. A peak at

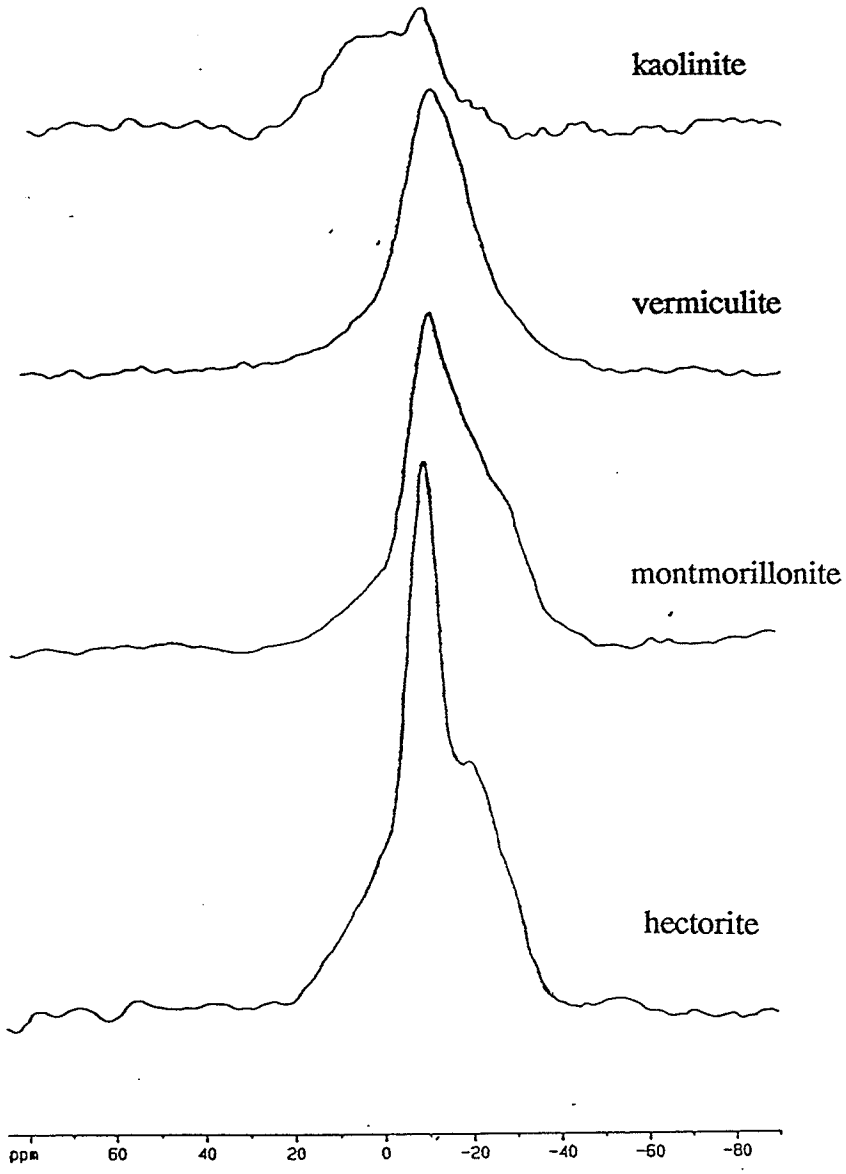

Fig. 5.5. ^{23}Na MAS NMR spectra of the clay minerals before lead exchange (11.74 T magnetic field)

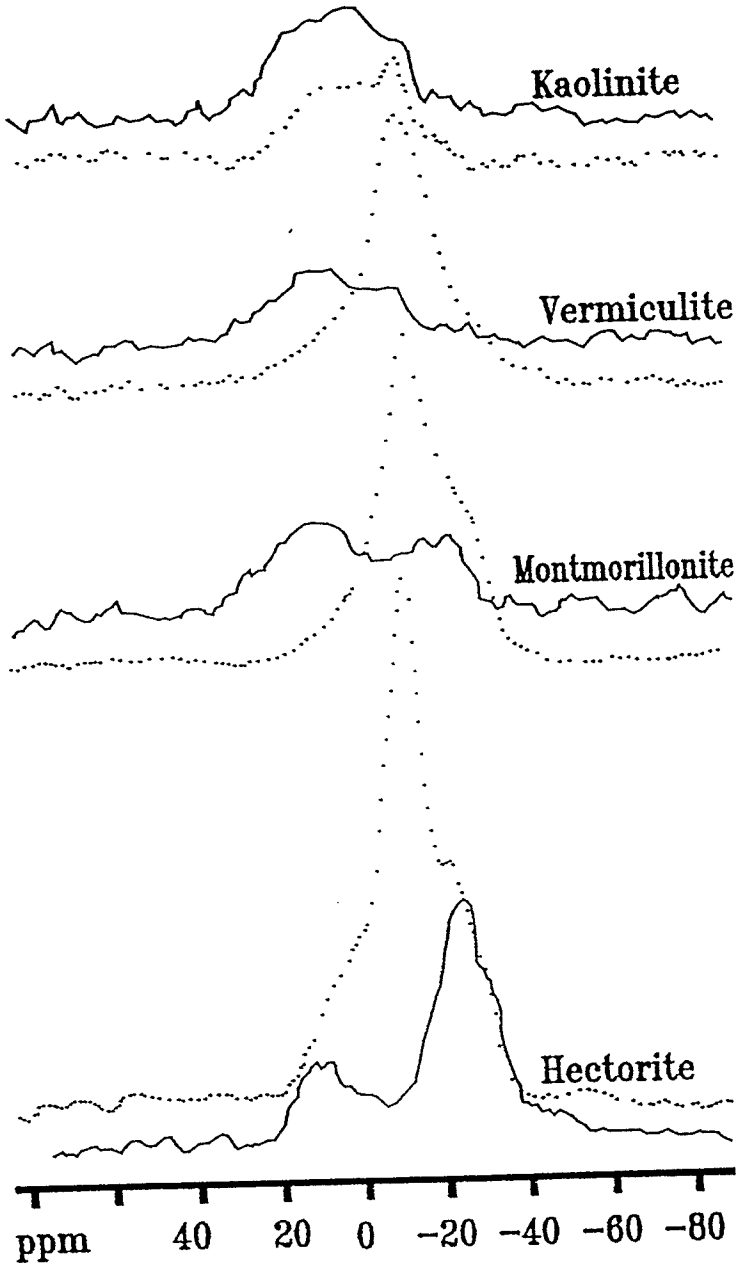

Fig. 5.6. ^{23}Na MAS NMR spectra of the clay minerals after lead exchange (solid lines) compared to that before lead exchange (dotted lines)

about -8 ppm, assigned to the interlayer site of the exchangeable cations in all four species, disappears after lead exchange (Fig. 5.6). The clay minerals have similar interlayer chemical environments which are available for cation-exchange by lead. Unlike chabazite, the clay minerals, except hectorite, can exchange almost all of the Na^+ cations in one single lead exchange experiment. Na^+ cations left in most of the clay minerals after lead exchange are not in crystallographic sites but are probably on surfaces or along grain boundaries.

5.3. Conclusions

The maximum lead contents gained through the ion exchange in Na-chabazite, vermiculite, montmorillonite, hectorite, and kaolinite can be 27%, 16%, 9%, 9%, and 0.4% respectively, when the initial lead nitrate solution concentration is 0.01 M. The ion exchange processes reached equilibrium within 24 hours of ion exchange for chabazite and vermiculite. Those in montmorillonite and hectorite were much faster with equilibrium being reached in less than 5 seconds.

Natural Ca(Na)-chabazite, which has the maximum lead content of 7%, is less efficient than Na-chabazite in taking up lead from the solution. There is, however, no such difference in the lead uptake capacities in the clay minerals with respect to different cation forms. This might be explained by the flexible interlayer spacing in the clay minerals, and hence less structure control over different types of exchangeable cations, on the contrast to the rigid framework structure of chabazite which imposes stronger

structure control over types of the exchangeable cations.

Calcite, which is often present in the clay minerals, precipitates lead as cerussite from the aqueous solution. The cerussite precipitate has the same granular form as calcite and the reaction causes no apparent volume increase.

^{29}Si and ^{27}Al MAS NMR data show that chabazite and vermiculite have structures in which exchangeable cations are close to the oxygens of the SiO_4 and AlO_4 tetrahedra. The other clay minerals do not display such close relationship.

^{23}Na MAS and DOR NMR did not separate the 3 peaks for the 3 Na^+ sites in Na-chabazite, revealing the fast chemical exchange of Na^+ cations in these sites. Low temperature MAS NMR showed that such fast chemical exchange slowed at sample temperature below -50 °C.

There are at least two sites for the exchangeable cations in hectorite. The corresponding peaks in the ^{23}Na MAS NMR spectrum can be tentatively assigned to the interlayer site and the site in the 6-membered ring in the tetrahedral sheet. Lead tends to occupy the interlayer site rather than the 6-membered ring site.

The chemical environments of the interlayer site in the clay minerals are similar in all the clay minerals studied. The exchangeable cation Na^+ in these sites disappeared completely after lead exchange, and therefore lead is presumed to have occupied the site.

Further work can be focused on lead extraction from the zeolite and clay minerals after lead exchange using the same experimental procedure. ^{207}Pb MAS NMR with larger sample size and lower magnetic field may succeed in monitoring the behaviour of lead during the ion exchange process. Synthetic clay minerals with controlled compositions

may be used in conjunction with MAS NMR and X-ray diffraction to help understand the structural details of these minerals, which are poorly understood but are important in the ion exchange processes.

REFERENCE

Baes C. F. Jr. and Mesmer R. E. (1974) The hydrolysis of cations. John Wiley & Sons. New York. pp489

Barlow S. M., Sullivan F. M. (1982) Lead. Reproductive hazards of industrial chemicals. London: Academic Press Inc. 360-369

Barrer R. M. and Sammon D. C. (1955) Exchange equilibria in crystals of chabazite. J. Chem. Soc. **1955**, 2838-2849

Barrer R. M. and Davies J. A., and Rees L .V. C. (1969) Thermodynamics and thermochemistry of cation exchange in chabazite. J. Inorg. Nucl. Chem. **31**, 219-232

Becker E. D. (1980) High resolution NMR. 2nd ed. Academic Press. pp354

Bicknell J., Clayton B. E., Delves H. T. (1968) Lead in mentally retarded children. J. Ment. Defic. Res. **12**, 282-293

Bish D. L. and von Dreele R. (1988) Rietveld refinement of the crystal structure of kaolinite. Ann. Meeting Clay Miner. Soc., East Lansing, Michigan (Abstr.)

Boey K. W., Jeyaratnam J. (1988) A discriminant analysis of neuropsychlogical effect of low lead exposure. Toxicology **49**, 309-314

Bovey F. A. (1988) Nuclear magnetic resonance spectroscopy. 2nd ed. Academic Press, Toronto. pp653

Breck D. W. (1974) Zeolite molecular sieves. Wiley-interscience Publication. Toronto.

pp771

Brindley G. W. (1980) Order-disorder in clay mineral structures. in Crystal structures of clay minerals and their X-ray identification. 125-195. G. W. Bridley and G. Brown ed. Mineralogical Society, London

Brown G. and Brindley G. W. (1980) X-ray diffraction procedures for clay mineral identification. in Crystal structures of clay minerals and their X-ray identification. 305-360. G. W. Brindley and G. Brown ed. Mineralogical Society, London

Byers R. K. (1959) Lead poisoning. Review of the literature and report on 45 cases. Paediatrics. **23**, 585-603

Byers R. K., Lord E. E. (1943) Late effects of lead poisoning on mental development. Am. J. Dis. Child. **66**, 471-494

de la Calle C. & Suquet H. (1988) Vermiculite. Rev. Miner. **19**, 455-492

Calligaris M., Nardin G., Randaccio L., and Chiaramonti P. C. (1982) Cation-site location in a natural chabazite. Acta Cryst. **B38**, 602-605

Cloghesy M. (1985) Canadian Paints and Coatings Association. Submission to the Royal Society of Canada Commission on lead in the environment, Toronto, April 26

Considine D. M. and Considine G. D. (1984) Encyclopedia of chemistry, 4th ed., 534-537. Van Nostrand Reinhold Company, Toronto.

Cooper W. C. (1976) Cancer mortality patterns in the lead industry. Ann. NY Acad. Sci. **271**, 250-259

Crutcher J. C. (1963) Clinical manifestations and therapy of acute lead intoxication due to the ingestion of illicitly distilled alcohol. Ann. Intern. Med. **59**, 707-715

Cullen M. R., Kayne R. D., Robins J. M. (1984) Endocrine and reproductive dysfunction in men associated with occupational inorganic lead intoxication. Arch. Environ. Health. **39**, 431-440

Elwood P. C. (1986) The importance of various sources of lead. in M. C. B. Hotz ed. Health effects of lead. Minister of Supply & Services Canada 123-150

Engelhardt G. and Michel D. (1987) High resolution solid state NMR of silicates and zeolites, John Wiley & Sons. Toronto. pp485

Fulton M., Raab G., Thomson G., Laxen D., Hunter R., Hepburn W. (1987) Influence of blood lead on the ability and attainment of children in Edinburgh. Lancet. **1**, 1221-1226

Fyfe C. A. (1983) Solid state NMR for chemists. C. F. C. Press, Guelph. pp593

Gallacher J. E., Elwood P. C., Phillips K. M., Davies B. E., Ginnever R. C., Toothill, C., and Jones, D. F. (1984) Relation between pica and blood lead in areas of differing lead exposure. Arch. Dis. Child. **59**, 40-44

Gilfillan, S. C. (1965) Lead poisoning and the fall of the Roman Empire. J. Occu. Med. **7**, 53-60

Gilani S. H. (1973) Congenital anomalies in lead poisoning. Obstet. Gynecol. **41**, 265-269

Goyer R. A., Tsuchiya K., Leonard D. L., Kahyo H. (1972) Aminoaciduria in Japanese workers in the lead and cadmium industries. Am. J. Clin. Pathol. **57**, 635-642

Grandjean P., Hollnagel H. and Olsen, N. B. (1981) Occupationally related lead exposure in the general population: a population study of 40-year-old men. Scand.

J. Work Environ. Health **7**, 298-301

Grant F. A. (1985) American Can Canada Inc. Submission to the Royal Society of Canada Commission on lead in the environment, April 26

Güven N. (1988) Smectite. Rev. Miner. **19**, 497-559

Harrison P. G., Healy M. A., and Steel A. T. (1983) ^{207}Pb chemical shift data for bivalent lead compounds: thermodynamics of the equilibrium $Pb(O_2CCh_3)_2 \rightleftharpoons [Pb(O_2CCH_3)]^+ + O_2CCH_3^-$ in aqueous solution in the temperature range 303 - 323 K. J. Chem. Soc. Dalton Trans. 1845-1848

Herzfeld J. and Berger A. E. (1980) Sideband intensities in NMR spectra of samples spinning at the magic angle. J. Chem. Phys. **73**, 6021-6030.

Hotz M. C. B. (1986) Lead and health--An editorial overview. in M. C. B. Hotz ed. Health effects of lead. Minister of Supply & Services Canada 1-26

Irwin P. J. (1985) Canada Metal Company Ltd. Submission to the Royal Society of Canada Commission on lead in the environment, Toronto, April 26

Jenkins C. D., Mellins R. B. (1957) Lead poisoning in children. A study of 46 cases. Arch. Neurol. Psychiatry. **77**, 70-78

Karalekas P. C., Jr., Ryan C. R., and Taylor F. B. (1983) Control of lead, copper, and iron pipe corrosion in Boston. J. Am. Water Works Assoc. **75**, 92-95

Klaussen, C. D. (1980) Heavy metals and heavy-metal antagonists. Lead. in : Gilman, A. G., Goodman L. S., Gilman A., eds. The pharmacological basis of therapeutics. 6th ed. New York: Macmillan. 1616-1622

Komarneni S., Fyfe C. A., Kennedy G. J., and Stroble H. (1986) Characterization of

synthetic and naturally occurring clay by ^{29}Si magic angle spinning nuclear magnetic resonance. J. Am. Cerm. Soc. **69**, C45-C47

Laperche V., Lambert J. F., Prost R., and Fripiat J. J. (1990) High-resolution solid state NMR of exchangeable cations in the interlayer surface of a swelling mica: ^{23}Na, ^{111}Cd, and ^{133}Cs vermiculites. J. Phys. Chem. **94**, 8821-8831

Lillis R., Gavrilescu N., Nestorescu B., Dumitriu C., Roventa A. (1968) Nephropathy in chronic lead poisoning. Br. J. Ind. Med. **25**, 196-202

Lin-Fu J. S. (1982) Children and lead: new findings and concerns. N. Engl. J. Med. **307**, 615-617

Lippmaa E. Mägi M., Samoson A. Tarmak M., and Engelhardt G. (1981) Investigation of the structure of zeolite by solid state ^{29}Si NMR spectroscopy. J. Am. Chem. Soc. **103**, 4992-4996

Lippmaa E., Samoson A., and Mägi M. (1986) High resolution ^{27}Al NMR of aluminosilicates. J. Am. Chem. Soc. **108**, 1730-1735

Little P., Fleming R. G. and Heard M. J. (1981) Uptake of lead by vegetable foodstuffs during cooking. Sci. Total Environ. **17**, 111-131

Lucchini V. & Wells P. R. (1980) Trimethyllead chloride distribution in aqueous and methanolic solutions. J. Organomet. Chem. **199**, 217-222

Maes A. & Cremers A. (1985) Highly selective ion exchange in clay minerals and zeolites. ACS Symp. Ser. **323**, 254-295

Mägi M., Lippmaa E., Samoson A., Engelhardt G., and Grimmer A. -R. (1984) Solid state high resolution ^{29}Si chemical shifts in silicates. J. Phys. Chem. **88**, 1518-

1522

Maruyama T., Hannah S. A., and Cohen J. M. (1975) Metal removal by physical and chemical treatment processes. J. WPCF. **47**, 962-975

Mazzi F. and Galli E. (1983) The tetrahedral framework of chabazite. N. Jb. Miner. Mh. **10**, 461-480

Mazzocco F. (1977) Optimization of the purifying process using sodium sulphate. Inquinamento **19**, 145-153

Méring J. and Oberlin A. (1971) The smectites, in The electron-Optical Investigations of Clays J. A. Gard, ed., Miner. Soc. Monogr. **3**, 193-229

Moore D. M. and Reynolds R. C., Jr. (1989) X-ray diffraction and the identification and analysis of clay minerals. pp179-268. Oxford University Press. New York

Nilsson R. (1971) Removal of metals by chemical treatment of municipal waste water. Water Research **5**, 51-60

Nolle A. (1977) ^{207}Pb magnetic shielding anisotropy in $Pb(NO_3)_2$, $PbCO_3$, $PbCrO_4$, $PbMoO_4$ and $PbWO_4$ by Fourier Transform NMR. Z. Naturforsch. **32a**, 964-967

Nowacki W., Koyama H., Mladeck M. H. (1958) crystal structure of the zeolite, chabazite. Experimentia **14**, 396

Nriagü J. O. (1986) Lead contamination of the Canadian environment. in M. C. B. Hotz ed. Health effects of lead. Minister of Supply & Services Canada 61-78

Oliver T. (1911) Lead poisoning and the race. Br. Med. J. **1**, 1096-1098

van Olphen H. V. and Friapiat J. J. (1979) Data handbook for clay materials and other non-metallic minerals. Perganmon Press, Toronto. pp346

Parker S. P. ed. in chief (1983) Encyclopedia of chemistry. 559-561. McGraw-Hill Company, New York

Palmisano P. A., Sneed R. C., Cassady G. (1969) Untaxed whisky and fetal lead exposure. J. Pediatr. **75**, 869-872

Partington J. R. (1973) A text book of inorganic chemistry. Fifth edition. McMillan, London. 910

Partington J. R. (1935) Origin and development of applied chemistry. Longmans, London

Patterson C. C. (1965) Contaminated and natural environments of Man. Arch. Environ. Health **11**, 344-360

Patterson J. W. (1975) Treatment technology for lead, in Wastewater treatment technology, Ann Arbor Science Publishers, Ann Arbor, MI, pp. 129-138

Piette L. H. & Weaver H. E. (1958) NMR chemical shifts of Pb^{207} in a few compounds. J. Chem. Phys. **28**, 735-736

Pines A., Gibby M. G., and Waugh J. S. (1973) Proton-enhanced NMR of dilute spins in solids. J. Chem. Phys. **59**, 569-590

Pluth J. J., Smith J. V., and Mortier W. J. (1977) Position of cations and molecules in zeolite with the chabazite framework. IV. Hydrated and dehydrated Ca^{2+}-exchanged chabazite. Mat. Res. Bull. **12**, 1001-1007

Pocock S. J., Shaper A. G., Walker M. et al. (1983) Effects of tap water lead, water hardness, alcohol, and cigarettes on blood lead concentrations. J. Epidemiol. Commun. Health **37**, 1-7

Pouchou J. L. and Pichoir F. (1985) A new model for quantitative X-ray microanalysis. Rech. Aerosp. **1984-3**, 13-38

Power W. P., Waysylishen R. E., Mooibroek S., Pettitt B. A., and Danchura W. (1990) Simulation of NMR powder line shape of quadrupolar nuclei with half-integer spin at low-symmetry site. J. Phys. Chem. **94**, 591-598

Saether O. M., Bolviken B., Lag J., and Steinnes E. (1988) Concentration and chemical form of lead during natural transportation in ground water. Chem. Geol. **69**, 309-310

Samoson A., Kundla E., and Lippmaa E. (1982) High resolution MAS NMR of quadrupolar powders. J. Mag. Reson. **49**, 350-357

Samoson A. and Lippmaa E. (1983) Excitation phenomena and line intensities in high-resolution NMR powder spectra of half integer quadrupolar nuclei. Phys. Rev. **1328**, 6567-6570

Sanders J. K. M. and Hunter B. (1989) Modern NMR spectroscopy. Oxford University Press. Toronto. pp308

Shannon R. D. (1976) Rvised effective ionic radii and systematic studies of interatomic distances in halides and chalcogenides. Acta Cryst. **A32**, 751-766

Schwartz J., Landrigan P. J., Feldman R. G., Silbergeld E. K., Baker E. L., Von Lindern I.H. (1988) Threshold effect in lead-induced peripheral neuropathy. J. Pediatr. **112**, 12-17

Sharma S. Weiden N., and Weiss A. (1987) ^{207}Pb and ^{207}Tl NMR on Perovskite type crystals $APbX_3$. Z. Naturforsch., **42a**, 1313-1320

Sherlock J. C., Smart G. A., Walters B., Evans W. H., McWeeny D. J., Cassidy W. (1983) Dietary surveys on a population at Shipham, Somerset, United Kingdom. Sci. Total Environ. **29**, 121-142

Sherriff B. L., Hawthorne F. C., and Bain A. D. (in prep.) Solid state lead-207 NMR of minerals: chemical shifts, anisotropies and relaxation times.

Sherriff B. L., Grundy H. D. Stephen H. J. (1991) The relationship between ^{29}Si MAS NMR chemical shift and silicate mineral structure. Eur. J. mineral. **3**, 751-768

Sherriff B. L., Grundy H. D., and Hartman J. S. (1987) Occupancy of T sites in the scapolite series: A multinulear NMR study using magic-angle spinning. Can. Miner. **25**, 717-730

Shirozu H. and Bailey S. W. (1966) Crystal structure of a two-layer Mg-vermiculite. Amer. miner. **51**, 1124-1143

Singh N., Donovon C. M., Hanshaw J. B., 1978. Neonatal lead intoxication in a prenatally exposed infant. J. Pediatr. **93** 1019-1021

Smith J. V., Knowles C. R., and Rinald F. (1964) Crystal structure with a chabazite framework III. Hydrated Ca-chabazite at +20 and -150 °C. Acta. Cryst. **17**, 374-384

Smith J. V., Rinaldi F., Glasser L. S. D. (1963) Crystal structure with a chabazite framework. II. Hydrated Ca-chabazite at room temperature. Acta Cryst. **16**, 45-53

Smith J. V. (1962) Crystal structures with a chabazite framework. I. Dehydrated Ca-chabazite. Acta Cryst. **15**, 835-845

Smyth J. R., Bish D. L. (1988) Crystal structures and cation sites of the rock-forming minerals. Allen & Unwin, Boston. pp332

Srivastava S. K., Tyagi R., Pant N., and Pal N. (1989) Studies on the removal of some toxic metal ions: Part II (removal of lead and cadmium by montmorillonite and kaolinite). Environ. Techn. Lett. **10**, 275-282

Stubbs R. L. (1972) In "Lead in the Environment" (P. Hepple ed.) pp. 1. Institute of Petroleum, London

Sylva R. N.and Brown P. L. (1980) The hydrolysis of metal ions. Part 3, Lead(II), J. Chem. Soc. Dalton Trans. **9**, 1577-1581

Taylor P. and Lopata V. J. (1983) Stability and solubility relationships between some solids in the system PbO-CO_2-H_2O. Can. J. Chem. **62**, 395-402

Thompson J. G. (1984) ^{29}Si and ^{27}Al nuclear magnetic resonance spectroscopy of 2:1 clay minerals. Clay Miner. **19**, 229-236

Townsend R. P. (1984) Ion exchange in zeolites - basic principles. Chem. Indust. **2 Apr.** 246-251

de Treville R. T. (1964) Natural occurrence of lead. Arch. Environ. Health **8**, 212-221

Waldron H. A. and Stöfen, D. (1974) Sub-clinical lead poisoning. Academic Press

Weiberg I. (1962) Chemical shift of the Pb^{207} NMR in some polar semiconductors. J. Chem. Phys. **36**, 1112-1113

Weiss C. A., Jr., Kirkpatrick R. J., and Altaner S. P. (1990) The structural environments of cations adsorbed onto clays: ^{133}Cs variable-temperature MAS NMR spectroscopic study of hectorite. Geochim. Cosmochim. Acta **54**, 1655-

1669

White A. F. and Yee A. (1986) Near-surface alkli diffusion into glassy and crystalline silicates at 25°C to 100°C. ACS Symp. **28**, 587-598

Wijin M., Duives P., Herber R., and Brunekreef B. (1983) Lead uptake from vegetables grown along highways. Int. Arch. Occup. Environ. Health **52**, 263-270

Winship K. A. (1989) Toxicity of lead: a review. Adverse Drug. Deact. Acute Poisoning Rev. **8**, 117-152

Woessner D. E. (1989) Characterization of clay minerals by ^{27}Al nuclear magnetic resonance spectroscopy. Amer. Miner. **74**, 203-215

Wrackmeyer B. & Horchler K. (1989) ^{207}Pb-NMR parameters. Ann. Report NMR Spetr. **22**, 249-306

Wu Y., Chanelka B. F., Pines A., Davis M. E., Grobet P. J., and Jacobs P. A. (1990) High resolution ^{27}Al NMR spectroscopy of the aluminophosphate molecular sieve VPI-5. Nature. **346**, 550-552

Zamzow M. J., Eichbaum B. R., Sandgren K. R., and Shanks D. E. (1990) Removal of heavy metals and other cations from waste water using chabazites. Seprat. Sci. Techn. **25**, 1555-1569

Zvyagin B. B. and Pinsker . G. (1949) Electron diffraction study of the montmorillonite structure. Dokl. Acad. Nauka SSR **68**, 30-35